DLR-IB-AE-GO-2023-162

Influence of more accurate propeller modelling on the whirl flutter stability of a propeller-driven aircraft

Masterarbeit

Julia Noël

Deutsches Zentrum
DLR für Luft- und Raumfahrt

Dokumenteigenschaften

Titel	Influence of more accurate propellermodelling on the whirl flutter stability of a propeller-driven aircraft
Betreff	DLR-IB-AE-GO-2023-162
Institut	Institut für Aeroelastik
Erstellt von	Julia Noël
Beteiligte	Christopher Koch, Jürgen Arnold
Geprüft von	Prof. Dr.-Ing. Holger Hennings
Freigabe von	Prof. Dr.-Ing. Lorenz Tichy
Datum	14.12.2023
Version	1.0
Dateipfad	

Influence of more accurate propeller modelling on the whirl flutter stability of a propeller-driven aircraft

Abstract:

Whirl flutter stability of propeller-driven aircraft is so far verified by introducing analytical propeller derivatives into frequency-domain flutter analysis, based on the assumption of rigid propeller blades. Recent studies on an isolated propeller model with a new method using identified, frequency-dependent transfer matrices for the propeller hub loads have shown that including blade elasticity in the analysis increases whirl flutter stability significantly. This work extends the transfer-matrix method to enable its application on complex aircraft models. To decouple the specific propeller model used for transfer-matrix generation from the structural model of the airframe, a few adaptions for the transfer-matrices are introduced, like eliminating the propeller mass influence from the transfer-matrices as well as aligning the propeller orientation with the coordinate system definition of the structural model. An interpolation routine for the transfer-matrices over the velocity steps is also introduced. Frequency-domain flutter analyses of a generic twin-turboprop aircraft are performed to demonstrate the introduced adaptions and evaluate the influence of blade elasticity and thrust. While investigations on an aircraft model showing bending-torsion flutter expose a very low impact due to these propeller modelling aspects on stability, it is successfully demonstrated that the whirl flutter stabilisation due to blade elasticity also occurs on full aircraft level, even though this stabilising effect has a limit for very soft blades.

DEUTSCHES ZENTRUM FÜR LUFT- UND RAUMFAHRT e.V.

Institut für Aeroelastik

Institutsleiter:

Prof. Dr.-Ing. Lorenz Tichy

Verfasserin:

Julia Noël

Abteilungsleiter:

Prof. Dr.-Ing. Holger Hennings

Gruppenleiter:

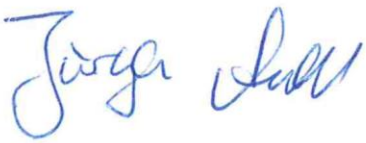

Jürgen Arnold

Master thesis

Influence of more accurate propeller modelling on the whirl flutter stability of a propeller-driven aircraft

Julia Noël

Matriculation Number: 5250318

DLR Institute of Aeroelasticity

Airbus Operations GmbH

First Examiner: Prof. Dr.-Ing. Lorenz Tichy
Second Examiner: Prof. Dr.-Ing. Sebastian Heimbs

Supervisors: M.Sc. Christopher Koch (DLR)
Dr.-Ing. Bernd Stickan (Airbus)

Deutsches Zentrum
für Luft- und Raumfahrt

AIRBUS

Institut für Aeroelastik

Deutsches Zentrum
DLR für Luft- und Raumfahrt

DLR e. V. Institut für Aeroelastik
Bunsenstr. 10, 37073 Göttingen

Ihr Zeichen
Ihr Schreiben
Unser Zeichen

Ihr Gesprächspartner Prof. Dr.-Ing. Lorenz Tichy

Telefon 0551 709- 2341
Telefax 0551 709-
E-Mail Lorenz.tichy@dlr.de

Task description Master thesis:

Influence of more accurate propeller modelling on the whirl flutter stability of a propeller-driven aircraft

In this master thesis the influence of a more accurate propeller modelling on the flutter behavior of a generic turboprop configuration should be examined. Classical methods of whirl flutter analyses neglect for example blade elasticity or thrust. Previous work at the Institute of Aeroelasticity has shown that these parameters can have a stabilising effect on simple whirl flutter models. In this thesis that should now be demonstrated for a complete aircraft configuration. For this purpose, existing aircraft and propeller models can be used. By means of parameter variations, the influence of model parameters such as blade elasticity, thrust setting and rotational speed on the whirl flutter stability should be examined and the results should be compared to the classical methods.

Tasks:

1. Familiarization with the subject of whirl flutter (classical methods, sensitivities, …)
2. Familiarization with software (MBS Simpack), methods (TM-method, flutter solution) and models (FE / DLM for aircraft / MBS for propeller)
3. Performing whirl flutter analyses with classical methods by use of the DLR flutter process
4. Identification of transfer behaviour for MBS propeller models in various settings
5. Performing whirl flutter analyses with identified propeller models
6. Comparison of results and derivation of trends
7. Documentation of the results in a scientific thesis

Starting date: 01.06.2023

Examiner: Prof. Dr.-Ing. Lorenz Tichy

Göttingen, 01.06.2023

Bunsenstr. 10
37073 Göttingen
Telefon 0551 709-0
Internet DLR.de

Statement of independence

I hereby confirm that I have written this thesis by myself and have not used any sources other than those cited.

I have not yet submitted the work in the same or similar form, including excerpts thereof, as part of another examination or course work.

I confirm that the submitted electronic version of the thesis is completely identical to the printed version.

30.11.2023 

Date, Signature

Abstract

This thesis demonstrates that using more accurate propeller modelling, especially regarding blade elasticity, has an important impact on whirl flutter stability of a full aircraft configuration.
Due to the general goal of reducing climate impact of aircraft, turboprop aircraft developments are currently increasing. Whirl flutter stability is an important certification criterion for these aircraft. This stability is so far verified using analytically derived propeller derivatives in frequency-domain flutter analysis. These derivatives are based on rigid blade assumptions though. Recent studies on an isolated propeller model with a new method using frequency dependent transfer-matrices for the propeller hub loads showed, that including blade elasticity in the analysis increases the whirl flutter stability significantly. However, this effect has not been examined on full aircraft level yet.
This work first reproduces these findings on two degrees of freedom level and performs some additional studies regarding eigenfrequency variation and scaling of blade stiffness. Then, the transfer-matrix method is extended to enable its application on complex aircraft models. To decouple the specific propeller model used for transfer-matrix generation from the structural model of the airframe, a few adaption procedures for the transfer-matrices are introduced, like eliminating the propeller mass influence from the transfer-matrices as well as aligning the propeller orientation with the coordinate system definition of the structural model. Furthermore, an interpolation routine for the transfer-matrices is introduced to reduce the number of necessary velocity steps for transfer-matrix generation. Then, frequency-domain flutter analyses of a generic twin-engine turboprop aircraft configuration are performed and the impact of the new propeller modelling approach and the influence of blade elasticity and thrust on stability are evaluated.
While investigations on an aircraft model showing bending-torsion flutter expose a very low impact due to these propeller modelling aspects on stability, the influence on whirl flutter is higher. It is successfully demonstrated that the stabilisation due to blade elasticity also occurs on full aircraft level. Even though this stabilising effect has a limit for very low blade elasticity, this investigation reveals an additional flutter stability margin, that should be examined further to take advantage of during future aircraft designs.

Zusammenfassung

In dieser Arbeit wird gezeigt, dass eine genauere Propellermodellierung einen großen Einfluss auf die Flatterstabilität einer propellergetriebenen Flugzeugkonfiguration hat.
Die Reduzierung des Klimaeinflusses von Flugzeugen ist aktuell ein wichtiges Ziel der Luftfahrtindustrie und führt zu immer mehr Entwicklungen von Turboprop-Flugzeugen. Ein wichtiges Zertifizierungskriterium für diese Propellerflugzeuge ist der Nachweis der Stabilität bezüglich Whirlflattern. Bisher wird dieser Nachweis mittels analytisch bestimmter Propellerderivativen durchgeführt, die in die Flatteranalyse im Frequenzbereich eingeführt werden. Bei der Herleitung dieser Derivative wird allerdings die Annahme steifer Propellerblätter getroffen. Neuere Studien haben gezeigt, dass Blattelastizität einen entscheidenden (stabilisierenden) Einfluss auf die Whirlflatterstabilität hat. Dabei wurde eine neue Methode verwendet, bei der frequenzabhängige Transfermatrizen für die Lasten an der Propellernabe bestimmt und in der Flatterlösung eines isolierten Propellermodells verwendet werden. Allerdings wurde dieser Effekt noch nicht an einer Gesamtflugzeug-Konfiguration untersucht.
Die vorliegende Arbeit reproduziert zunächst einige Ergebnisse des Zwei-Freiheitsgrad-Modells eines isolierten Propellers und untersucht weitere Aspekte, wie die Skalierung der Blatteigenfrequenzen und eine schrittweise Skalierung der Blattsteifigkeit, und deren Einfluss auf die Whirlflatterstabilität. Anschließend wird die Transfermatrix-Methode erweitert, um eine praktische Anwendung auf komplexere Flugzeugkonfigurationen zu ermöglichen. Um das Propellermodell, das zur Bestimmung der Transfermatrizen verwendet wird, unabhängig vom Strukturmodell, mit dem die Matrizen kombiniert werden sollen, zu machen, werden einige Methoden zur Anpassung der Transfermatrizen eingeführt. Dazu gehört ein Vorgehen, um den Einfluss der Propellermasse aus den Transfermatrizen herauszurechnen, und die Angleichung der Transfermatrizen an die Propellerorientierung im Koordinatensystem des Strukturmodells. Darüber hinaus wird eine Interpolationsroutine eingeführt, mit der die Anzahl der notwendigen Geschwindigkeitsschritte für die Bestimmung der Transfermatrizen reduziert wird. Nach diesen Modifikationen werden Flatteranalysen an einer generischen Turboprop-Konfiguration durchgeführt und der Einfluss der neuen Propellermodellierung und im Speziellen der Parameter Blattelastizität und Schub untersucht.
Der Fokus der Arbeiten liegt auf der Whirlflatterstabilität, allerdings werden zusätzlich auch Untersuchungen zur Stabilität bezüglich Biege-Torsions-Flattern durchgeführt, bei denen sich jedoch geringere Einflüsse der Propellermodellierung zeigen. Im Gegensatz dazu zeigte sich ein großer Einfluss der Propellermodellierung auf die Stabilität bezüglich Whirlflattern. Während der Einfluss des Schubzustands zwar nur gering ist, kann erfolgreich gezeigt werden, dass sich durch Berücksichtigung der Blattelastizität auch für das Gesamtflugzeug die Whirlflatterstabilität entscheidend erhöht. Darüber hinaus kann beobachtet werden, dass dieser Effekt bei niedrigen Blattsteifigkeitswerten deutliche Grenzen hat und ab einem gewissen Punkt wieder destabilisierend wirkt. Dennoch zeigt die Untersuchung einen größeren Spielraum bezüglich der Whirlflatterstabilität auf, der sich nach weiteren Untersuchungen vorteilhaft auf zukünftige Flugzeugentwicklungen auswirken kann.

Contents

List of acronyms and symbols

Acronyms

2DOF model	two degrees of freedom model
BTF	bending-torsion flutter
DOF	degree of freedom
FEM	Finite Element Method
FE-model	finite element model
HR-method	Houbolt/Reed method
ICAO	International Civil Aviation Organisation
IFASD	International Forum on Aeroelasticity and Structural Dynamics
MACX	modal assurance criterion extended for complex modes
ROM	reduced order model
STOL	short takeoff and landing
TAS	true air speed
TM-method	transfer-matrix method
TPS	Thin Plate Splines
WF	whirl flutter

Mathematical symbols

D	propeller diameter
$\underline{D}_{prop}$	propeller damping matrix
F_{prop}	vector of propeller forces and moments
f	frequency
$\underline{G}_{gen}$	generalised gyroscopic matrix
g	structural damping
$\underline{H}_{prop}$	propeller transfer-matrix
I_p, I_θ, I_ψ	inertia about x-, y-, or z-axis of propeller system
K	stiffness
$\underline{K}_{gen}$	generalised stiffness matrix
K_θ, K_ψ	rotational stiffness of engine mounts for rotation around y- or z-axis
$\underline{K}_{prop}$	propeller stiffness matrix
k_{scale}	scaling factor for stiffness of propeller blades
M	mass
M_{gyro}	gyroscopic moment
$\underline{M}_{gen}$	generalised mass matrix
m_{prop}	propeller mass
m_{scale}	scaling factor for mass of propeller blades
$\underline{Q}_{gen}$	generalised aerodynamic forces
q_h	vector of generalised coordinates

q	dynamic pressure
R	propeller radius
S	propeller disc area
s	Laplace variable
T	thrust
$\underline{T}$	transformation matrix for transfer-matrices or HR propeller matrices
V	airspeed
V_D	airframe dive airspeed
V_F	flutter speed
w_{kk}	aerodynamic pressure correction factor for axial propeller wake effect
x, y, z	coordinate axis directions
ρ	air density
ϕ, θ, ψ	angles of rotation about x-, y-, or z-axis
$\underline{\Phi}_{prop}$	modal matrix containing propeller hub displacements
Ω	rotational speed
ω_0	non-rotating blade eigenfrequency
ω_θ, ω_ψ	eigenfrequency of pitch or yaw motion

1. Introduction

1.1. Motivation

In the past decades, an increasing growth in aviation could be noticed and is predicted also for the future. This trend increases also the environmental impact of aviation emissions [1]. Therefore, reducing the emissions of future aircraft is the main challenge of current aeronautical research. For the aviation industry, this is not only part of its global responsibility, but also prescribed by external guidelines. In 2019, the European Union set a goal of climate neutrality for the EU until 2050, including also a target to reduce emissions from the transport sector by 90 % compared to 1990 [2]. In 2022, the International Civil Aviation Organisation (ICAO) set a similar guideline to achieve carbon emissionless international aviation until 2050 [3]. The aviation industry works a lot on different concepts to achieve these goals and reduce the climate impact of future aircraft. One important attempt for low-emission aircraft is the use of hybrid or full-electrical propulsion using propellers, because of their high propulsive efficiency and low emissions during flight [4].
An important aspect for the aeroelastic stability of propeller aircraft is the whirl flutter stability. Whirl flutter is a phenomenon arising for elastically mounted propellers performing a whirl motion that occurs due to gyroscopic coupling and can become unstable at a specific flutter speed [5]. For the new developments, it is important to be able to analyse the stability of the full aircraft-propeller system in an efficient way. Hereby, it is of great importance that not too conservative assumptions, e.g. regarding the propeller properties, are made to find the most efficient aircraft configuration, that is still stable.
One important aspect, that has been neglected so far in whirl flutter analyses, is the blade elasticity, which has a relevant impact on the whirl flutter stability, as it has been discovered recently [6]. Considering the blade elasticity in the stability analysis of a single, isolated propeller model has increased the whirl flutter stability of the system drastically. This stabilising effect indicates a big potential to reduce conservatism and improve the overall aircraft design, for example by reducing the structural mass at the propeller mounts. However, it needs to be investigated if this effect is only a theoretical artefact for isolated propellers or if it practically appears also on full aircraft level.
The investigations used the so-called transfer-matrix method (TM-method) [7] to consider parameters, like blade elasticity and propeller thrust, in the frequency-domain aircraft flutter analysis. This method should be applied and extended in this thesis with the aim to demonstrate that the method is also applicable on full aircraft configurations. Furthermore, it should be investigated if the influences observed for the isolated propeller can also be found in full aircraft stability analysis. For that, a generic twin-turboprop aircraft model is coupled with the transfer-matrices of a propeller model generated with a multibody simulation tool and the flutter stability is analysed. The focus is hereby mainly on the influence of propeller blade elasticity and thrust on whirl flutter stability, but also classical bending-torsion flutter is studied.

1.2. State of the art

Whirl flutter is a phenomenon whose detailed investigation began in the 1960s, after two accidents of Lockheed Electra aircraft caused by this type of instability occurred [5]. In the following, Houbolt and Reed [8] developed an analytical approach based on derived propeller derivatives to incorporate whirl flutter in flutter analyses to study the phenomenon. Bland and Bennett [9] later validated the method with experimental data and Rodden and Rose [10] developed a preprocessor to include the derivatives in MSC Nastran flutter analysis. The method makes some, for this thesis, crucial assumptions, such as rigid propeller blades. Still, it is up till now the standard method in the flutter analysis of turboprop aircraft and is also used for certification [11].
Developments in tilt-rotor applications required further investigations on whirl flutter stability. These configurations have larger and more flexible rotors which are additionally often mounted on the tips of flexible wings. This increases the whirl flutter risk. Therefore, even early investigations incorporate blade degrees of freedom by including hinges at the rotor hub in the analytical model for flutter calculation while the blades themselves remain rigid, as in [12] or [13]. By varying the stiffness of the rotational springs at the hinges, the influence of different eigenfrequencies of the blade degrees of freedom could be examined and even an optimum range for the smallest required engine mount stiffnesses found. These examinations showed further that blade elasticity might also change the unstable whirl mode from backward to forward whirl. The studies above only investigated separate, isolated propeller models fixed with the end of the propeller axis at a single pivot point. This pivot point permits only motion in two degrees of freedom, namely the tilting motions of the axis. Johnson [14] extended this approach by combining a theoretical rotor model with in-plane and out-of-plane blade motion with different wing/pylon models and examined their combined stability together.
With increasing computational capability, multibody simulation and numerical modelling of rotorcraft with flexible tilt-rotor blades became feasible. Shen et al. [15], for example, used one of these so-called rotorcraft comprehensive codes to model a rotor system attached to a wing and compared the results with experimental data. These methods have also been applied occasionally in aircraft applications. Studying even a full aircraft configuration, Hoover et al. applied this methodology on the electrical-driven technology testing aircraft X-57 to proof its whirl flutter stability [16] and further examined the influence of different parameters on whirl stability [17]. One parameter they studied was also the blade flexibility which appeared to have a mostly stabilising effect. Later, Yeo and Kreshock [18] showed with rotorcraft comprehensive code analysis that the blade elasticity influences not only the whirl stability, but also the whirl mechanism that becomes unstable (backward or forward whirl). Donham and Ostholt [19] have demonstrated that considering blade elasticity improves fidelity of the full aircraft whirl flutter results and in this case also increases the stability range.
A similar conclusion has been drawn, lately, by Koch and Koert [6] who used a new method [7], called transfer-matrix method (TM-method), to study the influence of blade elasticity on whirl flutter stability of a simple two degrees of freedom propeller model (2DOF model). Unlike most of the previously mentioned methods, which are time-domain methods, this new approach uses frequency-dependent transfer-matrices between hub motions and propeller hub loads to incorporate sophisticated propeller modelling in classical frequency-domain

flutter analysis. Frequency-domain flutter analysis is the standard procedure of stability analysis for fixed-wing aircraft.
There have been also other approaches to bring the whirl flutter analysis back into frequency domain but retain a more detailed propeller modelling. One approach is a procedure to determine propeller derivatives from time-domain simulations using an unsteady vortex-lattice method [20]. Gennaretti and Greco developed and applied an approach to create a reduced order model (ROM) for unsteady propeller aerodynamics to predict the aerodynamic loads, leading to a state-space model based on the approximation of frequency-domain aerodynamic solution [21, 22]. However, the basis of the TM-method used in this thesis is an approach as described in [23] and [24] where perturbations of a time-domain rotor model are used to determine transfer functions between hub motion and forces in the frequency domain. After that, a time-domain state-space ROM is built by approximating these generated transfer functions. The TM-method extends the idea, but keeps the transfer functions in frequency domain to incorporate them directly in the aircraft flutter analysis. Details on the method are explained in the following chapters, as it is the relevant method that is applied in this thesis. Yet, it has been only applied on the simple 2DOF model, so also method adaptions are presented with the aim to apply it on full aircraft configurations.

1.3. Outline

First, in chapter 2, the basis of the methodologies used and the aeroelastic phenomena studied is presented based on known theory from literature. After the relevant information about classical flutter analysis is summarised, details about the whirl flutter phenomenon and its analysis are described. In this chapter, also the TM-method used and the classical reference method from Houbolt and Reed (HR-method) is explained and some insights into the influence of different parameters on whirl stability are given. This last part of chapter 2 also includes, in section 2.3.3, the lessons learned from [6] about the influence of blade elasticity and thrust on the whirl flutter stability of a single, isolated propeller model that triggered further investigations on this topic by means of this thesis.
Chapter 3 first presents a similar 2DOF model of an isolated propeller that has been used to work on the TM-method and perform a few additional stability analyses on 2DOF level. This model description includes the presentation of the multibody simulation model of the propeller that is used to generate the transfer-matrices. These transfer-matrices are later also used for the full aircraft analysis. In the last section of this chapter, section 3.3, stability results for the 2DOF model are presented with the objective to reproduce the previous results from [6] with the model used in this work and to gain further insights into the observed effects. After the fundamental comparison of HR- and TM-method results, the influence of changing the blade eigenfrequency via mass or stiffness adaptions is compared. Finally, also a small parameter study regarding the blade stiffness is performed.
The TM-method used needs a few modifications to make it possible to apply it on a full aircraft configuration. Also, the HR-method needs some adaptions for practical applications on the generic aircraft model. These method extensions are explained in chapter 4.
Chapter 5 finally presents the stability analyses on full aircraft level. After the structural and aerodynamic model of the examined full aircraft are introduced, the results of performed flutter analyses with the modified TM-method are presented. Two structural models are

analysed: a model showing whirl flutter and a model showing classical bending-torsion flutter. For both structural configurations, the HR-method results are compared with the TM-method results and for the whirl flutter instability a parameter study regarding the blade elasticity is presented. Additionally, also the influence of thrust on flutter stability is studied for both structural configurations.
Concluding, chapter 6 summarises and discusses the work in this thesis and the gained results and gives a short outlook on potential future work.

2. Theoretical background

In this chapter, the relevant theoretical background from literature is summarised. First, in section 2.1, a small introduction on aeroelastic phenomena is given. After that, in section 2.2, the basics of flutter analysis in general are explained, before finally, in section 2.3, a focus is put on the whirl flutter phenomenon.

2.1. Basics of aeroelastic phenomena

Aeroelasticity describes the field of examination of interactions occurring between an elastic system and its surrounding airflow. Several different phenomena may appear which origin in the interactions of aerodynamic (A), elastic (E) and inertial forces (I). These correlations are often displayed in the so called "Collar's triangle" (figure 2.1) [25]. The three kinds of forces must form an equilibrium with potential external forces Q:

$$I + E + A = Q \tag{2.1}$$

If no external forces are considered, Q is zero.

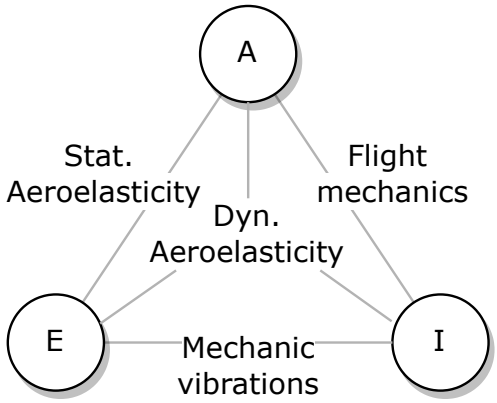

Figure 2.1.: Collar's triangle

Different interactions lead to different aeroelastic phenomena, which can be separated in two basic categories [25]: On the one hand, there are static aeroelastic phenomena which cover the interaction of static aerodynamic forces and elastic forces (e.g. divergence problems), so the inertial forces I in equation 2.1 are zero . On the other hand, there are dynamic aeroelastic phenomena which also consider unsteady aerodynamic and inertial forces. Furthermore, this second category can be split in response problems, where the reaction on an external excitation is analysed ($Q \neq 0$), and stability problems without external forces. Flutter phenomena, such as the whirl flutter phenomenon, are dynamic stability problems and appear in different forms depending on the involved aircraft parts and motions [25]. Flutter phenomena in general are self-induced oscillations. Their amplitudes can increase in the unstable case until a damage of the structure occurs and must be avoided in any

case. Whirl flutter is one kind of flutter phenomenon for aircraft with flexible mounted propellers [5]. In specific cases the whirl phenomenon can also occur as whirl divergence (a static stability phenomenon). Bending-torsion wing flutter is another, very typical, flutter mechanism for aircraft and is based on a coupling between wing bending and wing torsion modes [25].

2.2. General flutter analysis

The typical aim of flutter analyses is to identify the critical flutter speed where the system gets unstable. The oscillations of an aircraft can be described by a combination of their eigenmodes and the corresponding eigenvalues. During the flutter analysis, the damping and frequency of the occurring modes are determined depending on the flight velocity V_∞ to find instabilities which occur if the damping of a mode becomes negative. The typical process of a flutter analysis in the frequency domain is well presented in Schwochow's dissertation [26].

To solve the stability problem, first the equation of motion has to be set up on basis of equation 2.1 from the previous section. No external forces are considered in stability analyses [27]. In a general matrix form, with the elastic, damping and inertial forces on the left side of the equation and the aerodynamic forces on the right side of the equation, this leads to [26]:

$$\underline{M}\ddot{u}(t) + \underline{D}\dot{u}(t) + \underline{K}u(t) = A(t) \tag{2.2}$$

with the mass matrix $\underline{M}$, the stiffness matrix $\underline{K}$ and the velocity-dependent damping matrix $\underline{D}$ of the system. $A(t)$ stands for the unsteady aerodynamic force vector dependent on the motion of the structure (displacement and velocity) and the flow conditions and $u(t)$ for the vector of displacements.
Without any specific constraints, an aircraft can have a lot of degrees of freedom. If it is in free flight, also the rigid body modes have to be considered and, usually, also additional degrees of freedom of the control surfaces and other movables have to be taken into account [27]. This leads to a high number of physical degrees of freedom to consider. To reduce this number of degrees of freedom, a modal transformation is performed [26]. To do so, the motion $u_g(t)$ of the aircraft can be assembled by the combination of a limited number of modes with different participation rates:

$$u_g(t) = \underline{\Phi}_{gh} q_h(t) \tag{2.3}$$

where index g stands for the number of physical degrees of freedom and h for the number of modal degrees of freedom. $\underline{\Phi}$ includes the mode shapes. These mode shapes are orthogonal to each other, leading to a decoupling of the modal degrees of freedom q_h in the equation of motion for diagonal system matrices and no coupling through aerodynamic or external forces [26]. As modal degrees of freedom the eigenmodes of the system are used. These eigenmodes and eigenfrequencies can be determined numerically with the Finite Element Method (FEM).

Flutter phenomena usually do not appear at higher reduced frequencies than $k_{max} = 1.0$ [26]. The reduced frequency k is a dimensionless quantity characterising the time dependence of unsteady aerodynamics, defined with the reference length l_{ref} as half wing depth, the flight velocity V_∞ and the angular frequency of the motion ω:

$$k = \frac{\omega l_{ref}}{V_\infty} \tag{2.4}$$

Therefore, the range of stability analysis can be limited to a frequency range of:

$$0 \leq \omega \leq k_{max} \frac{V_{\infty,max}}{l_{ref}} \tag{2.5}$$

Accordingly, it is also sufficient to consider only eigenmodes in this frequency range [26]. Thereby, the high number of physical coordinates is transferred into a limited number of modal coordinates.
The modal transformation is put into the equation of motion and it is translated into the Laplace domain which transfers the equation to the basis of energy equilibrium [26]. That produces the general flutter equation in frequency domain as a complex eigenvalue-problem as followed:

$$(s^2 \underline{M}_{gen} + s\underline{D}_{gen} + \underline{K}_{gen} - q\underline{Q}_{gen})q_h = 0 \tag{2.6}$$

The index *gen* specifies the generalised form (in modal coordinates) of the system matrices. These system matrices can be determined also by using FEM in physical coordinates and transforming the results afterwards into the generalised form [26]. $\underline{Q}_{gen}$ describes the generalised aerodynamic forces which determination is one of the most expensive parts of the flutter analysis [27]. They couple the degrees of freedom and depend on the reduced frequencies and the Mach number. As the resulting oscillation frequencies of the modes are usually not know before the iterative solution of the flutter equation, the aerodynamic matrices are calculated for a set of reduced frequencies between which it will be interpolated later during the solution [26].
When all matrices in the flutter equation are determined, it can be solved for its complex eigenvalue $s = \sigma + i\omega$. The real part σ represents the damping and the imaginary part ω the oscillation frequency [26]. There are as many eigenvalues as modal degrees of freedom and they are calculated step by step for each flight velocity [26]. Due to many influencing factors the solution can only be performed numerically [27]. The calculated eigenvalues can be assigned to the eigenmodes of the system and become the eigenvalues of the oscillating system without aerodynamic forces for $V_\infty = 0$ [27].
To solve the eigenvalue problem, there are many different well known methods. In the following, the methods used in this thesis are explained shortly. There is the so called p-k-method [28] and the g-method [29].

p-k-method

The p-k-method is a classical solution method to solve the flutter equation giving a good approximation for damped or fanned oscillations. For the solution the dimensionless com-

plex eigenvalue p and the corresponding reduced frequency k and reduced damping g are introduced [26]:

$$p = \frac{l_{ref}}{V_\infty} s = \frac{l_{ref}}{V_\infty} (\sigma + i\omega) \tag{2.7}$$

$$k = Im(p) = \frac{l_{ref}}{V_\infty} \omega \tag{2.8}$$

$$g = Re(p) = \frac{l_{ref}}{V_\infty} \sigma \tag{2.9}$$

The flutter equation 2.6 is transformed in a form including the dimensionless eigenvalue p and for each modal degree of freedom and each flight velocity an iterative solution for the eigenvalue is performed [26]. During the solution, the reduced frequency k determines the value of the aerodynamic matrix $\underline{Q}_{gen}$ which is inserted into the transformed flutter equation and gives a new solution for p. This is repeated iteratively until a converged solution for p is found. Then, the dimensional frequency f and damping value ξ of the examined mode at the specific velocity can be determined as:

$$f = \frac{V_\infty}{2\pi l_{ref}} k \tag{2.10}$$

$$\xi = \frac{g}{|p|} \tag{2.11}$$

Repeating this process for each mode and each velocity step gives the frequency and damping trends for all considered modes [26].

g-method

The g-method is a subsequent development of the p-k-method. The typical used aerodynamic theories determine the aerodynamic forces only for the harmonic oscillating case with zero damping. So the forces and therefore the iterative solution of the p-k-method is only known exactly on the imaginary axis ($p = i\omega$) and not accurate outside this flutter case with $g = 0$. To improve the significance of the method for damped or fanned oscillations with $g \neq 0$, the g-method uses a Taylor series to expand the aerodynamic matrix $\underline{Q}_{gen}(ik)$ into the imaginary plane. The further solution of the flutter equation is performed similar to the p-k-method and can also be performed using a state space approach. [26]
The g-method is used for most flutter analyses in the following because it gives fast and robust results and a good damping approximation.

2.3. Whirl flutter

In this section, first the physical principles of whirl flutter are explained, before different methods to represent the propeller in the flutter equation are described. One of these methods is the transfer-matrix method, which is extended and applied later in this thesis on the generic aircraft configuration. Finally, the effects of different parameters on the occurrence of whirl flutter are presented, including the state-of-the-art findings on the influence of blade elasticity on a two-degree-of-freedom model.

2.3.1. Physical principles

Whirl flutter is a flutter phenomenon which can occur on separate propellers in elastic support or on aircraft with propellers, especially with low engine mount stiffness [5]. The general mechanism of whirl flutter is based on a coupling of the pitch and yaw motion of the rotating propeller due to aerodynamic forces and gyroscopic moments [30]. This leads to a circular whirl motion of the propeller axis, which can be stable or unstable. For classical aircraft, the dynamic instability usually occurs only when a failure case reduces the stiffness of the engine mounts drastically, as it happened in two accidents of a Lockheed Electra around the year 1960, which brought the topic on display and started further research about it [30].

As, for example, in Cecrdle's book about whirl flutter [30], the physical principle of the phenomenon is explained by means of an simple pylon model as it is shown in figure 2.2. The propeller is mounted on a rigid axis attached elastically to the aircraft structure. This attachment is represented by a bearing with two rotational degrees of freedom, in pitch and the yaw direction. The rotational stiffness in these directions are labelled as K_θ and K_ψ. The propeller rotational speed is denoted as Ω. Further, it is assumed that the propeller blades are rigid.

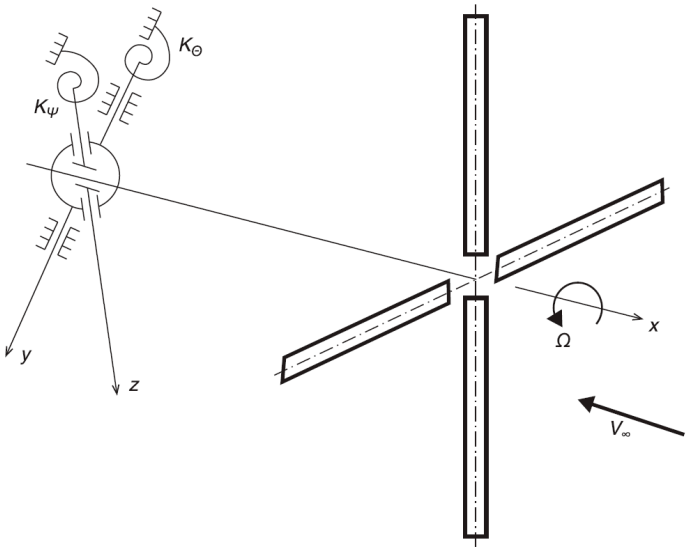

Figure 2.2.: Simple whirl system [30]

The equations of motion for the pitch and yaw motion of the system can be stated as:

$$I_y\ddot{\theta} + C_\theta\dot{\theta} + K_\theta\theta + I_x\Omega\dot{\psi} = M_y - aP_z \tag{2.12}$$

$$I_z\ddot{\psi} + C_\psi\dot{\psi} + K_\psi\psi - I_x\Omega\dot{\theta} = M_z + aP_y \tag{2.13}$$

where I indicates the moments of inertia of the system around the indicated axis, C the damping coefficients and P the aerodynamic forces and M the aerodynamic moments at the propeller [30]. In contrast to the classical flutter problem, besides the inertia, spring and damping forces also a gyroscopic term ($I_x\Omega\dot{\psi}$ respectively $I_x\Omega\dot{\theta}$) appears in both equations coupling both degrees of freedom.

To show the influence of the different occurring forces, the oscillation modes are explained step by step, as e.g. in [27] or [30]. First, the aerodynamic forces are neglected. Under this condition, for a non-rotating propeller, the motions in pitch and yaw are decoupled from each other, leading to two modes as illustrated in figure 2.3 (a). Taking the propeller rotation into account, both motions are coupled due to the gyroscopic moments. The propeller axis now moves on an elliptical path as displayed in figure 2.3 (b). There is a forward and a backward whirl mode that occur. In the forward whirl mode, the propeller axis rotates in the same direction as the propeller rotation and the eigenfrequency is higher. In the case of the backward whirl mode, the axis moves in the opposite direction than the propeller rotation and the eigenfrequency of the mode is lower.

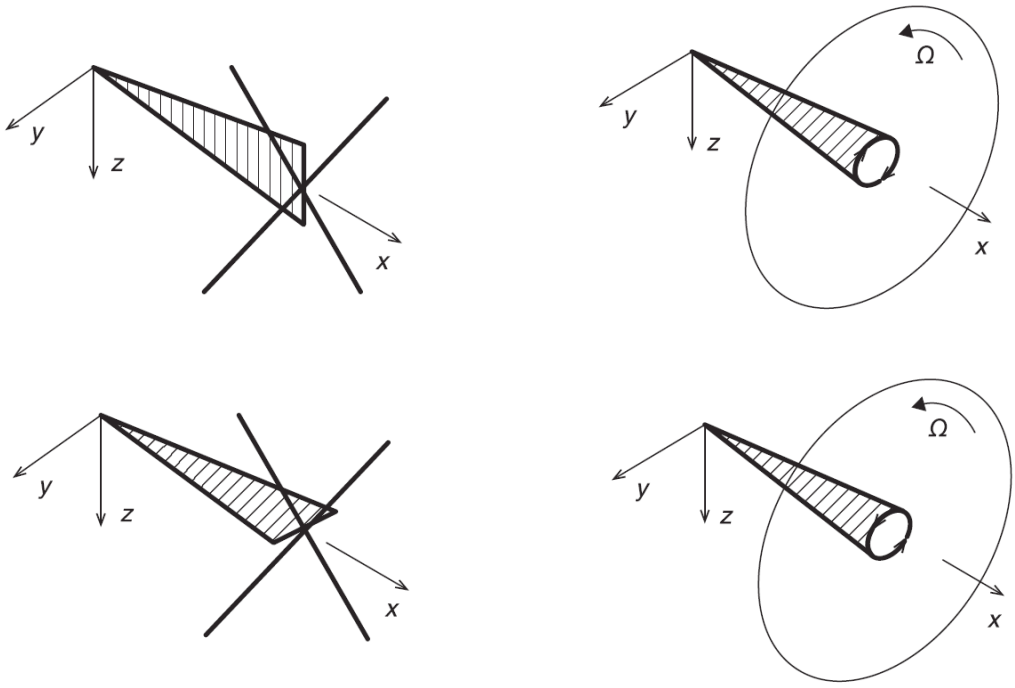

(a) Non-rotating propeller (b) Rotating propeller

Figure 2.3.: Propeller modes neglecting aerodynamic forces [30]

Considering the aerodynamics, the whirl motion of the propeller leads to harmonic changes of the blade angles of attack and therefore unsteady aerodynamic forces [30]. These forces can kindle the whirl oscillation and provoke whirl flutter. The velocity from which the system becomes unstable is called critical flutter speed V_F [27]. For $V_\infty < V_F$ the whirl motion decays after a small perturbation, whereas for higher velocities $V_\infty > V_F$ the whirl motion diverges to theoretically infinite amplitudes. Both cases are illustrated in figure 2.4. In general, for rigid blades, only the backward whirl mode becomes unstable [30]. Therefore, in the figure only this backward whirl mode is shown for a sub-critical and supercritical air stream velocity.
In the following, axial flow and a quasi-steady approach is used to explain the main effects creating the aerodynamic forces. In this case, the yaw and pitch motion is analogue because

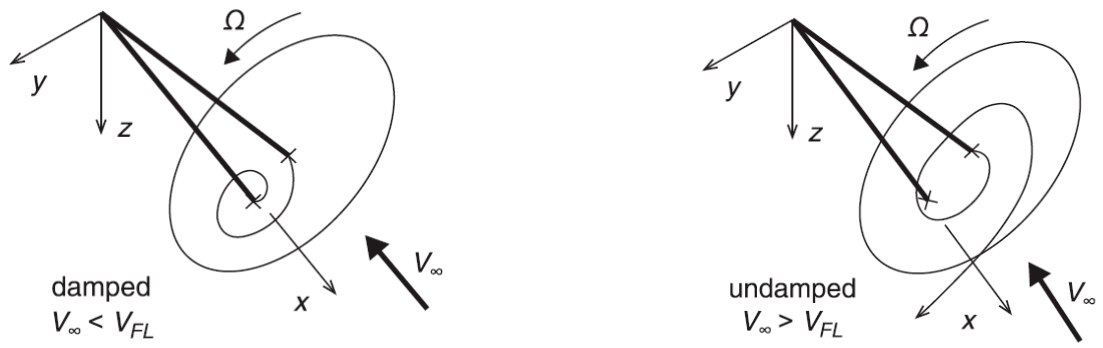

(a) Stable case (b) Unstable case

Figure 2.4.: Backward whirl mode for rotating propeller with aerodynamics, V_{FL} = critical flutter speed [30]

of the axial symmetry of the system. Therefore, only motions symmetric to the x,z-plane are analysed in the following.
Figure 2.5 shows the generated forces due to a pitch angle around θ. Due to the oblique flow on the propeller plane, a coupling moment $M_z(\theta)$ around the z-axis occurs which leads to the coupling of pitch and yaw motion. For the backward whirl mode, this moment acts in the same direction as the yawing velocity and is therefore destabilising [30]. Additionally, a vertical force $P_z(\theta)$ arises with an orientation such that it increases the angle θ further. The structure needs to counteract this effect by elastic restoring forces, otherwise the system is getting statically unstable and whirl divergence occurs [30].
Similar aerodynamic coupling moments and forces can be derived from a translation velocity $\dot{z}$ and an angular velocity $\dot{\theta}$, but these moments and forces do not increase the causal motion, so the motion is damped [30]. Therefore, the most important terms regarding to whirl flutter instability are the coupling moments between pitch and yaw frequency $M_z(\theta)$ and $M_y(\psi)$ respectively [30].

The occurrence of whirl flutter depends to a great extend on the present stiffness at the engine mounts, more precisely the stiffness values K_θ and K_ψ [27, 30]. This correlation can be well illustrated by a so called whirl flutter stability map as it is presented qualitatively in figure 2.6. It shows for which combinations of K_θ and K_ψ at a specific operation point the system becomes unstable. On the one hand, for a very low stiffness in only one degree-of-freedom the system becomes unstable due to whirl divergence. On the other hand, if both stiffness values are close to each other, the gyroscopic coupling is large and a higher stiffness is needed in general to prevent whirl flutter. These effects create the typical shape of the stability border. For different operating points and other parameter variations the range of instability can change. The change can be interpreted to show the influence of different methods or parameters on the stability results. Instead of K_θ and K_ψ also the uncoupled pitch and yaw frequencies of the system (ω_θ and ω_ψ) can be used as axis of the plot leading to similar figures with the same message.

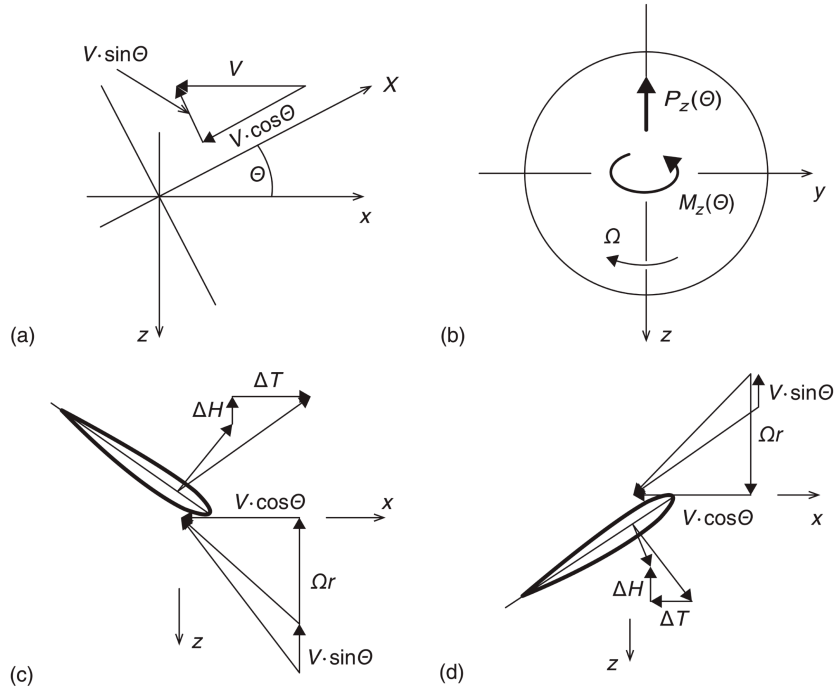

Figure 2.5.: Derivation of aerodynamic forces and moments due to a pitch deflection [30]
(a) Side view of declined propeller plane, (b) Propeller plane with occurring force and moment (looking in the x-axis direction), (c) Cross-section of down-going blade, (d) Cross-section of up-going blade

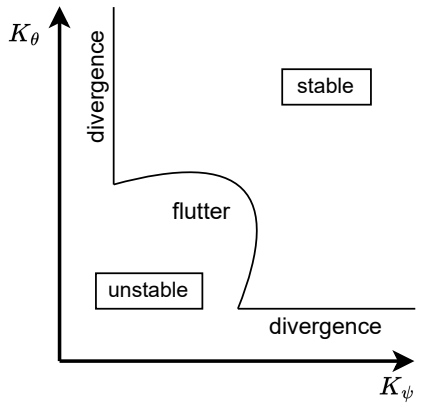

Figure 2.6.: Typical whirl flutter stability map

2.3.2. Integration of whirl flutter into the general flutter equation

As previously presented, whirl flutter is triggered by motion-induced unsteady aerodynamic forces on the propeller. Therefore, the transfer behaviour between hub displacements and hub forces is fundamental for whirl flutter analyses [7]. To perform whirl flutter analysis in the frequency domain, the propeller forces F_{prop} need to be described depending on the Laplace variable s, the hub motion X_{hub} and the operating point defined by the flight velocity V, the propeller revolution Ω and the air density ρ. For small perturbation about

a reference state, this transfer function can be linearised concerning the hub motion X_{hub} leading to a frequency-dependant matrix $\underline{H}_{prop}$ that describes the linear transfer behaviour of the propeller [7].

$$F_{prop} = \underline{H}_{prop}(s, V, \Omega, \rho)\Delta X_{hub} \tag{2.14}$$

The matrix $\underline{H}_{prop}$ depends on the Laplace variable s and the operating point. It is a 6x6 matrix due to the six degrees of freedom of the propeller. $\underline{H}_{prop}$ also contains the gyroscopic moment. Transforming the hub coordinates X_{hub} to modal coordinates q_h using the propeller mode shapes $\underline{\Phi}_{prop}$ and inserting the term into the aeroelastic equation of motion in modal coordinates leads to:

$$\underline{M}_{gen}\ddot{q}_h + \underline{K}_{gen}q_h = \left[q\underline{Q}_{gen}(s) + \underline{\Phi}^T_{prop}\underline{H}_{prop}(s, V, \Omega, \rho)\underline{\Phi}_{prop}\right] q_h \tag{2.15}$$

where $\underline{M}_{gen}$ and $\underline{K}_{gen}$ are the generalised mass and stiffness matrices of the structure and $\underline{Q}_{gen}$ the generalised aerodynamic force matrices (including unsteady aerodynamics from other aircraft components) [7]. When all matrices are known, equation 2.15 can be solved for its eigenvalues by means of the previously presented methods (see section 2.2) resulting in the frequency and damping values of the aircraft eigenmodes. The damping values can be interpreted for stability assessment of the aircraft showing also whirl flutter if it occurs. There are different methods to determine the matrix $\underline{H}_{prop}$. The first method used in this thesis is the classical Houbolt/Reed method [8] which is used in this work as reference for the second method, the transfer-matrix method [7], which is further developed in this thesis and is applied to perform the parameter studies on the generic aircraft configuration.

Houbolt/Reed method

The theory of Houbolt and Reed (further shortly called "HR-method"), as it has been applied in [31] and [7], uses stiffness and damping terms to determine the propeller forces and moments and build the linear description of F_{prop} as in equation 2.14:

$$F_{prop} = \underbrace{\left[\underline{K}_{prop}(V, \Omega) + s\underline{D}_{prop}(V, \Omega) - s\underline{G}(\Omega)\right]}_{\underline{H}_{prop}} \Delta X_{hub} \tag{2.16}$$

Forces and moments around the propeller axis are neglected in this method, causing the propeller matrices to be 4x4 matrices and the vector of perturbations ΔX_{hub} to consist only of the displacements in the propeller plane (translation in y and z direction and rotation θ and ψ around these axes). The matrix $\underline{G}$ describes the gyroscopic matrix containing $M_{gyro} = I_p\Omega$ [30]:

$$\underline{G} = \begin{bmatrix} 0 & 0 & 0 & 0 \\ 0 & 0 & 0 & 0 \\ 0 & 0 & 0 & M_{gyro} \\ 0 & 0 & -M_{gyro} & 0 \end{bmatrix} \tag{2.17}$$

The stiffness and damping matrices are described by non-dimensional derivatives as follows [7]:

$$\underline{K}_{prop} = 2\pi q R^3 \begin{bmatrix} 0 & 0 & \frac{C_{y\theta}}{2R} & \frac{C_{y\psi}}{2R} \\ 0 & 0 & \frac{C_{z\theta}}{2R} & \frac{C_{z\psi}}{2R} \\ 0 & 0 & C_{m\theta} & C_{m\psi} \\ 0 & 0 & C_{n\theta} & C_{n\psi} \end{bmatrix} \tag{2.18}$$

$$\underline{D}_{prop} = 2\pi q R^3 \begin{bmatrix} -\frac{C_{y\psi}}{2RV} & \frac{C_{y\theta}}{2RV} & \frac{C_{yq}}{2V} & \frac{C_{yr}}{2V} \\ -\frac{C_{z\psi}}{2RV} & \frac{C_{z\theta}}{2RV} & \frac{C_{zq}}{2V} & \frac{C_{zr}}{2V} \\ -\frac{C_{m\psi}}{V} & \frac{C_{m\theta}}{V} & \frac{C_{mq}R}{V} & \frac{C_{mr}R}{V} \\ -\frac{C_{n\psi}}{V} & \frac{C_{n\theta}}{V} & \frac{C_{nq}R}{V} & \frac{C_{nr}R}{V} \end{bmatrix} \tag{2.19}$$

with the flight velocity V and the propeller radius R. The first index of the derivatives specifies the resulting force or moment and the second index specifies the deflected degree of freedom that causes this component. The derivation of these derivatives is based on a linear strip theory approach, only including unsteady aerodynamic effects afterwards via a local Theodorsen function correction [8]. The coordinate system for the derivation is presented in figure 2.2 in the previous section. Further, to allow an analytical derivation, the propeller blades are assumed to be rigid and no steady state influence and no induced flow is considered [7].

Transfer-matrix method

The transfer-matrix-method (shortly "TM-method") has been developed to find a suitable method for propeller whirl flutter evaluations in the frequency domain that overcomes some of the limitations mentioned for the HR-method. Koch describes this method in his paper from the IFASD 2022 [7] in detail. In this method, the matrix $\underline{H}_{prop}$ is determined directly as a frequency-dependent transfer function between propeller hub motions and forces respectively moments without making use of damping and stiffness matrices, in the form of:

$$F_{prop} = \underbrace{\begin{bmatrix} F_{xx} & F_{xy} & F_{xz} & F_{x\phi} & F_{x\theta} & F_{x\psi} \\ F_{yx} & F_{yy} & F_{yz} & F_{y\phi} & F_{y\theta} & F_{y\psi} \\ F_{zx} & F_{zy} & F_{zz} & F_{z\phi} & F_{z\theta} & F_{z\psi} \\ M_{xx} & M_{xy} & M_{xz} & M_{x\phi} & M_{x\theta} & M_{x\psi} \\ M_{yx} & M_{yy} & M_{yz} & M_{y\phi} & M_{y\theta} & M_{y\psi} \\ M_{zx} & M_{zy} & M_{zz} & M_{z\phi} & M_{z\theta} & M_{z\psi} \end{bmatrix}}_{\underline{H}_{prop}} \Delta X_{hub} \tag{2.20}$$

where the items F_{ij} or M_{ij} in the matrix stand for a scalar depending on the frequency defining the force or moment response regarding the i-axis to a perturbation in j direction [7]. The perturbation vector ΔX_{hub} now consists of all six degrees of freedom of the propeller hub. The gyroscopic moments can be included in $\underline{H}_{prop}$ or added to the equation of motion separately as an additional gyroscopic matrix $\underline{G}$.
For the identification of these transfer functions, the simulation of a propeller model in the time domain is used and excited from its steady state for each degree of freedom. Simulation

tools for this type of time-domain perturbation are already widely spread, having a high fidelity which is carried forward directly into the fidelity of the transfer-matrices [7]. The perturbation response is then transformed in the frequency domain and provides the transfer functions for the different degrees of freedom and frequencies depending on the perturbation. As perturbation, a harmonic or pulse excitation can be used. While harmonic excitation can be used also for time-variant conditions (such as non-axial flow), for time-invariant and linear systems with pulse excitation a broad spectrum of frequencies can be excited in only one time simulation, reducing the computational costs [7].
Each degree of freedom of the propeller hub has to be excited separately to generate the full transfer-matrix [7]. But in some cases, practical simplification can be made. For axial symmetric systems (as e.g. a simple propeller in axial flow) the components identified from excitation around the y-axis can be mirrored to those about the z-axis, and for systems not including or neglecting any motion of the propeller hub in axial direction, these degrees of freedom do not need to be perturbed [7]. Both reduces the computational effort of the transfer-matrix generation significantly.
The derived set of transfer-matrices is coupled with a suitable node of the structural model representing the propeller hub node. Because this step is performed after the matrix generation, the structural model is independent from the propeller modelling [7]. Therefore, the used structural models can be exchanged easily, making the method favourable for parameter studies. As the transfer-matrices are already present in frequency domain, they can be easily combined with the typical flutter equation 2.15 [7].

Comparison of the methods

On the IFASD 2022 [7], Koch has presented the TM-method and compared it to the classical HR-method and a time-domain reference, for the case of a simple two-degree-of-freedom system. Figure 2.7 presents the achieved results in form of a whirl flutter stability map for one operating point. It can be seen that the stability border from the TM-method fits almost perfectly with the time-domain results. In contrast to the other two methods, the HR-method shows a slightly larger instability area regarding whirl flutter. So, it gives a bit more conservative results. The whirl divergence borders are for all methods quite close to each other. The differences between the HR-method and the TM-method or time-domain reference can be explained by the assumptions made in the HR-method as already mentioned previously [7]. As a conclusion, the TM-method allows a more accurate propeller modelling than the classical HR-method [7].

Consideration of the slip stream effect

Rodden and Rose have written a paper about the developement and application of a pre-processor to include propeller/nacelle aerodynamics and gyroscopic effects in MSC Nastran flutter analysis [10]. In this paper, they also described a possibility to consider aerodynamic interference effects between propeller and wing within the flutter calculations. One part of that is the incorporation of the propeller slipstream effect on the wing air stream by introducing a correction factor w_{kk} which multiplies the aerodynamic forces in the area of

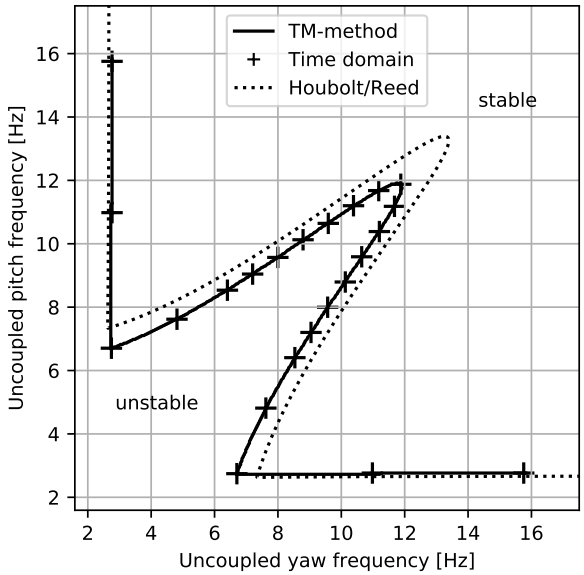

Figure 2.7.: Whirl flutter stability map created using different methods [7]

the propeller wake. This accounts for the higher flow velocity in the propeller wake. w_{kk} has been derived from a simple momentum theory, leading to following definition:

$$w_{kk} = 1 + \frac{D}{\Delta y} \cdot \sqrt{1 + \frac{1}{\sqrt{1 + 2T/(\rho V^2 S)}}} \cdot \frac{\sqrt{2}T}{\rho V^2 S} \tag{2.21}$$

with the propeller diameter D, the propeller area $S = \pi \cdot (D/2)^2$, the air stream velocity V and density ρ, the propeller thrust T and the width Δy which specifies the width of the area where the factor is applied. Only the axial velocity components in the propeller wake are represented by this factor, no tangential components.
The same paper presents a procedure to include the influence of wing downwash on the propeller coefficients. But, this method is not applied in the thesis because it is not compatible with the used tools for the flutter analysis. Therefore, it is not explained further at this point.

2.3.3. Influence parameters

Several parameters have been shown to have a relevant influence on whirl flutter stability. Most investigations have been made with the assumption of rigid propeller blades. In his book about whirl flutter [30], Cecrdle presented several influence parameters for this condition. The most important ones are the effective stiffness of the propeller mount K_θ and K_ψ and their ratio K_θ/K_ψ as it has already been mentioned in section 2.3.1 when explaining the classical whirl flutter stability map. Further important factors are the structural damping γ_θ and γ_ψ of the modes, the propeller revolution Ω and the propeller advance ration $J_0 = V_\infty/(\Omega R)$.
Figure 2.8 (a) illustrates the influence of structural damping γ and aerodynamic damping which comes from the distance between propeller hub and pivot point increasing the

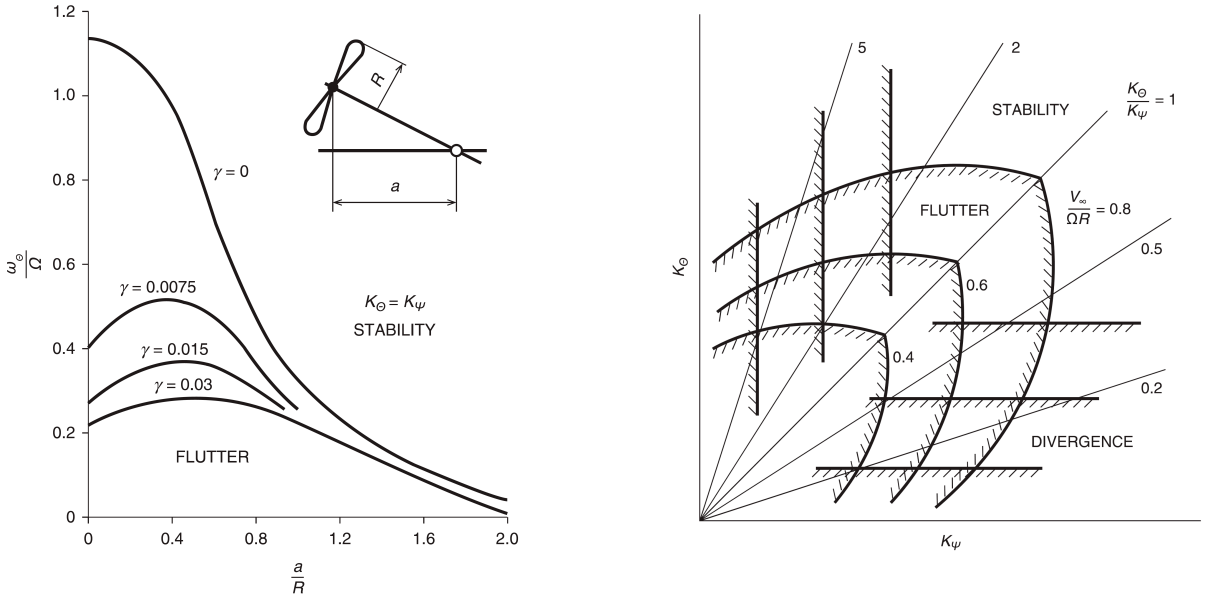

(a) Influence of damping (b) Influence of advance ratio

Figure 2.8.: Influence of different parameters on the whirl flutter stability [30]

damping force $P_z(\dot{z})$ in z-direction induced by a velocity in z-direction. Both damping effects decrease the critical eigenfrequency of the engine mounts which is determined by the stiffness values K_θ and K_ψ, so they have a stabilising effect [30]. Though, the sensitivity regarding structural damping decreases for higher aerodynamic damping in the system [30]. Figure 2.8 (b) shows the influence of the propeller advance ratio on the necessary stiffnesses K_θ and K_ψ which increase when increasing the advance ratio [30]. Further, the importance of the ratio K_θ / K_ψ can once again be detected.

Influence of blade elasticity and thrust on propeller with elastic propeller blades

As already mentioned in section 2.3.2, the classical method using aerodynamic derivatives based on Houbolt and Reed neglects blade flexibility in the flutter analyses. As the dynamic response of the propeller blades affects the overall transfer function of the propeller, the inclusion of blade elasticity has an effect on the whirl flutter prediction [6]. More complex methods applied on tiltrotor aircraft have already shown a stabilising effect of blade elasticity compared to analyses with the assumption of rigid blades (see section 1.2). For normal aircraft propeller the TM-method has been developed to incorporate such effects [7]. Koch and Koert have already applied this method examining an isolated turboprop propeller [6, 32]. Their results are the basis of the examinations on the generic full aircraft configuration in this thesis. Therefore, their result are presented briefly in the following.

Variations of the blade stiffness of the examined model have shown that the necessary pitch and yaw stiffness to prevent the propeller from whirl flutter instability is reduced significantly by considering the blades as elastic, with a constant trend to lower stiffness requirements for lower blade stiffness [6]. This is displayed in the whirl stability map in

figure 2.9 (a). The blades in this case varied between a first eigenfrequency of $1.3P$ ($33.4\ Hz$) and $2.3P$ ($60.8\ Hz$), with $1.5P$ ($40.7\ Hz$) in the nominal case, also compared to a propeller with rigid blades. Even though the influence of blade elasticity on whirl flutter stability has been significant, even for relatively stiff blades, the influence on static divergence has been found quite small which may, however, vary for different structural configurations [6].

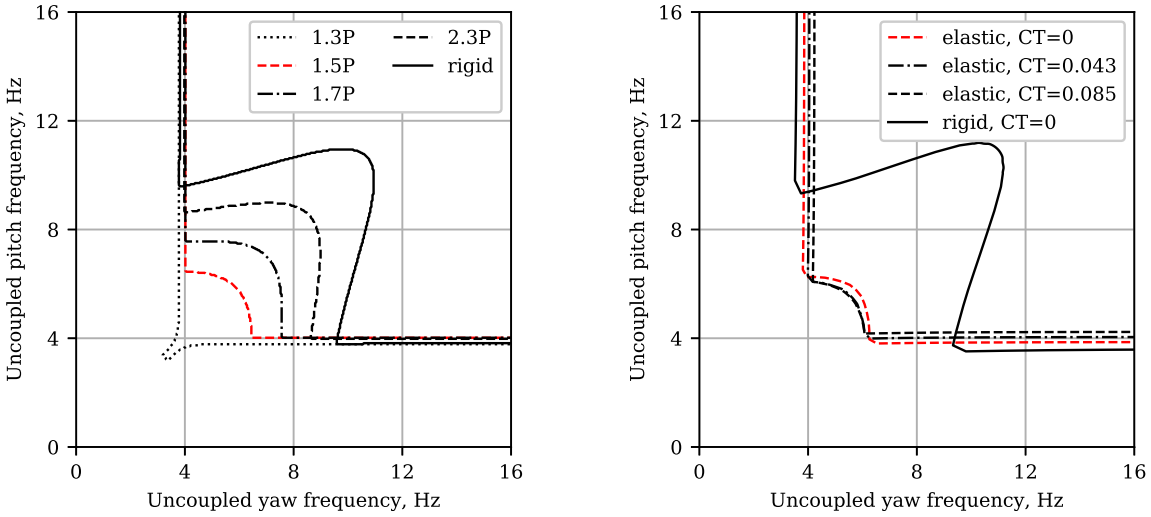

(a) Influence of elasticity

(b) Influence of thrust

Figure 2.9.: Whirl flutter stability map for elastic propeller blades [6]

The reason for this stabilisation has been examined by analysing the propeller hub transfer functions. The coupling moment between pitch and yaw motion, which is the main reason for the whirl flutter instability, is reduced in the transfer-matrices in the elastic cases. This happens due to periodic deformations of the propeller blades which occur because the angle of attack varies over one revolution for a propeller that is deflected around the pitch or yaw axis. This leads on the one hand to a shift of the maximum load in azimuthal direction (closer to the axis of the coupling moment) and on the other hand to an offset of the centrifugal loads which creates a moment in opposite direction of the coupling moment. Both effects lead to a reduced coupling moment about the axis around which the propeller is not perturbed. [6]

Further on, the influence of thrust has been examined briefly for the elastic propeller. The results can be found in figure 2.9 (b) where CT labels the dimensionless thrust coefficient of the propeller. The thrust coefficient has been increased by increasing the collective blade pitch angle of the propeller. For higher thrust coefficients, the whirl flutter instability range decreases slightly, so it seems to have an stabilising effect. However, observing the whirl divergence boundary, it can be noticed that here the thrust has an slightly destabilising effect. Even though, the influence is small. [6]

3. Preliminary studies with the 2DOF model

In this chapter, a similar 2DOF model as used in [6] is presented, as well as the propeller model used in this work for transfer-matrix generation. Details on the models are described in the first section of this chapter. After that, the second section provides a short description about the performed transfer-matrix generation procedure. Finally, the chapter concludes with results from parameter studies conducted with the 2DOF model to deepen the understanding of the results shown in [6].

3.1. 2DOF model

In this section, the simple 2DOF model of a single, isolated propeller-pylon system is presented. The model has been used in this work to test the implemented improvements to the TM-method and study a few additional aspects, before starting with the analysis on the generic aircraft configuration. The system is presented in figure 3.1. It consists of a single propeller with 5 blades and a stiff propeller axis that is mounted elastically on a pivot point. The unrestricted degrees of freedom of the model are, besides the propeller rotation around the x-axis, only pitch (θ) and yaw motion (ψ). The x-axis of the coordinate system points towards flight direction and against the vector of propeller rotation. y- and z-axis are spanning the propeller plane. The dive speed of the system is defined as $V_D = 142\ m/s$. Table 3.1 summarises relevant properties of the 2DOF model. The total rotational inertia of the propeller around the x-axis I_P includes the inertia from the propeller blades, the hub and additional engine parts that should be considered in the calculation. The inertia of the system around the y- and z-axis is $I_{\theta,\psi} = 34.82\ kg \cdot m^2$. The non-rotating eigenfrequencies in pitch and yaw arise as the result from

$$\omega_{\theta,\psi} = \sqrt{k_{\theta,\psi} / I_{\theta,\psi}} \tag{3.1}$$

with the defined spring stiffness values and the inertia of the system around y- and z-axis. The structure is modelled in MSC Nastran [33]. The model consists of nodes representing the pivot point and the propeller hub and RBE2 elements connecting the nodes to model

propeller axis length	a	$0.85\ m$
rotational pitch spring stiffness	K_θ	$1.37 \cdot 10^5\ Nm$
rotational yaw spring stiffness	K_ψ	$1.66 \cdot 10^5\ Nm$
total rotational inertia around the x-axis	I_p	$6.69\ kgm^2$
inertia of the system around the y- and z-axis	$I_{\theta,\psi}$	$34.82\ kgm^2$
non-rotation eigenfrequency in pitch	ω_θ	$62.73\ rad/s \approx 10\ Hz$
non-rotation eigenfrequency in yaw	ω_ψ	$69.05\ rad/s \approx 11\ Hz$

Table 3.1.: Properties of the 2DOF model

the rigid propeller axis and the bearing of the pivot point. A mass element (CONM2) includes the propeller mass at the hub node. For the HR-method calculations, the damping and stiffness matrices of the propeller are calculated based on the classical derivation as explained in 2.3.2. For the analyses with the TM-method, a multibody simulation model of the propeller using the software Simpack [34] is used to generate transfer-matrices. This model is presented in the next section. For flutter analyses, both kinds of matrices are coupled with the structural model at the hub node.

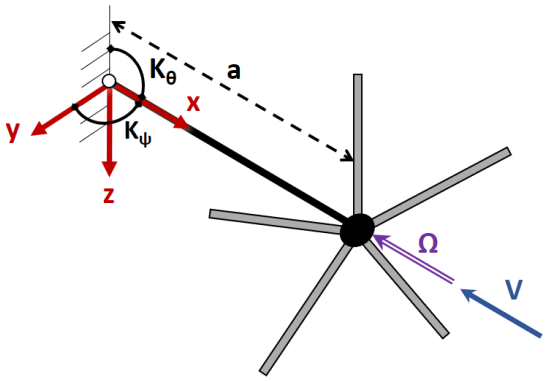

Figure 3.1.: 2DOF model

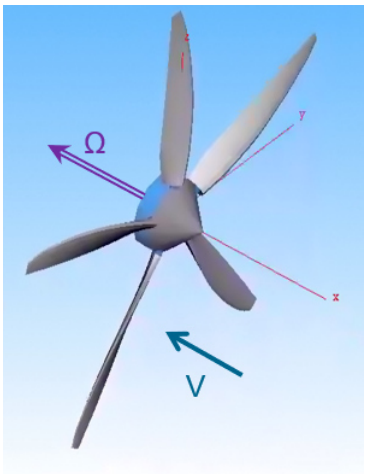

Figure 3.2.: Propeller model in Simpack

3.1.1. Propeller model

The propeller model used in this thesis has been created by Koert during his master thesis [32]. The propeller can be operated at constant rotational speed. That means the blade pitch angles can be adjusted during flight to trim the propeller to a specific thrust condition without changing the propeller rotational speed dependent on the flight velocity. The nominal rotational speed Ω is set to 168.3 rad/s. Figure 3.2 shows the Simpack model of the propeller which already existed before the work on this thesis. The model includes the five propeller blades and the hub, but no further pylon structure. The global properties of the propeller are summarised in table 3.2.

blade number	N_B	5
rotor diameter	D	2.5 m
blade mass	m_B	1.542 kg
total mass	m_{prop}	7.71 kg
blade inertia (x-axis)	$I_{p,blades}$	3.597 kgm^2
blade inertia (y- and z-axis)	$I_{\theta,blades} = I_{\psi,blades}$	1.806 kgm^2
nominal rotational speed	Ω	168.3 rad/s

Table 3.2.: Technical details of propeller

The propeller blades are modelled as linear beam finite element models consisting of 26 nodes and 25 beam elements. The beam model used is a Timoshenko beam. The model is parameterised, so the blade properties can be adjusted, e.g. to scale the stiffness, which is explained in more detail in section 3.1.2. Also, the number of considered blade modes can be defined. That makes it possible to model the propeller blades as rigid or elastic by defining either zero elastic blade modes to consider or more. In the following, for the elastic case three blade modes are included, following [32].
The rotational inertia of the blades around the propeller axis add up to $I_{p,blades} = 3.597\ kgm^2$. A complete rotational inertia for the system can be defined in the model to include also additional inertia, representing engine parts which are not modelled in detail. As mentioned before, the system should have a total I_p of $6.69\ kgm^2$. Therefore, besides the blade inertia, an additional rotational inertia of $I_{p,add} = 3.093\ kgm^2$ needs to be included in the calculations to represent additional rotating engine parts and their gyroscopic influence. $I_{p,add}$ can be included in the calculations either by setting the rotational inertia of the Simpack model at $I_p = 6.69\ kgm^2$ or by including an additional gyroscopic matrix during the flutter solution. The second option is chosen in most cases to reduce the parameters affecting the TM generation. Then, the total rotational inertia of the propeller in Simpack is reduced to $I_{p,blades} = 3.597\ kgm^2$.

The propeller aerodynamics are based on an unsteady strip theory approach, which is implemented in the Simpack model by means of 12 force elements per blade, each arranged along blade segments in radial direction of the blades. The force elements define the profile aerodynamics for each segment with a linear lift slope of $C_{L,\alpha} = 2\pi$, a maximal lift coefficient of $C_{L,max} = 1.5$ and a minimal drag coefficient of $C_{D,min} = 0.15$. The aerodynamic moment is neglected. The flow velocity at each force element is composed of the flight velocity, the propeller rotation and possible blade motion. Other induced velocities are neglected, as well as influences between the single propeller blade elements. Therefore, especially for high thrust conditions, the aerodynamics are not modelled precisely [6].
In the aerodynamic modelling of the propeller, the propeller blades are assumed to have an infinite length. The implementation of the HR-method contains a correction factor representing the fact that the blades have a finite radius and therefore a loss of lift at the tips [30, Eq. 5.51]. The Simpack model does not take this into account. For a better comparison, the aspect ratio parameter used to determine the correction factor is set to a very high value to practically disable this correction in the HR-method.

3.1.2. Variation of blade stiffness and mass

In the Simpack model, the propeller blades can be modelled as elastic or rigid bodies by including the elastic states of the propeller blades into the model or not. Furthermore, the number of considered blade mode shapes is set to zero for rigid blades and to 3 for elastic blades. In the later studies, not only the difference between rigid and elastic blades should be evaluated, but also the elasticity is increased gradually to see the tendency of the effect. For that, a factor to scale the blade stiffness that is already implemented in the used propeller model in Simpack can be used. This factor effects all blade stiffness values and is labelled as k_{scale}. $k_{scale} = 1$ corresponds to the nominal blade stiffness. Higher values

increase the stiffness and lower values decrease it. The alteration of the stiffness affects the non-rotating blade eigenfrequency ($\omega_0 = \sqrt{K/M}$) with a factor of $\sqrt{k_{scale}}$.
This eigenfrequency can also be altered by changing the blade mass. For this variation, a scaling factor m_{scale} has been introduced in the Simpack model similar to the already existing factor k_{scale}. It has to be remarked, that in this case, the total polar inertia of the propeller model in Simpack is defined such that it remains constant even for changing blade masses. So, the propeller model still contributes an inertia of $3.597\ kgm^2$ to the total system and the overall inertia in the flutter analyses (together with the $I_{p,add}$) stays $6.69\ kgm^2$. The effect of both scaling factors on the eigenfrequency can be shown as follows:

$$\omega_0 = \sqrt{\frac{K}{M}} = \sqrt{\frac{k_{nominal} \cdot k_{scale}}{m_{nominal} \cdot m_{scale}}} \tag{3.2}$$

As visual in the equation, changing k_{scale} has the same effect on the eigenfrequency as setting m_{scale} to a value of $1/k_{scale}$. Also, changing both factors by the same amount leads to no change in eigenfrequency.
Later, the effect of both scaling factors on the stability of the system is studied. The aim of these examinations are to further underline the origin of the stabilising effect of the blade elasticity as it has been stated in Koch and Koert's examinations [6].

3.1.3. Trim for constant propeller speed

During flight with different air speeds, there are different ways to adjust the propeller to the operating conditions. On the one hand, if the blade pitch angle is kept constant, the rotational speed of the propeller has to be scaled with the air speed to keep a constant thrust value. However, the usual operating mode for large aircraft is to use constant speed propellers where the propeller rotational speed stays always the same, but the propeller blade pitch angle changes to retain a specific thrust condition [35]. So, the engine can run always in its optimal operating range. The process of adapting the blade pitch angle is called trim. There are different possible target conditions for trim, such as a constant thrust coefficient or propeller power. In the following, three trim conditions should be presented that are all used in this thesis:

- windmilling, torque = 0
- maximal power $P = P_{max} = 500\ kW$
- constant thrust to dynamic pressure ratio T/q

The first trim condition, the windmilling condition, is used as the standard no-thrust case. The second condition with constant power is used later on to examine the influence of thrust on the flutter results. The thrust is not constant over the flight speed, but the propeller operates always in maximum power conditions, being $P_{max} = 500\ kW$ for this propeller. The third condition leads also to a propeller producing thrust, but it is scaled with the air speed and is later used to include a slipstream correction factor in the calculations. In addition to that, this trim corresponds to operating with constant drag coefficient, when the drag W is assumed to be equivalent to the thrust T, as the drag coefficient is defined

as $c_w = W/(q \cdot S)$. The constant value for the thrust to dynamic pressure ratio T/q is selected from the operating condition of the second trim case at flight velocity $V = V_D$ leading to a value of $T/q = 0.2851\ m^2$.
The trim is performed by iteratively adjusting the collective blade pitch angle to reach the defined trim target. Figure 3.3 displays the resulting blade pitch angles and also the resulting power, thrust and T/q values for each trim case and each flight velocity. The diagrams show the results for rigid and elastic propeller blades which, however, barely differ.

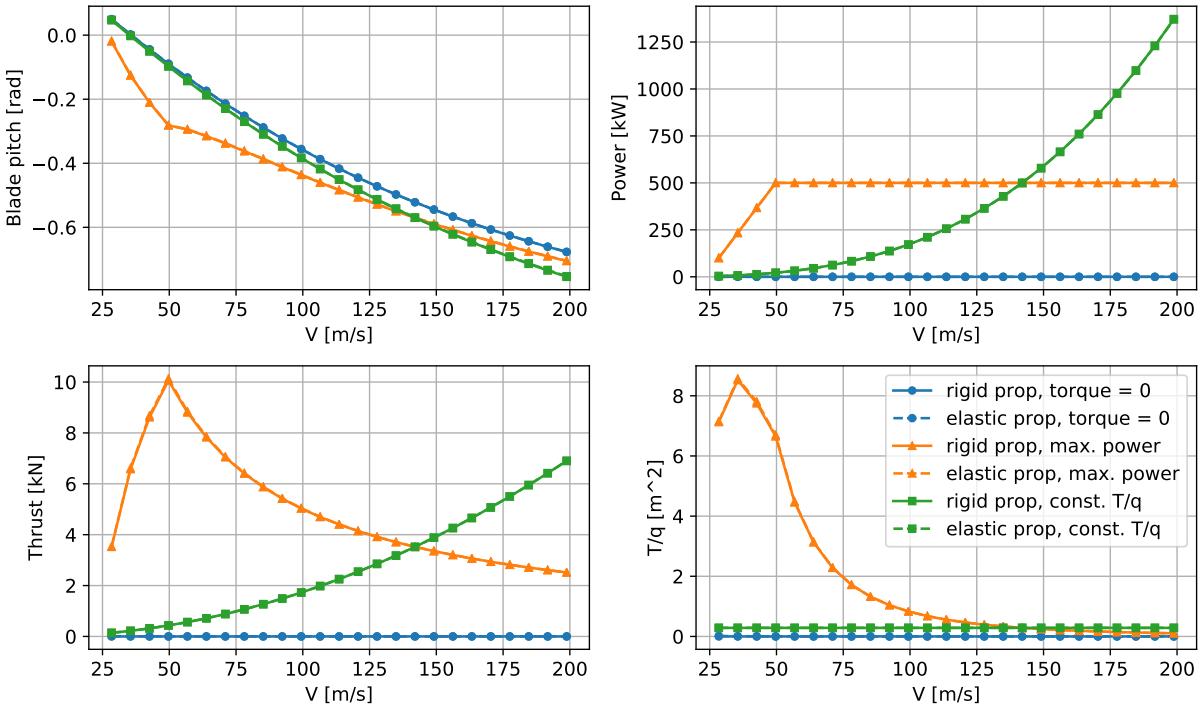

Figure 3.3.: Propeller trim

For low air speeds, the blade pitch angles need to be higher to reach the given target thrust values, as it can be seen in the top left plot. The occurring blade angle of attack of the trim conditions with thrust result from the difference between the trimmed pitch angle and the blade pitch angle for windmilling trim. In the simple linear aerodynamic model used for the blades, the physical behaviour in the range of high blade angles of attack leading to lift coefficients close to the maximum lift coefficient $c_{L,max}$ is not modelled correctly. Therefore, these angles of attack should be avoided for all blade sections. For constant propeller speed, this has been difficult to achieve for air speeds below $V = 0.2V_D$, especially for the higher thrust conditions. Therefore, for air speeds below $0.2V_D = 28.4\ m/s$ no trim values are calculated and no transfer-matrices are identified. Instead for later evaluations, for lower air speeds, the transfer-matrices for the state at $0.2V_D$ is used, but scaled down quadratically with the air speed.
The same problem occurs for the second trim condition (max. power) for air speeds below $0,35V_D$. In this case, the transfer-matrices are generated, but the target power is reduced linearly between $V = 0.2V_D$ and $V = 0.35V_D$, so the maximum blade angles is not exceeded.

This can be seen in the top right plot of figure 3.3. At $V = 0.2V_D$ the power is reduced to $P = 0.2P_{max} = 100\ kW$. At $V = 0.35V_D$ the power is back to its full value and stays constant afterwards.
In figure 3.3, the different curves of the two trim conditions with thrust (max. power and const. T/q) intersect all at $V = V_D$ because this operating point has been selected as reference point for the definition of the constant thrust to dynamic pressure ratio.

3.2. Transfer-matrix generation

The previously presented Simpack model has been used to generate transfer-matrices following a workflow that has already been explained in section 2.3.2. After trimming the model for its steady state in the different operating points, pulse excitation is used as perturbation. The velocity range spans from $0.2V_D$ up to $1.4V_D$ with intermediate steps of $0.05V_D$.
Depending on its properties, the perturbation pulse covers a specific frequency range. First, transfer-matrices up to a frequency of 250 Hz have been generated. In figure 3.4, it can be easily seen that the transfer-matrices in this range appear very nonlinear with respect to frequency due to elastic blade poles. The figure shows the transfer functions of the resulting matrices for force and moment response according to the y- and z-axis due to pitch perturbation with different maximum frequencies ω_{max}.

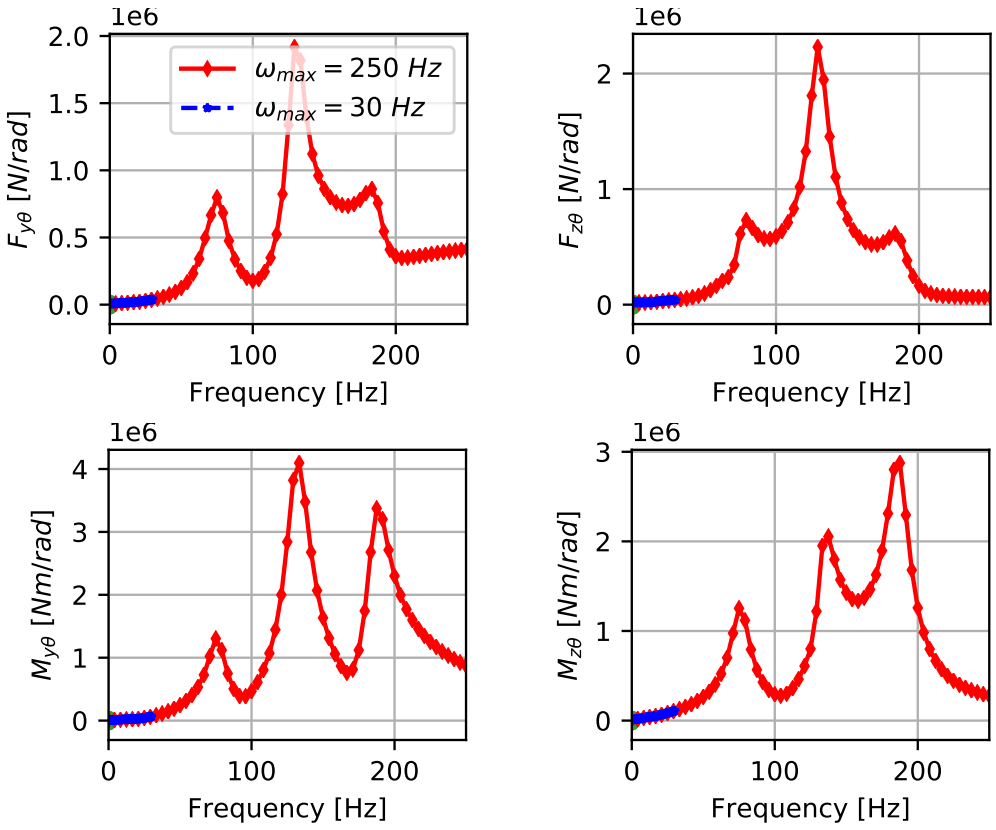

Figure 3.4.: Transfer-matrix entries for response due to pitch perturbation (absolute values, elastic blades, $V = V_D$)

The relevant frequency spectrum for whirl flutter is much lower than 250 Hz. Examinations on the 2DOF model has been shown that using only transfer-matrices up to a frequency of 30 Hz (or even 20 Hz) leads to the same flutter results. Therefore, it seems sufficient to only generate and use transfer-matrices up to a frequency of 30 Hz. As shown in figure 3.4, in this range no poles appear yet. This simplifies further plans on including interpolating routines. Further, it has been detected that reducing the maximum frequency of the pulse reduces numerical noise in some entries of the transfer-matrices.
Table 3.3 summarises the properties of the used pulse excitation and figure 3.5 shows an exemplary pulse response time series for the hub loads according to the y- and z-axis due to pitch perturbation at velocity V_D. From these pulse responses, the transfer functions in frequency domain are derived (as seen in figure 3.4) composing the transfer-matrices.

ω_{max}	30 Hz
amplitude	0.0005 m or 0.0005 rad
time steps per pulse width	402
length of time response	50 pulse widths

Table 3.3.: Parameters for pulse excitation

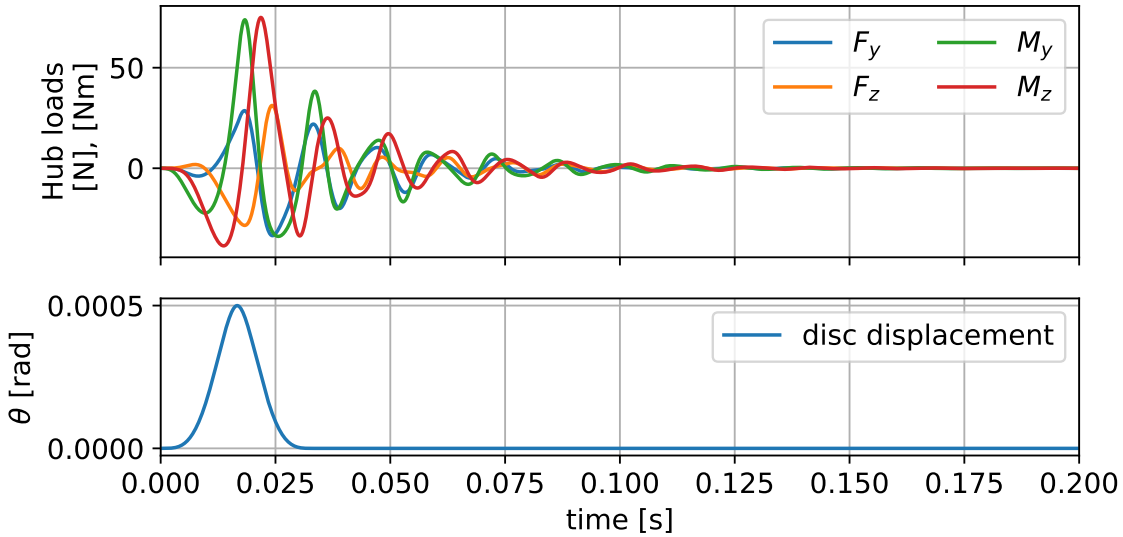

Figure 3.5.: Extraction of pulse response for pitch excitation according to table 3.3 for elastic propeller model at $V = V_D$

3.3. Stability analyses with the 2DOF model

Several stability analyses with a 2DOF model have been conducted by Koch and Koert [6] as already presented shortly in section 2.3.3. Even though, their used model is similar to the 2DOF model previously presented, a few parameter studies are performed in the following to underline the past lessons learned and gain additional understanding of the obtained results.
The flutter analyses are performed with a frequency-domain flutter solver similar as in the paper [6] for airspeeds up to $1.4V_D$ under sea level conditions ($\rho = 1.255\ kg/m^3$). As propeller trim the windmilling condition with constant propeller speed at $\Omega = 168.3\ rad/s$ is used.

3.3.1. Comparison HR vs. TM-method

First, the stability of the 2DOF model in the windmilling trim condition is examined. For that, in this section, the results for flutter analysis with the HR-method and the TM-method for rigid and elastic propeller modelling is presented. Following the results from [6], it is to be expected that the unstable mode is stabilised by integrating the more accurate propeller model via the TM-method. That should be the case already for the rigid propeller modelling, but especially for the elastic propeller modelling.
Figure 3.6 shows the resulting frequency f and structural damping values g over the velocity range from $0.2V_D$ to $1.4V_D$ for the three cases. Two modes can be identified: Mode 1 representing the backward whirl mode and mode 2 representing the forward whirl mode.
The frequencies of the modes are displayed in the upper subplot. It can be observed that both modes are shifted slightly. While for mode 1 the difference can be found mostly in the higher velocity range, mode 2 is affected over the whole displayed velocity range. Especially, the elastic propeller modelling leads to higher differences. This is due to the altering of aerodynamic stiffness terms, which are already present at low speeds due to the constant speed trim.
The structural damping g is displayed in the lower subplot and is the most relevant to assess flutter stability. When the value g becomes positive, it indicates negative damping of the mode leading to instability. For the HR-method and the TM-method with rigid propeller blades, the damping of the backward whirl mode crosses the zero-damping line and becomes unstable. To take a closer look on the flutter velocity, a close-up view on the zero-crossing is displayed. It can be seen that the flutter velocity of the TM-method result is slightly higher than that from the classical HR calculations ($146.79\ m/s$ compared to $138.22\ m/s$). This implies an increase of about 6.2 %. Looking at the damping of mode 1 for the TM-method results with elastic propeller modelling (dotted line), it can be noticed that the damping is greatly increased leading to a stabilisation of this mode.
The forward whirl mode (mode 2) stays stable for all cases. However, it can be noticed that its damping increases for the TM-method with rigid propellers compared to the HR-method results. In contrast to that, the elastic blade modelling leads to a lower damping. But, this effect is not critical for stability of the whole system.
To summarise, the stability of the system increases due to the more accurate propeller modelling in the TM-method calculations. This confirms the findings gained from [6].

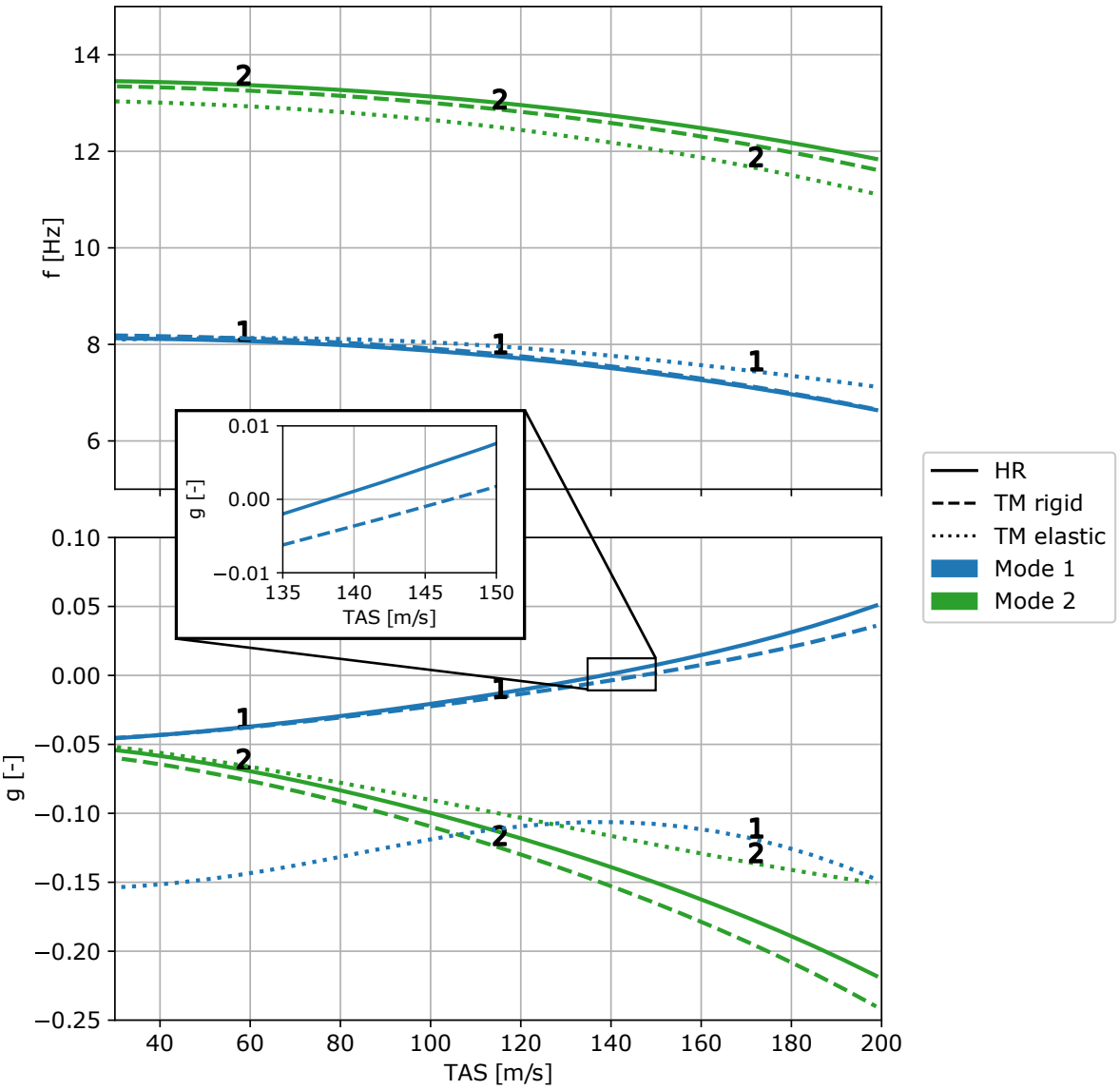

Figure 3.6.: Frequency and reduced damping trends for the 2DOF model with HR-method and TM-method with rigid and elastic propeller, windmilling condition

3.3.2. Blade eigenfrequency variation

In the previous section, a stabilisation due to blade elasticity has been identified for the 2DOF model. For the elasticity of propeller blades, often the non-rotating eigenfrequency of the blades is used as a comparison value. However, this eigenfrequency is not only affected by the blade stiffness but also the blade mass as seen in equation 3.2. Koch and Koert explained the stabilising effect by means of deformations of the propeller blades (c.f. section 2.3.3 and [6]). The deformability of the blades is determined by its stiffness. The stiffness should therefore be the main driver for the stabilisation or destabilisation of the whirl flutter, while the mass should have a minor effect. In the following, the influence of scaling stiffness and mass of the propeller blades on the whirl flutter stability is examined.

The scaling has been performed on the elastic propeller model by changing the in section 3.1.2 described parameters k_{scale} and m_{scale} and keeping the total polar inertia of the system constant. To assess the stability of the different cases, whirl flutter stability maps, as shown in figure 2.6, have been created. The cases are compared at velocity V_D and nominal propeller rotational speed. Two comparisons are presented in figure 3.7.

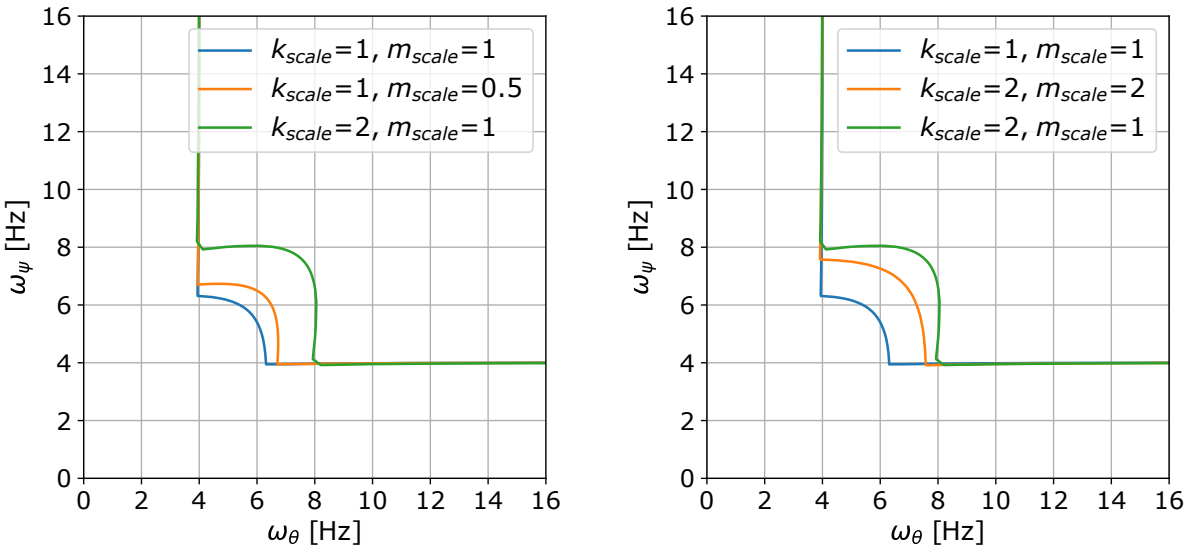

(a) (b)

Figure 3.7.: Influence of stiffness and mass scaling on the whirl flutter stability map, displayed for 2DOF model with elastic propeller blades at $V = 142\ m/s$

First, the blade eigenfrequency is increased compared to the nominal case in two ways, on the one hand, by increasing the stiffness by $k_{scale} = 2$ and, on the other hand, by decreasing the mass by $m_{scale} = 0.5$. Both scales lead to the same alteration of eigenfrequency compared to the nominal case ($\sqrt{K/0.5M} = \sqrt{2K/M} = \sqrt{2}\ \omega_0$).
In figure 3.7 (a) the results for the two scaled cases and the nominal case is shown. The blue line is the reference case for nominal blade stiffness and mass ($k_{scale} = 1$ and $m_{scale} = 1$). For the orange line, the mass is scaled down with $m_{scale} = 0.5$ and for the green line the stiffness is increase by the factor $k_{scale} = 2$. The stiffer blades ($k_{scale} = 2$) are less flexible than the blades from the nominal case. So, a destabilisation of the system is expected. This can be observed in the plot as the instability range increases from blue to green. For the lighter blades ($m_{scale} = 0.5$), whose stiffness has not been changed, it is expected that the instability area is smaller than for the $k_{scale} = 2$ case. This can be seen in the plot. However, it can also be noticed that the instability range is a bit larger than for the nominal case. But, the effect of increasing the stiffness is larger than the effect of reducing the mass, even tough the blade eigenfrequency is the same for both cases.
The second comparison is presented in figure 3.7 (b). Here, again the nominal case and the case with $k_{scale} = 2$ and $m_{scale} = 1$ is plotted. Additionally, a case were mass and stiffness are scaled both by the same factor can be seen. This scale leads to no change in eigenfrequency compared to the nominal case ($\sqrt{2K/0.5M} = \sqrt{K/M} = \omega_0$). However, it

can be observed that the instability area is larger than for the nominal case. But, it remains a bit more stable than the case were only the stiffness is scaled ($k_{scale} = 2$ and $m_{scale} = 1$). From both comparison, it can be concluded that not the blade eigenfrequency itself is crucial for the stability of the system. The effect of stabilisation or destabilisation depends highly on the blade stiffness. That underlines the importance of the blade deformation for stabilisation. But, also the mass or the eigenfrequency seems to have an effect. For the same stiffness, a higher mass seems to be stabilising, which implies that also dynamic effects affect the whirl flutter stability. However, the blade stiffness is still the dominating parameter. Therefore, in the further examinations with scaled elasticity only the factor k_{scale} is used.

3.3.3. Influence of low blade stiffness on the stability of the 2DOF model

Previously, it has been shown that the propeller with flexible blade is more stable than the rigid one. Furthermore, it has been detected that the scaling of the blade stiffness has a decisive effect on the stability. In this section, the blade stiffness is varied, as explained in section 3.1.2, to examine trends in the influence on the stability. Figure 3.8 shows the damping and frequency of the two present modes over the flight velocity for flutter analysis with the TM-method. Besides the results from the rigid propeller model, five different cases for the elastic propeller model are shown which differ in the applied scaling factor k_{scale} on the blade stiffness. $k_{scale} = 1$ refers to the nominal case, while higher values ($k_{scale} > 1$) imply stiffer blades and lower values ($k_{scale} < 1$) more flexible blades.
The left subplot (Fig. 3.8 (a)) shows mode 1 (the backward whirl mode). Comparing in the upper subplot the frequency of the rigid propeller results with the $k_{scale} = 10$ and $k_{scale} = 2$ case, it can be seen that it barley changes. For $k_{scale} = 1$ the frequency is increased slightly for higher velocities. For more flexible blades ($k_{scale} = 0.5$ and $k_{scale} = 0.25$) the frequency is larger even for lower velocities, but runs in a similar range. In damping in the lower subplot, a slight difference is visible already between the rigid propeller case and $k_{scale} = 10$. The flutter velocity is shifted to $167.66\ m/s$ for the $k_{scale} = 10$ case. Increasing the flexibility up to the nominal case, further stabilises the mode. For $k_{scale} = 2$ and $k_{scale} = 1$ no instability of the system can be detected in the examined velocity range. But, lowering k_{scale} beyond the nominal case leads again to a decrease in the damping. For lower velocities, the damping of the $k_{scale} = 0.5$ case is higher than for the other cases, but then decreases rapidly to even lower damping values than for the $k_{scale} = 2$ case. As a result, even the instability reappears at the end of the velocity range. For $k_{scale} = 0.25$ the damping is decreased further, leading to an even lower flutter speed than for all the other cases. Between the damping curves for mode 1 $k_{scale} \geq 1$ and the curves $k_{scale} < 1$ a change in the shape of the damping curves can be noticed. The flutter velocities of the different cases, together with the rigid propeller modelling results, are summarised in table 3.4. For the stiffer blades, the damping decreases over the velocity only slightly (or even increasing again at higher velocities for $k_{scale} = 1$ and $k_{scale} = 2$). For lower stiffness, the damping trend changes to a curve that starts close to $V = 0\ m/s$ with high damping values, but then the damping decreases already at low velocities rapidly, before the rate of decline becomes moderate again.

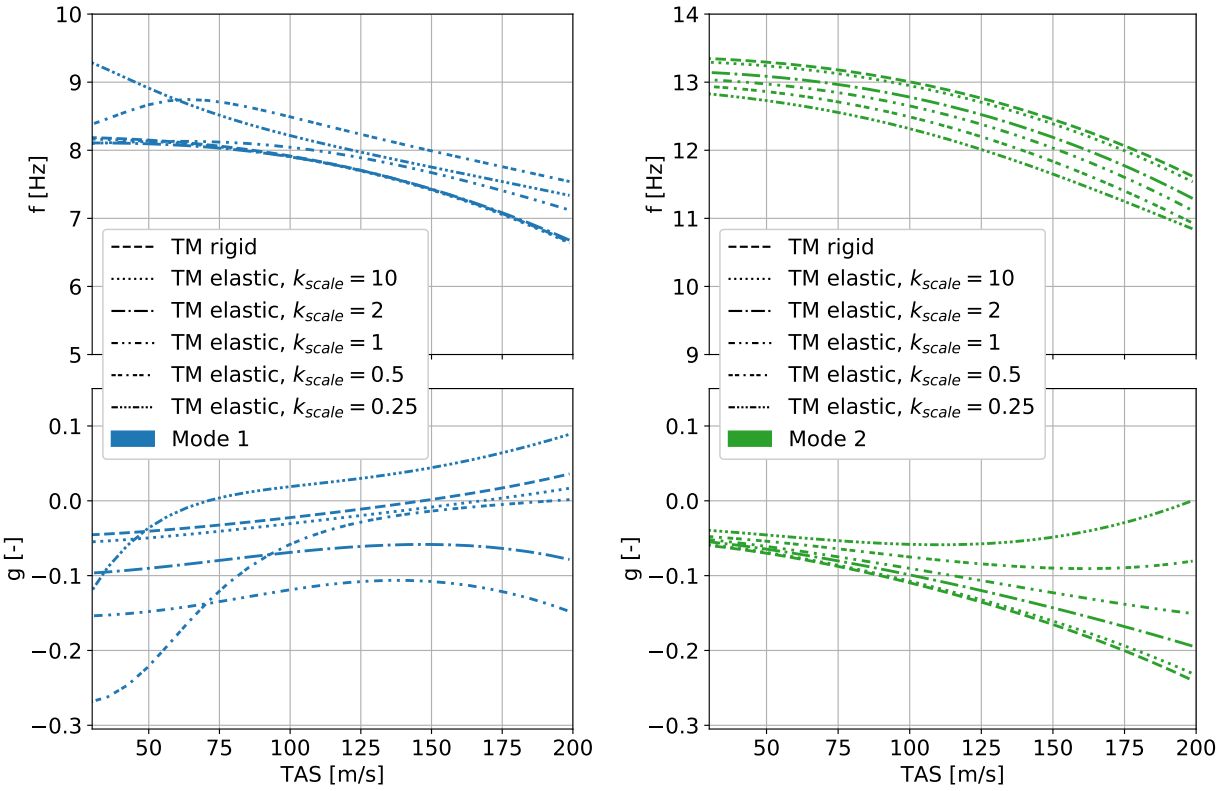

(a) Mode 1 (b) Mode 2

Figure 3.8.: Frequency and reduced damping trends for the 2DOF model analysis with TM-method, rigid and elastic propeller model with different blade stiffness values, windmilling condition

The right subplot (Fig. 3.8 (b)) shows mode 2, the forward whirl mode. With increasing blade elasticity, the frequencies of this mode decrease slightly over the whole velocity range. For the damping, a clear trend to lower damping of the system with increasing blade elasticity can be observed. Especially in the higher velocity range, the impact increases. For the most flexible case $k_{scale} = 0.25$, the damping even crosses the zero-damping line at the very end of the velocity range ($V_F = 198.61\ m/s$). This means that the forward whirl mode would get unstable here. However, mode 1 for this case has an even smaller flutter speed, so the flutter point of mode 2 would anyway not be reached.
To summarise, up to the nominal blade stiffness for this configuration, the stabilisation trends due to blade elasticity determined as known already from literature [6] could be confirmed. However, for even more flexible blades, this effect seems to change and the stability is decreased again. Not only the forward whirl is also critically destabilised, but also the flutter velocity of the backward whirl is reduced drastically. The origin of this effect should now not be investigated further. Only a few further findings from analysing these configurations should be shortly presented.

Having a look on the damping trends for mode 1 of case $k_{scale} = 0.25$ in figure 3.8 (a) shows that the damping gradient changes strongly over the velocity range, which differs

	V_F $[m/s]$
HR	138.22
TM rigid	146.79
TM elastic, $k_{scale} = 10$	167.66
TM elastic, $k_{scale} = 2$	-
TM elastic, $k_{scale} = 1$	-
TM elastic, $k_{scale} = 0.5$	192.71
TM elastic, $k_{scale} = 0.25$	70.88

Table 3.4.: Flutter velocities for mode 1 for the 2DOF model with different propeller models

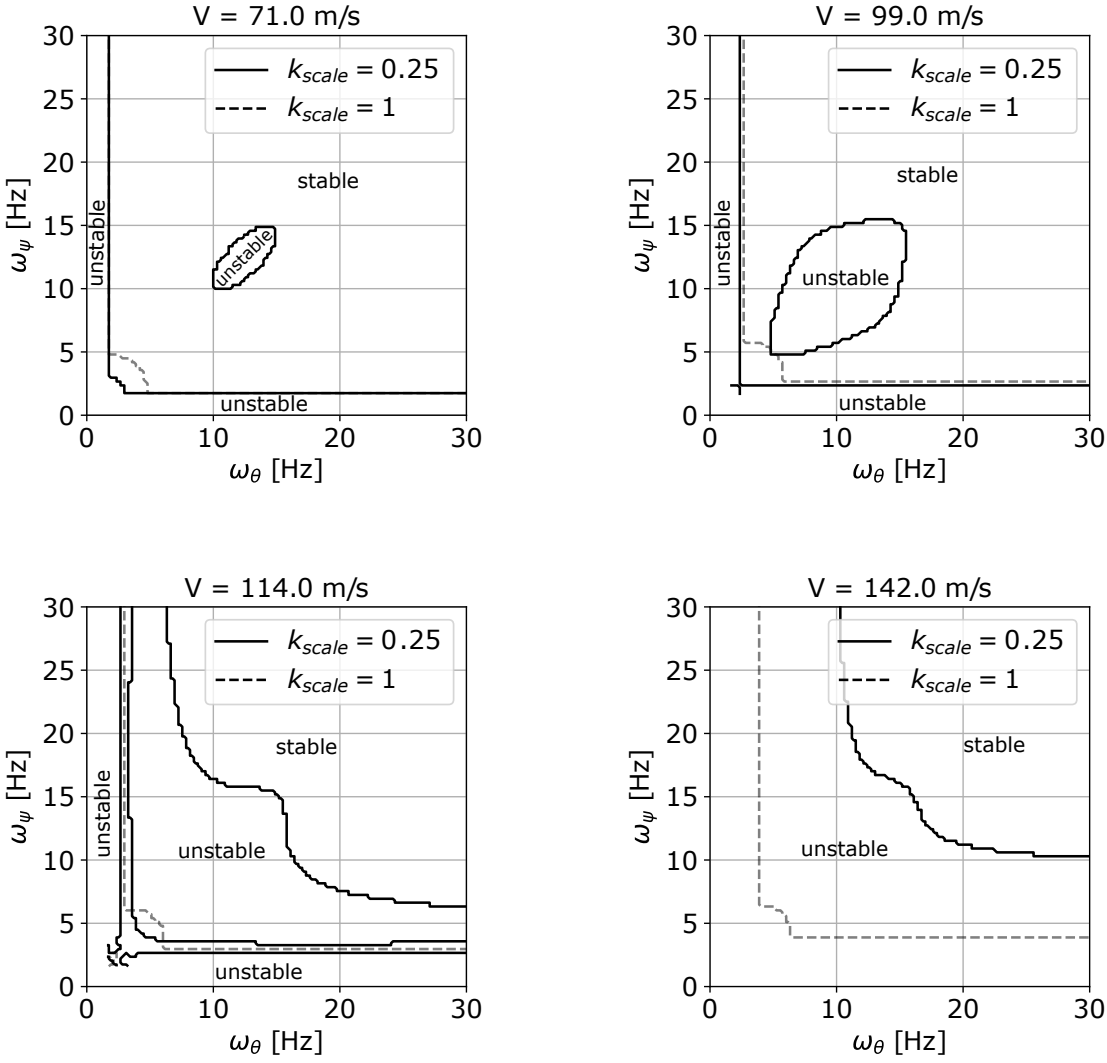

Figure 3.9.: Whirl flutter stability map for the 2DOF model with $k_{scale} = 0,25$ case at different velocities

from the damping trends of the cases with $k_{scale} \geq 1$. That suggests that a difference in the instability mechanism appears. This is also what the whirl flutter stability maps, that can be seen in figure 3.9, indicate. In the figure, the stability borders for the $k_{scale} = 0.25$

case for different velocities are displayed, as well as the stability borders for the nominal case transparently in the background. The stability has been analysed for several points in the presented frequency range with a pk-method approach and then the border between stable and unstable regions is marked by the plotted lines. Comparing the two cases shows that the shape of the stability border is different. For the nominal case, a classical bell curve that slightly grows with increasing velocities can be observed. In contrast, for the $k_{scale} = 0.25$ case for $V = 0.5V_D = 71\ m/s$ an additional unstable bubble in the higher mount stiffness area can be observed. Figure 3.10 shows the damping values of the points from the whirl flutter stability map for $k_{scale} = 0.25$ at $0.5V_D$. The determined damping values are coloured by its magnitude. The colour scale is chosen irregular and refined close to zero to picture this area more precisely. Here, not the structural damping but the viscous damping value is displayed. Still, a negative value means stability. In the unstable area, the damping is positive. Having a look on the damping values in the unstable bubble reveals that the damping is indeed positive, but only marginal (between 0.01 and 0, light blue colour). This is significant lower than the damping in the (small) area of conventional whirl flutter of the bell curve. The area where the damping values are 1 indicate divergence (red coloured).

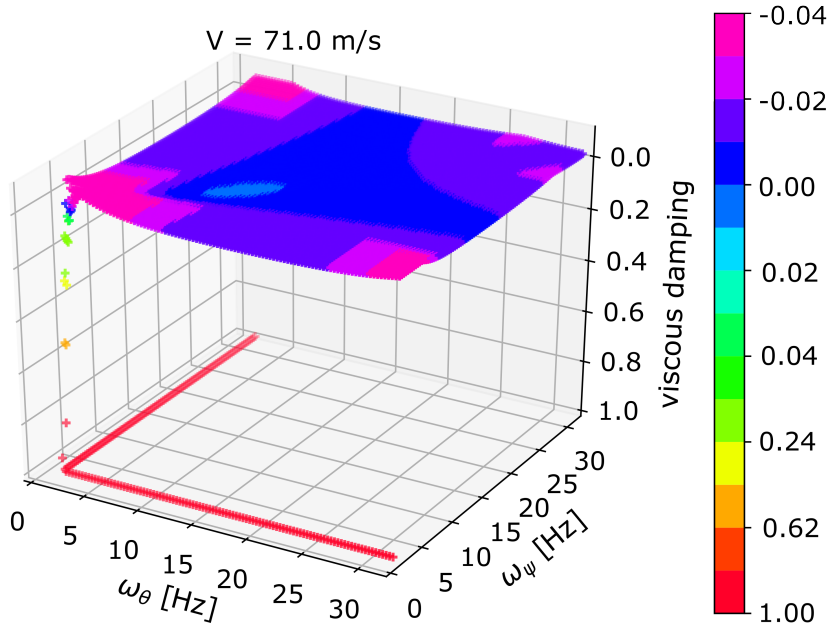

Figure 3.10.: Damping values of the points from the whirl flutter stability map for the 2DOF model with $k_{scale} = 0.25$ case at $V = 0.5V_D$, coloured by damping value

The unstable bubble grows with increasing velocity (see again figure 3.9) and finally merges with the unstable divergence area. At V_D, the unstable area is much larger than for the nominal case. Similar whirl plots could have been found by Johnston in [13] who varied the stiffness of rotational springs at rotor blade hinges and also found differently shaped whirl plots as a result. During this parameter study, he also detected that there is an optimum range of stiffness for best stability results. Same can be concluded from the previously

presented results. Even though, the rising blade elasticity first increases stability, there is a point where the mechanism is changing and the system gets destabilised. However, the examined very flexible blades might not be representative for real propeller blades. No further effort has been put in analysing the origin of this phenomenon because it has not been part of this work and the TM-method might not be the best method for analysing models with such flexible blades. For a deeper understanding of these effects, this would be necessary, though. Nevertheless, it can be concluded, that there is a certain limit for the stabilising influence of blade elasticity.

4. Method modifications for the practical application on complex configurations

So far in past applications of the TM-method, only examinations on a simple two-degree-of-freedom propeller model have been conducted, just as in the previous chapter. The used transfer-matrices have been generated using a propeller model in the multibody simulation tool Simpack [34]. After that, they have been combined with the structural model in a frequency-domain flutter solver. For these previous studies, the Simpack model was intentionally built based on the definitions of the structural model. But, if other models, especially more complex aircraft configurations, should be evaluated, the current method has some aspects that prohibits its direct application on these models in practice. To overcome these limitations and extend the TM-method, in the following necessary modifications are introduced in the workflow as preparation to apply the method on the generic aircraft configuration presented in the next chapter.
Beside the modifications on the TM-method, which are presented in detail in the first section of this chapter, also some adaptions on the implemented HR-method were necessary to apply it on the generic aircraft configuration due to differences in the propeller orientation. The second section of this chapter gives a detailed explanation on these adjustments.

4.1. Modifications of the TM-method

In the following, the implemented changes in the TM-method are presented that make it possible to apply the method on a more complex model in an efficient way. There are three main challenges that need to be solved and are treated in greater detail in the next subsections:

- The influence of the propeller mass that is included in the propeller model in Simpack, but usually also in the structural model, and must not be accounted for twice.
- The necessity to generate transfer-matrices for each operational point that should be evaluated in the flutter analysis, which can get very time consuming for complex models
- The required alignment of the propeller model, which is used to generate the transfer-matrices, and the structural model, with which it should be combined (e.g. regarding coordinate system orientations)

Further on, a possibility to define masking mechanisms is explained, which is useful to neglect elements in the transfer-matrices, more precisely in the axial degrees of freedom.

4.1.1. Elimination of the mass influences from the transfer-matrices

The propeller modelled in Simpack always contains the masses of the propeller blades. These masses can not be eliminated from the Simpack model before the transfer-matrix generation, at least for elastic propeller blades, and therefore always influence the generated transfer-matrices. However, the propeller masses are usually also part of the finite element model (FE-model) and must not be considered twice. Therefore, the masses need to be either subtracted from the FE-model or from the generated transfer-matrices. A general goal is to keep the FE-models independent from the method used to include the propeller in the flutter analysis, so different structural configurations can be used in the analysis without modifying all of them. Hence, the second option, removing the mass influence from the transfer-matrices, is the more practical solution and is elaborated in the following. Mass has a quadratic influence with increasing frequency in the flutter equation, as seen in equation 2.6. This is transferable to the mass part in the transfer-matrix term $\underline{H}_{prop}$. Because it is included in the flutter equation on the right side of the equation, the term has an negative sign. The mass from the propeller blades is known from the Simpack model as a mass matrix $\underline{M}_{prop}$ referenced about the propeller hub point. Therefore, with the simplification of $\sigma = 0$ and so $s = i\omega$, the mass part in the transfer-matrices can be calculated as:

$$-\underline{M}_{prop}\, s^2 = -\underline{M}_{prop}(i\omega)^2 = \underline{M}_{prop}\, \omega^2 \tag{4.1}$$

This term can then be subtracted from the generated transfer-matrix:

$$\underline{H}_{prop,new} = \underline{H}_{prop} - \underline{M}_{prop}\, \omega^2 \tag{4.2}$$

with the simplified propeller mass matrix $\underline{M}_{prop}$:

$$\underline{M}_{prop} = \begin{bmatrix} m_{prop} & 0 & 0 & 0 & 0 & 0 \\ 0 & m_{prop} & 0 & 0 & 0 & 0 \\ 0 & 0 & m_{prop} & 0 & 0 & 0 \\ 0 & 0 & 0 & I_p & 0 & 0 \\ 0 & 0 & 0 & 0 & I_\theta & 0 \\ 0 & 0 & 0 & 0 & 0 & I_\psi \end{bmatrix} \tag{4.3}$$

with $m_{prop} = 7.71\ kg$, $I_p = 3.597\ kgm^2$ and $I_\theta = I_\psi = 1.806\ kgm^2$ for the presented propeller model (see table 3.2). Elements beside the main diagonal, that may occur due to differences between centre of gravity and the reference point at the hub, are neglected. The new transfer-matrix $H_{prop,new}$ can now be combined with a full FE-model without considering the propeller mass twice.

As mentioned in section 2.3.2, it is not unusual to create transfer-matrices only for perturbations in and around the y- and z-axis, neglecting the x-axis terms. For these transfer-matrices, no mass term must be subtracted in the first and forth degree of freedom. Otherwise, negative masses would be added in these degrees of freedom leading to incorrect results if motion in these directions are not completely neglected in the model.

Similar to this procedure, also the gyroscopic effects that are part of the transfer-matrices can be eliminated after their generation. That would make it possible to incorporate the complete gyroscopic moment as a damping matrix in the flutter equation, just as in the HR-method definition, and simplifies the interpretation of the transfer-matrices itself. However, this is not used in the following and is therefore, not presented further.

4.1.2. Interpolation of the transfer-matrices for more velocity steps

For complex models, many operating points, e.g. velocity steps, have to be considered in the flutter analysis. For each of these operating points, there needs to be a transfer-matrix as input in the flutter analysis. That might make the TM generation quite time consuming. To decouple the number of velocity steps used for the TM generation and those used during the flutter analysis, an interpolation routine is introduced in the procedure to enable the refinement of the velocity steps after the generation of the transfer-matrices.
For the interpolation routine, a simple linear method implemented in Python is used that interpolates every TM value, separately for each base frequency, over the velocity steps. The routine can also extrapolate over the limits of the given velocity steps, but this might lead to wrong results in this range and should be avoided as far as possible. If no transfer-matrix set has been created for $V = 0$, it is therefore also preferable to include a matrix filled with zeros for this velocity step as interpolation input to avoid extrapolation and improve the interpolation results in the lower velocity range. This is only a simplification, that is not valid for every case, because a rotational speed different from zero at $V = 0$ produces transfer-matrices different from zero. However, this approach fits to the interpolation approach defined for the trim conditions in section 3.1.3 and is therefore suitable at this point.

4.1.3. Alignment of the transfer-matrices with the structural model

The transfer-matrices are generated by using a specific Simpack model and are connected directly with the attachment node in the structural model. So, the motion of the structural node is the direct dimensional input for the transfer-matrices. Now, problems may occur if the Simpack model and the structural model differ in their unit system definition or the propeller orientation in the coordinate system because input and output magnitudes and signs are interpreted differently by the transfer-matrices and the structural model. Further, it is important in which direction the propeller rotation is defined regarding the orientation of the coordinate axis.

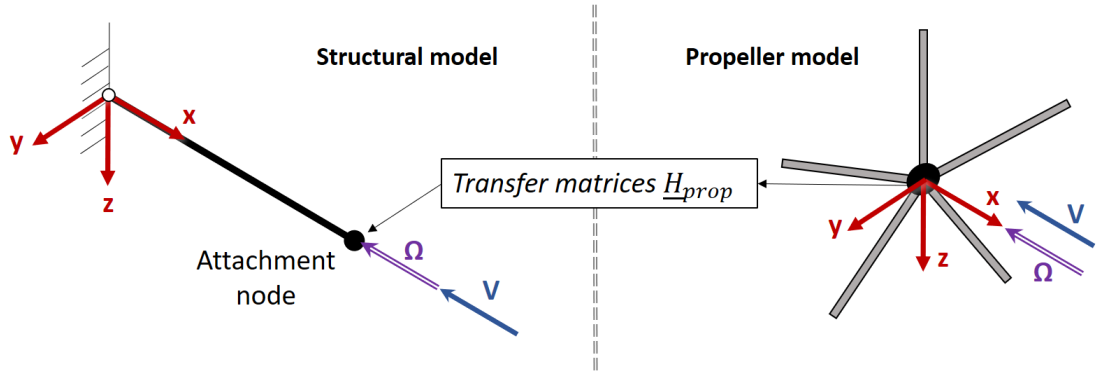

Figure 4.1.: Illustration of the combination of propeller model and structural model

The transfer-matrices used in this thesis are created by means of the Simpack model shown in section 3.1. The propeller rotation and coordinate system orientation are indicated in figure 3.2. Figure 4.1 provides a schematic overview about its connection with the structural

model exemplary for the 2DOF model from the previous chapter. It also displayed the present coordinate system and propeller orientations of the models.
In the pictured case, both models fit perfectly to each other regarding propeller orientation and coordinate system definition. The propeller model uses *kg* as mass unit and *m* as length unit. For the 2DOF structural model the same definitions are present, so for this combination the transfer-matrices also need no adaption in this point. However, it is not unlikely that the method should be applied on models where differences appear, as it is also the case for the generic aircraft configuration in the next chapter. Then, because the structural method should still be kept independent from the used propeller method, the transfer-matrix method needs to be aligned to the structural model.
As shown in equation 2.20, a fully identified transfer-matrix consists of the following elements:

$$\underline{H}_{prop} = \begin{bmatrix} F_{xx} & F_{xy} & F_{xz} & F_{x\phi} & F_{x\theta} & F_{x\psi} \\ F_{yx} & F_{yy} & F_{yz} & F_{y\phi} & F_{y\theta} & F_{y\psi} \\ F_{zx} & F_{zy} & F_{zz} & F_{z\phi} & F_{z\theta} & F_{z\psi} \\ M_{xx} & M_{xy} & M_{xz} & M_{x\phi} & M_{x\theta} & M_{x\psi} \\ M_{yx} & M_{yy} & M_{yz} & M_{y\phi} & M_{y\theta} & M_{y\psi} \\ M_{zx} & M_{zy} & M_{zz} & M_{z\phi} & M_{z\theta} & M_{z\psi} \end{bmatrix} \tag{4.4}$$

Each element depends on different degrees of freedom, specified by the indices, and needs to be adapted accordingly. These adaptions are introduced in the following.

Adapt the unit system of the transfer-matrices according to the FE-model

After the transfer-matrix generation, no normalisation or nondimensionalisation is performed before including the matrices in the flutter process. So, in the process so far, the transfer-matrices kept the units used in the Simpack model. But, if the structural model used is defined in a different unit system than the Simpack model, the values in the transfer-matrices need to be adapted, so they return the perturbation response in the correct dimension. In the following, the conversion of an unit system with mass in *kg* and length in *m* into an unit system with the mass in *t* and the length in *mm* is shown. Angular deflections have the unit *rad* in both systems. Table 4.1 shows the units of different quantities in the systems before and after the transformation.

Quantity	Before transformation	After transformation
length	*m*	*mm*
mass	*kg*	*t*
time	*s*	*s*
force	*N*	*N*
moment	*Nm*	*Nmm*
angle	*rad*	*rad*

Table 4.1.: Units of relevant quantities in the unit systems before and after the presented transformation

The elements of the 6x6 transfer-matrices (see equation 4.4) have different input and output quantities and the transformation needs to be aligned accordingly. The matrix can be

divided in four parts regarding the input and output magnitude, each with nine elements that need the same conversion. The upper left elements (row 1-3 and column 1-3) transfer a length perturbation (Δx, Δy or Δz) into an force output (F_x, F_y or F_z). Before any changes in the considered case, the length input has the unit m and the force output the unit N (see also table 4.1) causing the values in this area of the transfer-matrix to have the unit N/m. In the changed unit system the force unit stays N, as it is defined as $N = \frac{kg \cdot m}{s^2} = \frac{t \cdot mm}{s^2}$. Therefore, the values in the upper right area of the transfer-matrix now need to be changed, so that a input in mm leads to an output in N. To do this, each element must be multiplied by 0.001.
The transformation of the other values in the transfer-matrix can be derived analogously and brought together in a transformation matrix $\underline{T}_{unit}$, which is multiplied element-wise with the transfer-matrices. The unit conversion of the transfer-matrices can then be formulated as follows:

$$\underline{H}_{prop/t,mm} = \underline{H}_{prop/kg,m} \circ \underbrace{\begin{bmatrix} 0.001 & 0.001 & 0.001 & 1 & 1 & 1 \\ 0.001 & 0.001 & 0.001 & 1 & 1 & 1 \\ 0.001 & 0.001 & 0.001 & 1 & 1 & 1 \\ 1 & 1 & 1 & 1000 & 1000 & 1000 \\ 1 & 1 & 1 & 1000 & 1000 & 1000 \\ 1 & 1 & 1 & 1000 & 1000 & 1000 \end{bmatrix}}_{\underline{T}_{unit}} \tag{4.5}$$

The lower left and upper right elements need no multiplication factor because they have the unit N respectively N/rad which both do not differ between the systems. The lower right elements have the unit Nm/rad leading to a multiplication by 1000 to transform the values in Nmm/rad.
For cases with a gyroscopic moment added separately from the transfer-matrices $M_{gyro,add}$, this value also needs be adapted to the new unit system. Due to the definition as multiplication from inertia and rotational frequency, $M_{gyro,add}$ has the unit $kgm^2 \cdot rad/s$ before and $tmm^2 \cdot rad/s$ after the transformation. For the transformation the value need to be multiplied by 1000:

$$M_{gyro,add/t,mm} = M_{gyro,add/kg,m} \cdot 1000 \tag{4.6}$$

Naturally, other transformations might be required in various use cases due to different unit systems in the applied models which can be derived similarly. Though, for the application in this thesis, the presented transformation is sufficient.

Rotate the coordinate system of the propellers

To align the coordinate system in which the transfer-matrices have been generated and the one from the structural model, a transformation matrix similar to $\underline{T}_{unit}$ from the previous subsection can be derived. First of all, both coordinate systems need to be right-handed Cartesian coordinate systems. It is further assumed that the axes of the propeller model and the structural model are parallel to each other and the propeller axis, especially, is in both models parallel to the x-axis. Then, the y-z-plane is parallel to the propeller plane. Further, the exact orientation of the y- and z-axis in the propeller model is irrelevant

because the Simpack model is rotational symmetric around the x-axis. Therefore, the only relevant difference can appear in the x-axis orientation which can be turned by 180°. Of course, either the y-axis or the z-axis needs to change also its direction to remain a right-handed coordinate system. It is assumed in the following that the z-axis remains constant and the y-axis rotates also by 180°. Figure 4.2 illustrates the possible coordinate system orientations.

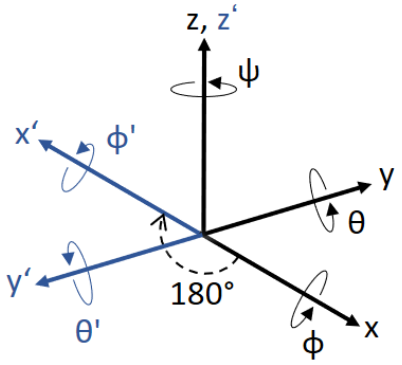

Figure 4.2.: Coordinate system transformation

The rotation affects the single elements in the transfer-matrix differently because of the different involved degrees of freedom shown by the indices in equation 4.4. No complex coordinate transformation that would require trigonometric functions to derive the effect on the different coordinates is applied, but only simple rotations by 180°. Therefore, the effects are reflected only by sign changes in some elements of the matrix. Due to the transformation, the degrees of freedom x, y, ϕ and θ experience a change in sign. But, if two of these mentioned degrees of freedom are involved in a transfer-matrix element, the sign changes cancel each other out. For the whole transfer-matrix this leads to the following transformation, with again an element-wise multiplication:

$$\underline{H}_{prop,cos} = \underline{H}_{prop} \circ \underbrace{\begin{bmatrix} 1 & 1 & -1 & 1 & 1 & -1 \\ 1 & 1 & -1 & 1 & 1 & -1 \\ -1 & -1 & 1 & -1 & -1 & 1 \\ 1 & 1 & -1 & 1 & 1 & -1 \\ 1 & 1 & -1 & 1 & 1 & -1 \\ -1 & -1 & 1 & -1 & -1 & 1 \end{bmatrix}}_{\underline{T}_{COS}} \tag{4.7}$$

The change of orientation of the x-axis also affects the definition of the additional gyroscopic moment $M_{gyro,add}$. This value also needs to change its sign because it depends on the inertia around the x-axis:

$$M_{gyro,add/cos} = -M_{gyro,add} \tag{4.8}$$

Analogously to the matrices $\underline{T}_{unit}$ and $\underline{T}_{COS}$ a transformation matrix for a difference in propeller rotation direction can be determined and found in the appendix (see equation A.2). But, this matrix is not used in the following.

4.1.4. Masking of axial components

Not always all elements of the generated transfer-matrices should be included in the flutter analyses, especially due to additional assumptions regarding the axial degrees of freedom (DOF 1 and 4) which usually have a lower impact on whirl flutter. Depending on the stated assumptions, the elements that should not be considered in the further analyses are set to zero ("masking"). Three relevant masking configuration are introduced:

- **Mask 1**: all elements in rows and columns affected by DOF 1 or 4 are set to zero
- **Mask 2**: only element F_{xx} retains in the columns and rows of DOF 1 and 4, the other elements in these rows and columns are set to zero
- **Mask 3**: all elements coupling DOF 1 or 4 with other degrees of freedom are zeroed out; F_{xx}, $F_{x\phi}$, M_{xx} and $M_{x\phi}$ remain

In the generated transfer-matrices very small, oscillating values appeared for the elements coupling the axial degrees of freedom with other degrees of freedom. These findings seem to have no real physical source, but are only noise in the data. To reduce this, it seems favourable to neglect these elements, leading to the definition of mask 3. But, also in both other masking configurations, it is useful to zero out these elements. Further, Mask 1 is similar to the assumption of the HR-method that neglects the axial degree of freedom completely. Mask 2 is applicable if the torsional degree of freedom should be omitted. This seems appropriate for models where no engine shaft is modelled, but it would absorb a lot of axial rotation of the propeller axis in reality.
For models where motion in DOF 1 and 4 is neglected in the structural model, the variation makes no difference. The described masking methods are compared later during the flutter evaluations with the generic aircraft configuration.

4.2. Adaptions on the HR-method

The influence of different orientations of propeller has not been taken into account in implemented HR-method so far, but specific requirements had to be met by the model to gain correct results. The standard assumptions for the derivation of the HR propeller matrices are illustrated in figure 2.2 and again in figure 4.3 (a). This definition leads to the analytical description for the propeller forces:

$$\begin{bmatrix} F_y \\ F_z \\ M_y \\ M_z \end{bmatrix} = \underbrace{\begin{bmatrix} 0 & 0 & \frac{C_{y\theta}}{2R} & \frac{C_{y\psi}}{2R} \\ 0 & 0 & \frac{C_{z\theta}}{2R} & \frac{C_{z\psi}}{2R} \\ 0 & 0 & C_{m\theta} & C_{m\psi} \\ 0 & 0 & C_{n\theta} & C_{n\psi} \end{bmatrix}}_{\underline{K}_{prop}} \cdot \begin{bmatrix} y \\ z \\ \theta \\ \psi \end{bmatrix} + \underbrace{\begin{bmatrix} -\frac{C_{y\psi}}{2RV} & \frac{C_{y\theta}}{2RV} & \frac{C_{yq}}{2V} & \frac{C_{yr}}{2V} \\ -\frac{C_{z\psi}}{2RV} & \frac{C_{z\theta}}{2RV} & \frac{C_{zq}}{2V} & \frac{C_{zr}}{2V} \\ -\frac{C_{m\psi}}{V} & \frac{C_{m\theta}}{V} & \frac{C_{mq}R}{V} & \frac{C_{mr}R}{V} \\ -\frac{C_{n\psi}}{V} & \frac{C_{n\theta}}{V} & \frac{C_{nq}R}{V} & \frac{C_{nr}R}{V} \end{bmatrix}}_{\underline{D}_{prop}} \cdot \begin{bmatrix} \dot{y} \\ \dot{z} \\ \dot{\theta} \\ \dot{\psi} \end{bmatrix} \quad (4.9)$$

If the matrices should be used as implemented, the examined structural model needs to match with these assumptions. However, other coordinate system orientations or an opposite propeller rotational direction can be imagined for structural models and should be taken into account in the following considerations. The previously examined 2DOF model only differs from the HR-method in the rotational direction of the propeller. No difference arises in the flutter results for this variation on the 2DOF model because it is a rotational symmetric system. Other models, such as the generic aircraft configuration, can differ also in the coordinate system orientation or be not rotational symmetric, so the models and the method need to be aligned in this points. As previously for the TM-method, also for the HR-method it is more practical to adapt the method to the used model and not change the structural model. However, not the definitions of the HR derivatives, as they are implemented in the flutter solver, should be changed. Rather, the influence of these adaptions on the propeller matrices used in the HR-method are derived, so the effect can be incorporated by adapting these matrices before entering them in the flutter analysis.
In the following, the adaptions for two variations towards the standard HR-method should be presented. These two examined cases are shown in figure 4.3 (b), with an opposite propeller rotational direction, and (c), with a rotated coordinate system. Combining the adaptions of case (b) and (c) would lead to a hypothetically case with opposite flight direction definition.

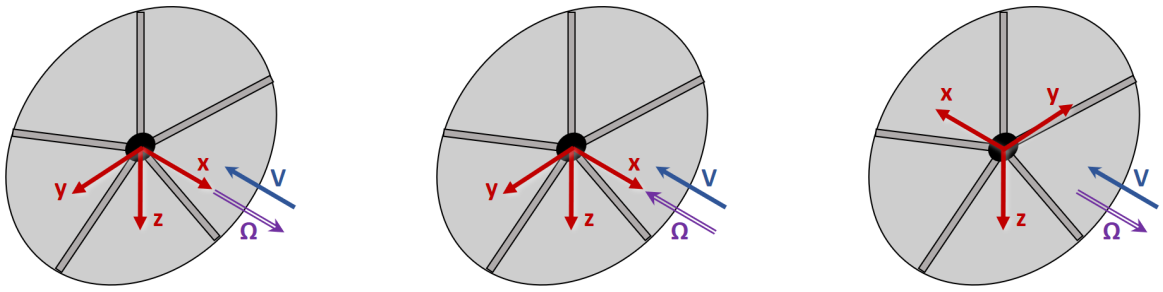

(a) Standard HR

(b) Opposite propeller rotation

(c) Rotated coordinate system

Figure 4.3.: Propeller orientation

The propeller matrices $\underline{K}_{prop}$ and $\underline{D}_{prop}$ and the included derivatives used in the HR-method can be derived as shown in Cecrdle's book about whirl flutter [30] for the standard propeller orientation 4.3 (a). Similar to this derivation, the influence of a change in propeller rotation direction and opposite flight direction has been derived. This leads to a change in sign for some elements of the matrices. To introduce these changes into the flutter process, transformation matrices T_i can be determined with which the propeller matrices are adapted according to the existing propeller orientation. The index specifies the kind of transformation that is performed with the matrix. In general, the transformations of the stiffness and damping matrices can be described as element-wise multiplication of the transformation matrix:

$$\underline{K}_{prop,i} = \underline{K}_{prop} \circ \underline{T}_i \tag{4.10}$$

$$\underline{D}_{prop,i} = \underline{D}_{prop} \circ \underline{T}_i \tag{4.11}$$

Three transformation matrices, for opposite rotational speed T_Ω, turned coordinate system T_{XY} and the combination of both (opposite flight direction) T_{FD} have been derived.
First, the derivations for case (a) and (b) have been compared leading to the transformation matrix regarding a change in propeller rotation direction:

$$\underline{T}_\Omega = \begin{bmatrix} 1 & -1 & -1 & 1 \\ -1 & 1 & 1 & -1 \\ -1 & 1 & 1 & -1 \\ 1 & -1 & -1 & 1 \end{bmatrix} \tag{4.12}$$

For a change of the coordinate system, similar considerations can be made as in section 4.1.3 for the transfer-matrices. This leads to the following transformation matrix T_{XY} for a coordinate system rotation around the z-axis with x- and y-axis pointing in opposite directions:

$$\underline{T}_{XY} = \begin{bmatrix} 1 & -1 & 1 & -1 \\ -1 & 1 & -1 & 1 \\ 1 & -1 & 1 & -1 \\ -1 & 1 & -1 & 1 \end{bmatrix} \tag{4.13}$$

Considering the hypothetical case of an opposite flight direction in the matrix derivation in relation to the classical case (a), the following transformation matrix can be stated:

$$\underline{T}_{FD} = \begin{bmatrix} 1 & 1 & -1 & -1 \\ 1 & 1 & -1 & -1 \\ -1 & -1 & 1 & 1 \\ -1 & -1 & 1 & 1 \end{bmatrix} \tag{4.14}$$

It can be seen that changing both the rotational speed and the coordinate system orientation leads to the same alterations as this hypothetical case of opposite flight direction:

$$\underline{T}_{FD} = \underline{T}_{XY} \circ \underline{T}_\Omega \tag{4.15}$$

These transformation matrices for the HR propeller matrices can be seen as special cases for the transformations of the 6x6 transfer-matrices. For example, $\underline{T}_{XY}$ can be compared with the transformation matrix $\underline{T}_{COS}$ for the transfer-matrices neglecting the axial degrees of freedom (see equation 4.7). Analogously to $\underline{T}_\Omega$, also a full transformation matrix for the opposite propeller rotation for the transfer-matrices can be stated and found in the appendix (see equation A.2).

5. Stability analyses with the full aircraft configuration

The TM-method, as described in literature, has been extended in the previous chapter to enable its application for stability analysis of complex aircraft models. This is now demonstrated on a full aircraft configuration. For this purpose, a generic regional aircraft with two propellers is used. The study makes use of the existing FE-model and aerodynamic model of a generic aircraft configuration which has been only slightly modified to encounter the desired flutter mechanisms inside the aeroelastic envelope. Besides the most important whirl flutter analysis, also an aircraft configuration showing regular bending-torsion flutter has been studied. For these two flutter cases, the influence of blade elasticity and thrust on the flutter stability is examined.

5.1. Full aircraft configuration

In this section, the aircraft model used for the flutter analyses on full aircraft level is described. Figure 5.1 shows a sketch of the generic aircraft configuration. The aircraft is a high-wing, twin-turboprop aircraft with a conventional tail and a wingspan of about 16 m. It represents a short-distance, short takeoff and landing (STOL) commuter aircraft for 20 passengers. Both propellers, mounted each on one wing, rotate in the same direction (clockwise as viewed from the front). The installed propellers are the same as described and used in the previous chapter. The rotational speed is also the same ($\Omega = 168.3\ rad/s$) and the trim conditions described in 3.1.3 are applicable. Therefore, the same already generated transfer-matrices with the presented Simpack model can be reused. Also, for this model the flight speed V_D is 142 m/s.

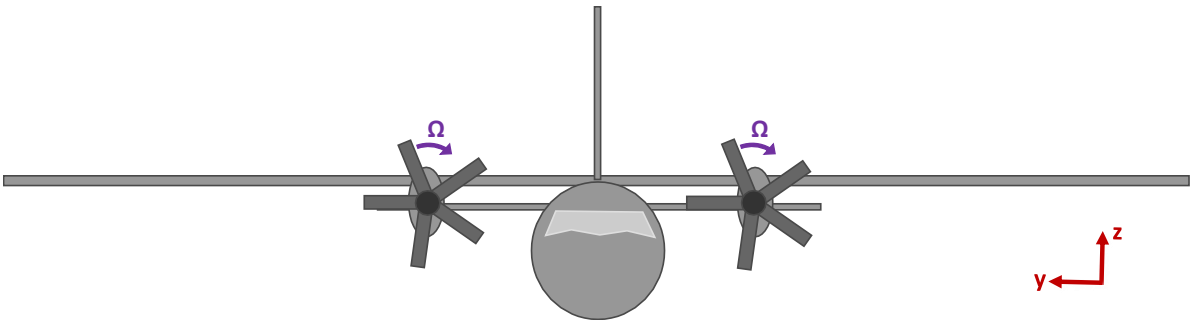

Figure 5.1.: Generic aircraft configuration

5.1.1. Finite element model

The FE-model used is a full-span aircraft model for MSC Nastran [33]. The fuselage is modelled using bar elements, while the wing and empennage, as well as the control surfaces,

consist of shell elements, which each have a specified material and density. Because in the evaluations only whirl flutter and bending-torsion flutter should be studied, the motion of the control surfaces relatively to the wing and the empennage is blocked to avoid appearance of control surface phenomena. This simplifies identifying clear whirl and bending-torsion modes. The components are connected by multi-point-constraints (RBE2 and RBE3) or springs (CBUSH). The aircraft mass not already included in the model by the shell elements is added to the model using point masses (CONM2 elements). The mass configuration is a representative Maximum Take Off Weight (MTOW) configuration.
For each propeller, an attachment node is defined that is connected with the pylon structure on the wing through four CBUSH elements each. These elements represent shock mounts with a specific stiffness carrying the engine. Therefore, they determine the engine mount stiffness, which is relevant for the whirl flutter stability. On the propeller nodes the propeller mass is added as point masses. These nodes are also the points where the transfer-matrices or propeller matrices are included in the model.
The unit system used in the model is t-mm-s. The main coordinate system is defined with its x-axis pointing against the flight direction and the z-axis pointing upwards. For the later performed flutter analyses, the model is reduced to 50 structural modes, including the rigid body modes in the first 6 modes. However, later in the flutter results only the modes 7 to 30 are displayed, which is sufficient to show the whirl flutter and bending-torsion phenomena. The first 30 structural modes are listed in table A.1 in the appendix A.3.

The FE-model used in this work was supplied as an input. It is only slightly modified to show flutter instabilities in the examined velocity range. This allows studying the effects of blade elasticity and other parameters on different flutter phenomena. These modifications are presented in the following.

Whirl flutter configuration

The most important phenomenon that should be examined is whirl flutter. To trigger whirl flutter on the model, the stiffness of the engine mounts (shock mounts) has been reduced until whirl flutter occurred for the flutter analysis with the classical HR-method. This structural configuration is called **"Tuned WF"** in the following.

Bending-torsion configuration

In addition to the whirl flutter configuration, also a structural model showing bending-torsion flutter should be examined. To trigger this instability, tuning beams in the wings are used to increase the stiffness of wing bending. Also, the material properties of the wing panels have been modified to decrease the stiffness of wing torsion. This brings the eigenfrequencies of these modes closer together, creating an adverse coupling and thus flutter. Additionally, extra masses have been inserted on the wing trailing edge further amplifying the flutter phenomenon. This structural configuration is called **"Tuned BTF"**.

5.1.2. Aerodynamic model

To model the unsteady aerodynamics of the aircraft, the commercial aeroelastic software ZAERO [36] was used. The model used is a panel model and can be seen in figure 5.2. For the lifting surfaces (empennage and wing) CAERO7 panels are defined while for the other components BODY7 elements are used. The splining between structural nodes and aerodynamic panels is performed with Thin Plate Splines (TPS). The aerodynamic data is generated with the linear subsonic unsteady aerodynamic ZONA6 method of ZAERO. Details on the method can be found in the theoretical manual of ZAERO [37].

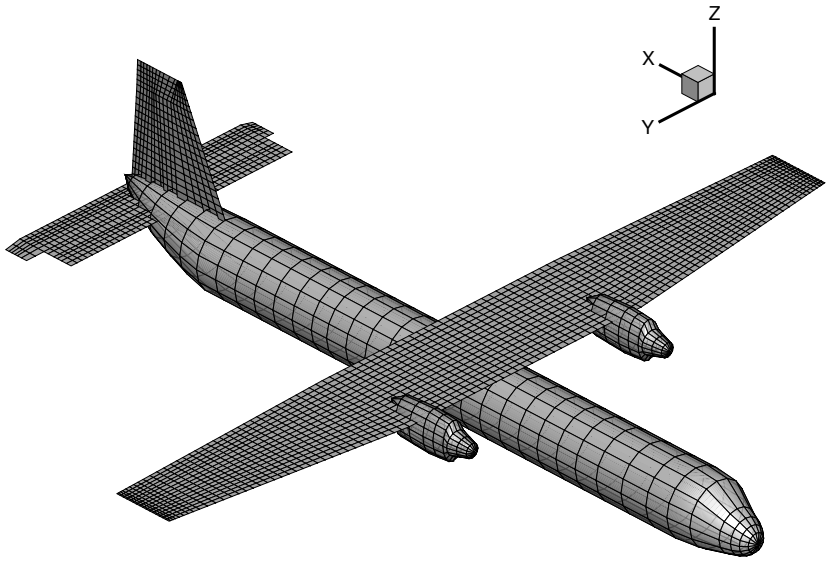

Figure 5.2.: Aerodynamic model of generic aircraft configuration

5.2. Flutter analysis setup

For the flutter analysis, the described FE-model is coupled with the aerodynamic model and the propellers are added to build the generalised equation of motion of the coupled system. As already seen in equation 2.15, for a specific airstream velocity V and an additional gyroscopic matrix $\underline{G}_{gen}$ this leads to the equation:

$$\underline{M}_{gen}\ddot{q}_h + \underline{K}_{gen}q_h + \underline{G}_{gen}\dot{q}_h = \left[q\underline{Q}_{gen}(s) + \underline{\Phi}^T_{prop}\underline{H}_{prop}(s, V, \Omega, \rho)\underline{\Phi}_{prop}\right] q_h \tag{5.1}$$

$\underline{M}_{gen}$ and $\underline{K}_{gen}$ are the generalised mass and stiffness matrices from the structural full aircraft model. The generalised gyroscopic matrix $\underline{G}_{gen}$ includes gyroscopic terms that are not already part of $\underline{H}_{prop}$. For the TM-method this concerns the additional gyroscopic moment $M_{gyro,add}$. For the classical flutter analysis with the HR-method, $\underline{G}_{gen}$ contains no values

because in this case the gyroscopic terms are included completely in $\underline{H}_{prop}$. The term $\underline{Q}_{gen}$ determines the generalised aerodynamic forces. They are calculated from the coupling of aerodynamic and structural model using ZAERO [36] for a given set of reduced frequencies between which an interpolation for the current frequency can be performed. $\underline{H}_{prop}$ determines the propeller matrices which are also frequency dependant. For the classical flutter analysis, the HR matrices are included in the calculations at this point, including also the gyroscopic moment (see equation 2.16). For the TM-method, the generated transfer-matrices first need to be adjusted to the coordinate system definitions of the FE-model as described in the previous chapter and then interpolated over the examined velocity range. Then they are added to the equation as $\underline{H}_{prop}$. Thereby, $\underline{H}_{prop}(s)$ is approximated by the determined $\underline{H}_{prop}(i\omega)$, according to the assumptions of the g-method. The propeller matrices are included in the model at the two defined propeller attachment nodes of the structural model. $\underline{\Phi}_{prop}$ determines the mode shapes of these nodes and performs the generalisation of the propeller matrices.
The flutter analyses are performed with a frequency-domain flutter solver that solves the flutter equation following an iterative g-method approach, as in [26]. All computations are performed under sea level conditions ($\rho = 1.255\ kg/m^3$) in a non-matched flutter analysis (fixed density and Mach number) at the Mach number $Ma = 0$. The airspeeds investigated range from $0\ m/s$ in steps of $1\ m/s$ to $200\ m/s$, which is equivalent to approximately $1.41V_D$.

5.3. Stability analyses with the Tuned WF model

First, the structural model with the whirl flutter modification is examined to study the influence of blade elasticity and thrust on the whirl flutter stability of the generic aircraft configuration. However, first the flutter results with the HR-method and the TM-method for rigid propeller blades are compared for verification purposes.

5.3.1. Comparison HR vs. TM-method

If the performed flutter calculations have been defined properly, the analysis results from the HR and TM-method calculations for the rigid propeller model should be similar. This implies also that the transfer-matrix and HR matrix transformations that need to be applied have been performed appropriately to the model definitions. From previous analysis on the 2DOF model, a slightly higher flutter velocity for the TM-method results with the rigid propeller model could be expected.
Figure 5.3 shows the frequency f and structural damping value g for the first 30 structural modes, except the rigid body modes, of the Tuned WF model combined with the HR propeller and the rigid TM propeller. For the TM-method, three different masking configurations where examined, as they have been explained in section 4.1.4. Only the values starting from $0.2V_D$ are shown. It can be seen that the overall trends of the frequency and damping curves for the different modes are quite similar between the different methods. So, it can be assumed that the method has been implemented correctly.
A positive value of g indicates negative damping of a mode and, thus, flutter. Two modes can be found that cross the zero-damping line and go unstable. They are therefore high-

lighted in the plot: Mode 9 and Mode 10. Both instabilities are induced by backward whirl modes. For mode 10, the whirl motion of the two propellers occurs in the same phase, so both propeller axes are deflected upwards at the same time. In this case mostly symmetric structural modes with respect to the xz-plane are involved. Even though, both propellers still perform a backward whirl motion and the mode is therefore not fully symmetrical, this mode is referred to as "symmetric mode" in the following. In the other case, for mode 9, the whirl motion of both propellers occur with an temporal offset. When one axis is deflected upwards, the other axis is deflected downwards. Still, both propellers are performing an backward whirl motion, but mostly antisymmetrical structural modes are involved in the airframe motion. In the following, this mode is referred to as "antisymmetric mode".

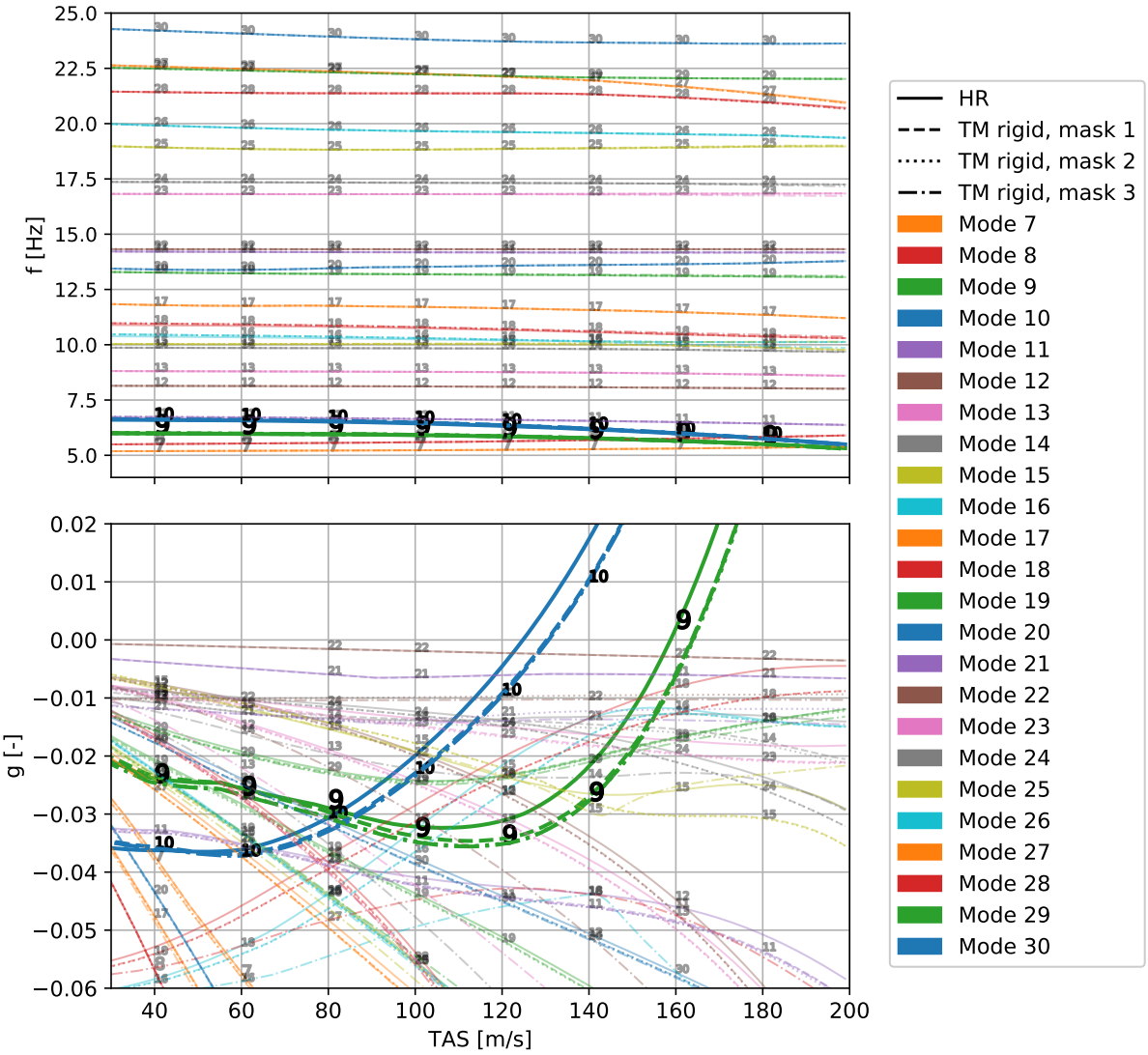

Figure 5.3.: Frequency and damping trends for the Tuned WF model with HR-method and TM-method for rigid blades and different masking configurations, windmilling condition, see figure 5.4 for close-up of damping at flutter point

All displayed methods show these two instabilities. However, the point of zero damping, that determines the flutter speed V_F, differs from case to case. Especially, the HR-method

results show lower flutter speeds (124.81 m/s and 158.77 m/s) than the TM-method results, which differ much less from each other (130.32 m/s and 163.64 m/s for mask 1). So, the TM-method determines even for rigid propeller blades approximately 3.1 % respectively 4,4 % higher flutter velocities than the HR-method. This difference is slightly smaller than for the 2DOF model analysis where the deviation has been 6,2 % (see section 3.3.1).

The difference between HR-method and TM-method even for rigid propeller modelling has already been present in the analysis of the 2DOF model. Therefore, it was to be expected to appear also on full aircraft level and can be explained the same way by simplifications in the HR-method. As the HR-method results in lower flutter speed, it is still the more conservative method.
Figure 5.4 shows a closer view on both zero-crossings for mode 9 and 10. In this close-up, also the flutter speeds for the different masking configurations for the TM-method can be separated. Even though, the differences between them are very small, the comparison shows that masking configuration 1 is for both cases the most conservative one and, therefore, also the closest to the HR-method results which is the reference method. This is reasonable because this masking configuration only incorporates elements for degree of freedom 2, 3, 5 and 6 just as in the HR-method. Having a closer look on other structural modes reveals for some modes stronger differences in the damping values g. These modes might have higher parts of axial motion which explains why masking configurations considering the axial degrees-of-freedom show different trends than those that neglect the entries.
For conservative results, in all following analyses the masking configuration 1 is used.

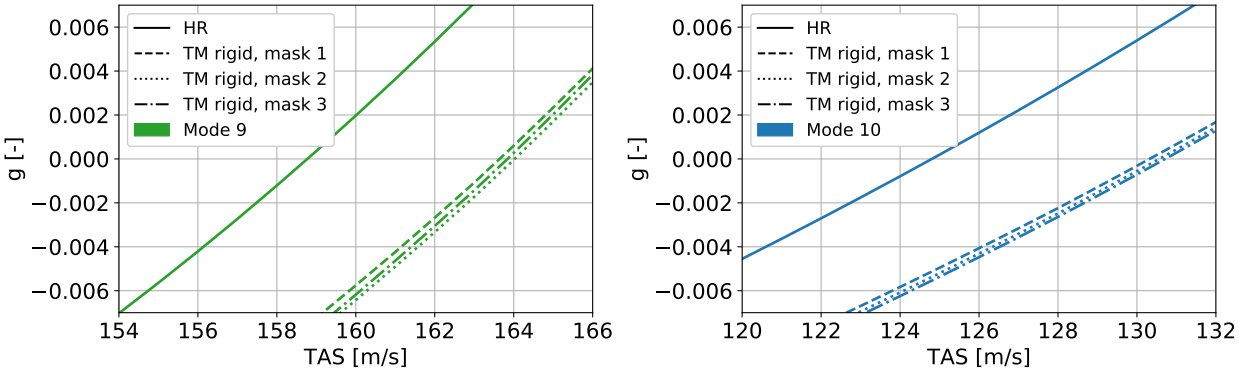

(a) Mode 9 (antisym. whirl) (b) Mode 10 (sym. whirl)

Figure 5.4.: Close-up of damping at flutter point for both flutter modes from figure 5.3

5.3.2. Influence of blade elasticity

In this section, the influence of the blade elasticity on the whirl flutter stability is investigated. For these evaluations, the transfer-matrices generated with the Simpack model including the blade degrees of freedom are used. To show the effect on the flutter stability, the blade elasticity is increased by using the scaling factor k_{scale} (see section 3.1.2). Three stiffness values have been examined: a relatively stiff value of $k_{scale} = 10$, $k_{scale} = 2$ and

$k_{scale} = 1$ being the nominal blade elasticity. All examination have been made for the windmilling trim condition.

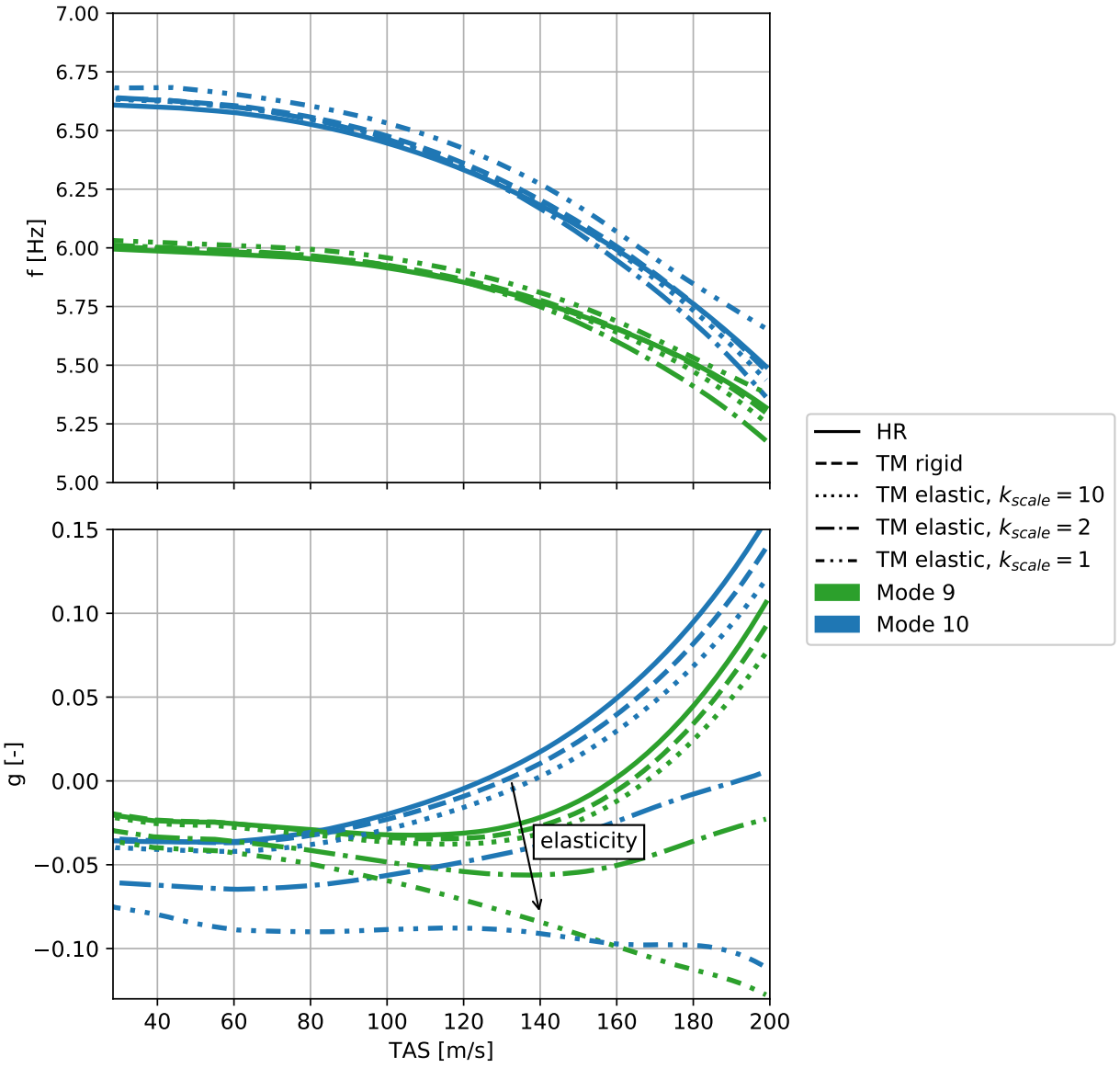

Figure 5.5.: Frequency and damping trends for the unstable modes of the Tuned WF model with HR-method and TM-method for rigid and elastic blades, windmilling condition

Figure 5.5 shows the frequency and damping trends over the velocity. For clarity, only the in the previous section determined unstable modes are displayed. In the appendix A.4, the full frequency and damping plots for all modes can be found in figure A.4 to A.6. Besides the new results for the cases with blade elasticity, also the results from the HR-method and the TM-method with rigid blades are shown in the plot. As expected from the former results with the 2DOF model (cf. figure 3.8), the two modes are stabilised when blade elasticity is included in the simulation. Even for relatively stiff blades with $k_{scale} = 10$, the frequency and damping curves are close to the results from the rigid propeller modelling, but indicate higher flutter velocities for both flutter modes. When the elasticity is increased

further, the flutter points are shifted to higher velocities. For nominal blade stiffness, no instability occurs in the examined velocity range. The difference in damping increases with the velocity.
As already studied with the 2DOF model, the blade elasticity has been increased even further to lower values than $k_{scale} = 1$. This leads to the frequency and damping trends as displayed in the two plots of figure 5.6. In the graphs, also the former results for the blade elasticity from rigid to nominal are shown and only the curves for $k_{scale} = 0.5$ and $k_{scale} = 0.25$ are added. In the appendix A.4, also the full frequency and damping plots for all modes of these cases can be found in figure A.2 and A.3. For the symmetric whirl mode (Mode 10), in the mode tracking during the flutter analysis of the case with $k_{scale} = 0.25$ a mode switch appears. Therefore, in figure 5.6 (b) for this configuration also Mode 11 is displayed which represents (at higher velocities) the actual whirl mode to compare. In table 5.1 the determined flutter velocities for the different cases at windmilling condition are summarised, as well as the modal assurance criterion for complex modes (MACX), which indicates the correlation of the compared modes [38]. Each MACX value is calculated between the HR-method and the respective TM-method used for mode 9 or 10 at the velocity V_D. For the $k_{scale} = 0.25$ case, mode 11 is used instead of mode 10 due to the mode switch. All values are close to 1, so the mode shapes are similar and they represent the correct modes to compare.

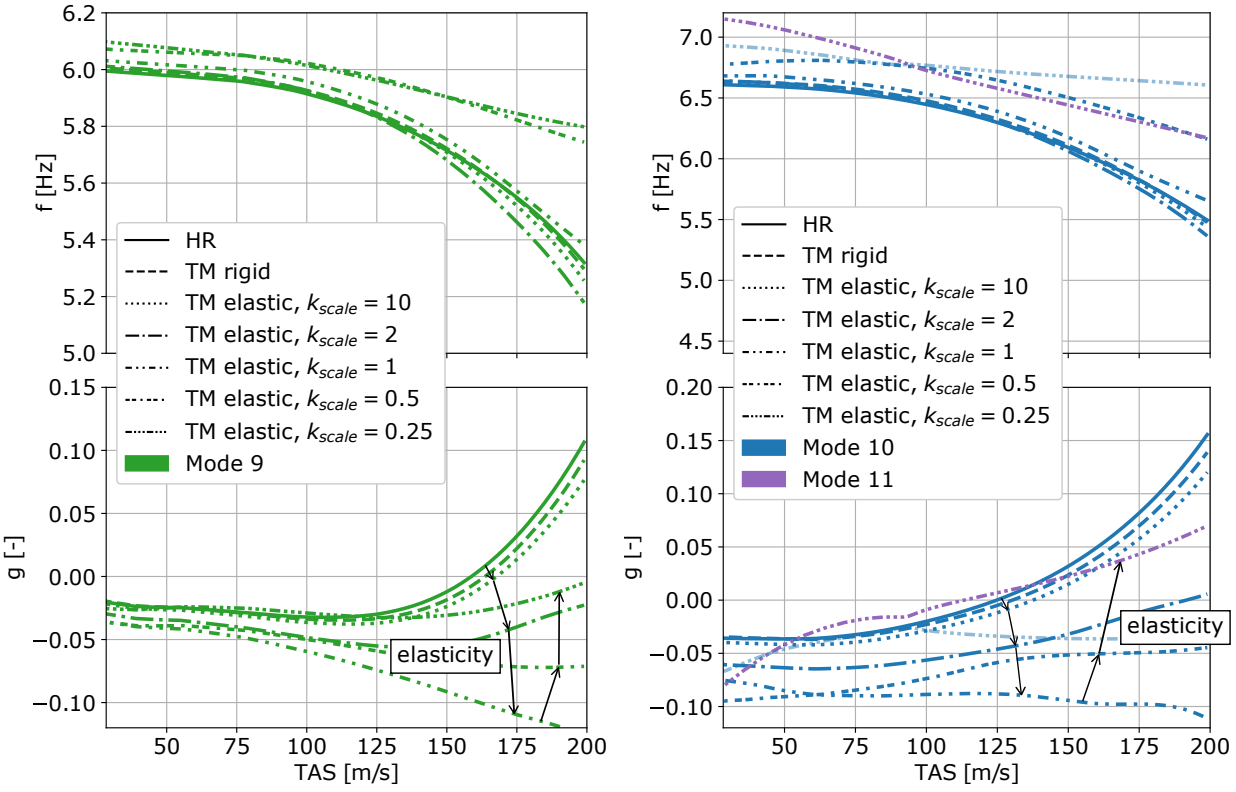

(a) Mode 9 (antisym. whirl)

(b) Mode 10 (sym. whirl)

Figure 5.6.: Influence of lower blade elasticity on frequency and damping of flutter modes of the Tuned WF model, windmilling condition

In figure 5.6, it can be seen that more flexible blade stiffness than nominal ($k_{scale} < 1$) results in a destabilisation of the system compared to the nominal case. This is true for both whirl modes. While the case with $k_{scale} = 0.5$ remains for both modes stable in the examined velocity range, the $k_{scale} = 0.25$ case reveals an instability in the symmetric whirl mode with a flutter speed of $V_F = 113.28\ m/s$. This is even lower than the HR-method result, which leads to the fact that for this blade property the HR approach would not be conservative anymore. However, the results for blades as flexible as this have to be handled with caution because, as already seen for the 2DOF model in section 3.3.3, the kind of instability seems to change for this cases and it has to be investigated further how the TM-method depicts this new effects. In this specific case, for $k_{scale} = 0.25$ even a few other new flutter modes appear on other structural modes. This can be seen in the full frequency and damping plots for all modes, as displayed in figure A.2 in the appendix. These new instabilities have not been examined any further. Additionally, it can also be seen that during the calculation one mode is lost at the beginning of the velocity range. But, as already observed for the 2DOF system, without further investigations on these new effects, it can be stated that the stabilisation due to blade elasticity seems to have a certain limit. The blade elasticity can not be increased over a certain extent without the risk of destabilisation of the system. Aircraft configurations with propeller blades with very low elasticity need to be handled with care. For detailed knowledge about the arising effects, further studies would be necessary.

	Sym. whirl mode (mode 10/11)		Antisym. whirl mode (mode 9)	
	$V_F\ [m/s]$	MACX	$V_F\ [m/s]$	MACX
HR	124.81	1.0 (Ref.)	158.77	1.0 (Ref.)
TM rigid	130.32	0.9995	163.64	0.9999
TM elastic, $k_{scale} = 10$	13764	0.9979	167.79	0.9998
TM elastic, $k_{scale} = 2$	191.64	0.9684	>200	0.9964
TM elastic, $k_{scale} = 1$	>200	0.9435	>200	0.9886
TM elastic, $k_{scale} = 0.5$	>200	0.9892	>200	0.9588
TM elastic, $k_{scale} = 0.25$	113.28	0.9961	>200	0.9684

Table 5.1.: Flutter velocities and MACX values for different propeller models for the Tuned WF model in windmilling condition, MACX calculated between each case and HR-method as reference at $V = V_D$

5.3.3. Influence of thrust

For the examination of the influence of thrust on the whirl flutter stability of the generic aircraft configuration, two trim conditions have been defined as explained already in section 3.1.3: the maximum power condition and the constant T/q condition.

Maximum power condition

First, the constant maximum power trim case is examined. The results are compared with the windmilling trim condition for the propeller model with rigid and elastic propeller

blades. Therefore, the frequency and damping values are plotted over the velocity and compared between the two conditions. In this section, only TM-method results are shown. The two, for the rigid propeller, unstable modes, mode 9 and mode 10, are highlighted in the different plots and are mainly compared in the study.

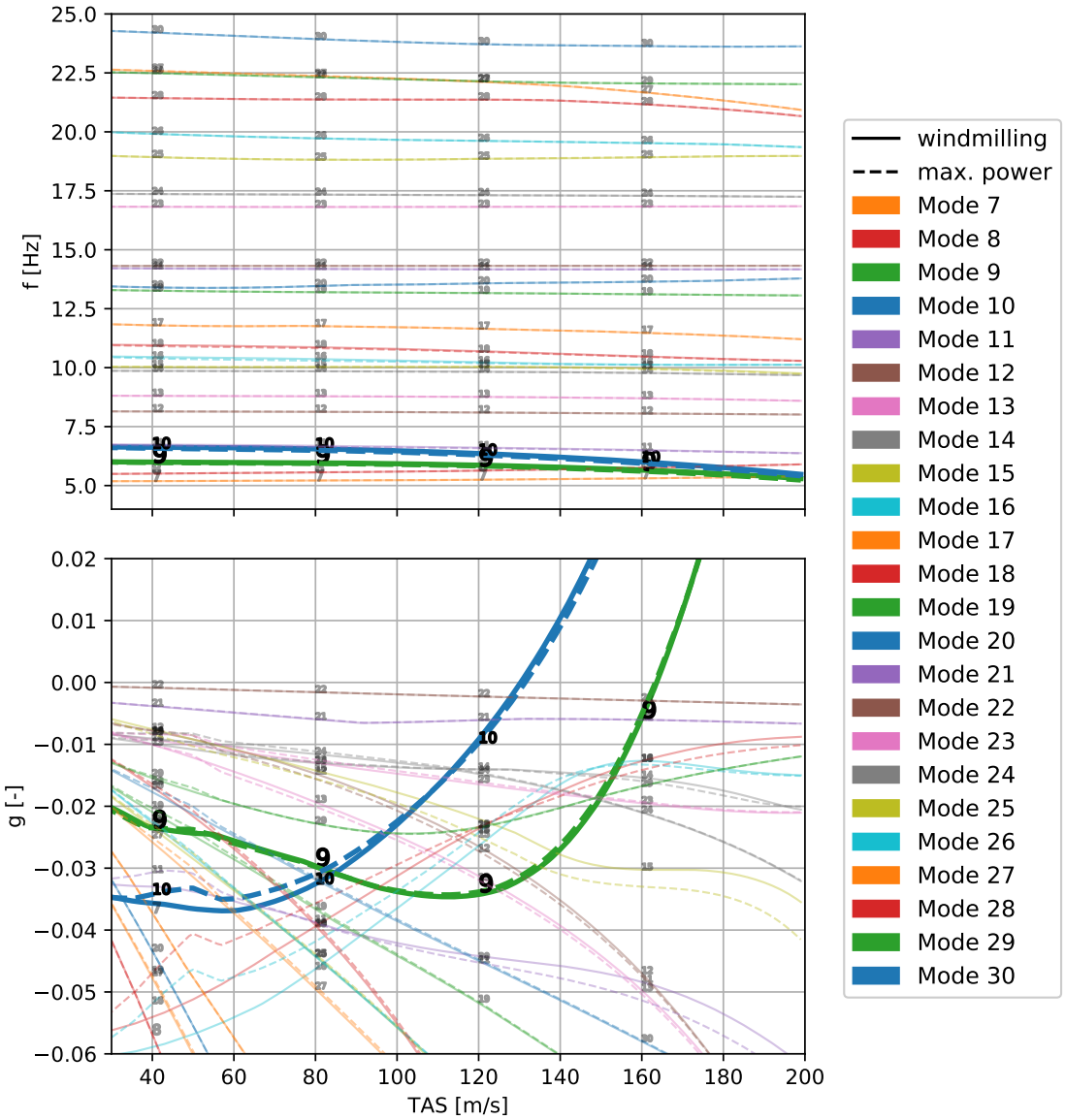

Figure 5.7.: Frequency and damping trends for the Tuned WF model with TM-method for rigid blades and different trim conditions, see figure 5.8 for close-up of damping at flutter point

In figure 5.7, the calculation results for the rigid propeller model are displayed. The top subplot shows the frequency trends. It can be noticed that the influence on the frequency is very low for all modes, even for the not highlighted ones. In the subplot below, the damping ratio g can be seen. The influence of thrust on damping is more noticeable (see e.g. mode 15), but especially for the unstable modes 9 and 10 no big differences appear. A closer view on the zero-crossing of the damping (the flutter points) for both unstable modes

is displayed in figure 5.8. In the left subplot (a), it can be seen that the flutter velocity for the unstable mode 9, which is the antisymmetric whirl mode, is slightly decreased due to thrust (from 163.64 m/s to 163.32 m/s, only -0.2%). In the right plot (b), the zero-crossing for mode 10 (symmetric whirl instability) is plotted. Different to mode 9 in (a), here it can be seen that the thrust has a slight stabilising effect. The flutter velocity increases from 130.32 m/s to 131.40 m/s. The difference is a bit higher than for the mode 9, but still the change is only approximately 0.83%.
So overall, the influence of thrust on the whirl flutter stability seems to be small, but not clearly stabilising or destabilising for this aircraft configuration with rigid propeller blades.

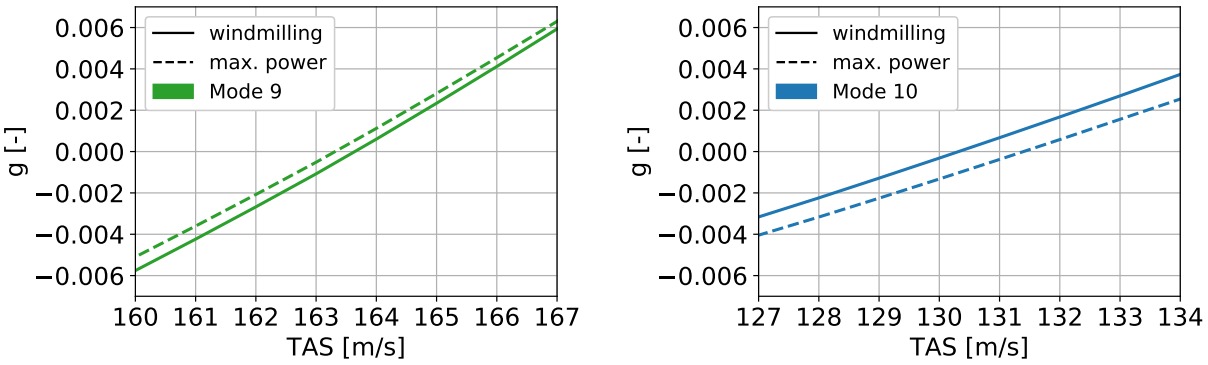

(a) Mode 9 (antisym. whirl) (b) Mode 10 (sym. whirl)

Figure 5.8.: Close-up of damping at flutter point for both flutter modes from figure 5.7

Now, the influence of thrust on the frequency and damping trends of the configuration with the elastic propeller blades is examined. The corresponding frequency and damping trends are displayed in figure 5.9. In this case, as for the elastic blade with $k_{scale} = 0.25$ from the previous section, a mode switch between mode 10 and 11 appears in the flutter solution. Therefore, here mode 11 is highlighted for the thrust case instead of mode 10. The effect of the thrust on the frequency trends are still low. But, in the lower subplot, it can bee seen for both highlighted modes that higher thrust has a significant influence on the damping level. g gets smaller over the full velocity range for both highlighted modes which means that they are more damped. The impact in the lower velocity range is larger than for higher velocities, except for the very low velocities up to approximately 50 m/s where the power is ramped up and not yet on full level. This appearance fits to the trim condition that leads to higher thrust at lower velocities to keep the power constant (see also figure 3.3). It needs to be remarked that due to the assumptions made in the g-method, the damping besides the flutter point is not determined exactly, so the difference in damping should not be interpreted too precisely.

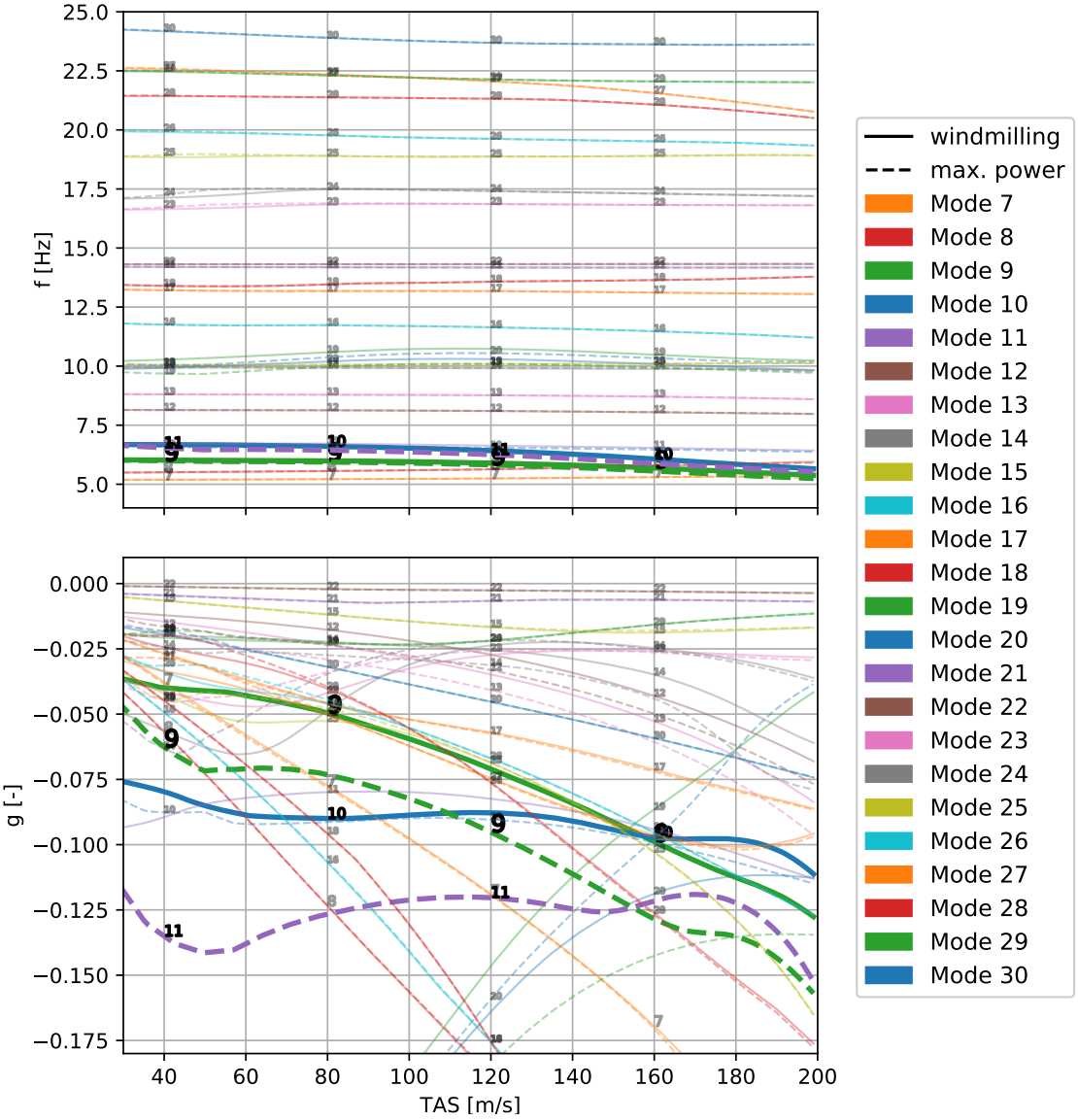

Figure 5.9.: Frequency and damping trends for the Tuned WF model with TM-method for elastic blades and different trim conditions

Consideration of the slipstream effect

The second trim condition with thrust has been established to enable integrating a correction factor for the propeller wake influence on the wing aerodynamics in the calculations. This factor has been determined by Rodden and Rose [10] and has been presented already in section 2.3.2:

$$w_{kk} = 1 + \frac{D}{\Delta y} \cdot \sqrt{1 + \frac{1}{\sqrt{1 + 2T/(\rho V^2 S)}}} \cdot \frac{\sqrt{2}T}{\rho V^2 S} \tag{5.2}$$

$$= 1 + \frac{D}{\Delta y} \cdot \sqrt{1 + \frac{1}{\sqrt{1 + T/(qS)}}} \cdot \frac{\sqrt{2}T}{2qS} \tag{5.3}$$

D determines the propeller radius and S the propeller area. Δy labels the width of the area where the factor is applied. It can be remarked that the factor depends on the flight velocity V, but remains constant for a constant ratio of thrust T to dynamic pressure q. Therefore, for the specific trim condition with constant T/q the factor remains constant over the velocity range. That makes it possible to implement the factor on the aerodynamic pressure coefficients in the flutter calculation using the CPFACT module from ZAERO [36].

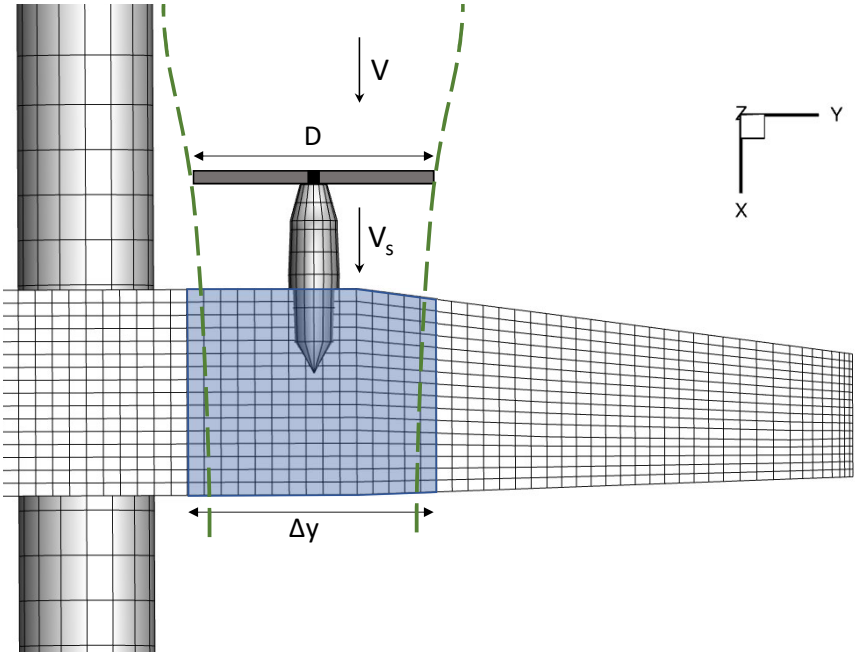

Figure 5.10.: Affected wing panels due to propeller slipstream

Figure 5.10 shows a sketch of the wake of the attached propeller (green dashed lines). In this area the propeller causes a higher stream velocity (marked as V_S in the picture) than the free stream velocity V. Without knowing the exact flow of the wake, for axial flight conditions, the possibly affected wing area is the area behind the propeller with a diameter of D. The definition from equation 5.3 is now used to identify the suitable correction factor w_{kk} for the generic aircraft configuration. This factor is then applied on selected aerodynamic panels of the ZAERO model of the aircraft. The propeller diameter is $D = 2.5\ m$ leading to a propeller area of $S = \pi \cdot (D/2)^2 = \pi \cdot (1.25\ m)^2 = 4.9087 m^2$. Δy is the width of the area where the factor is applied and arises from the total width of the selected aerodynamic panels. The panels are chosen such that the propeller wake behind the propeller is fully inside. In figure 5.10 the selected aerodynamic panels are highlighted. The panels have a total width of $\Delta y = 2.5712\ m$ and cover the propeller area and its wake. The T/q ratio is defined in the trim condition as $T/q = 0.2851 m^2$. This leads to a factor w_{kk} of:

$$w_{kk} \approx 1.056 \tag{5.4}$$

This factor is quite small. Therefore, it is expected that its influence on the flutter stability is also small.

Figure 5.11 shows the frequency and damping values over velocity for the windmilling propeller and the trim condition with constant T/q for the rigid propeller. Hereby, the trim with thrust is displayed with and without included slip stream correction factor. Figure 5.12 shows a close-up view on the flutter points of both unstable modes.

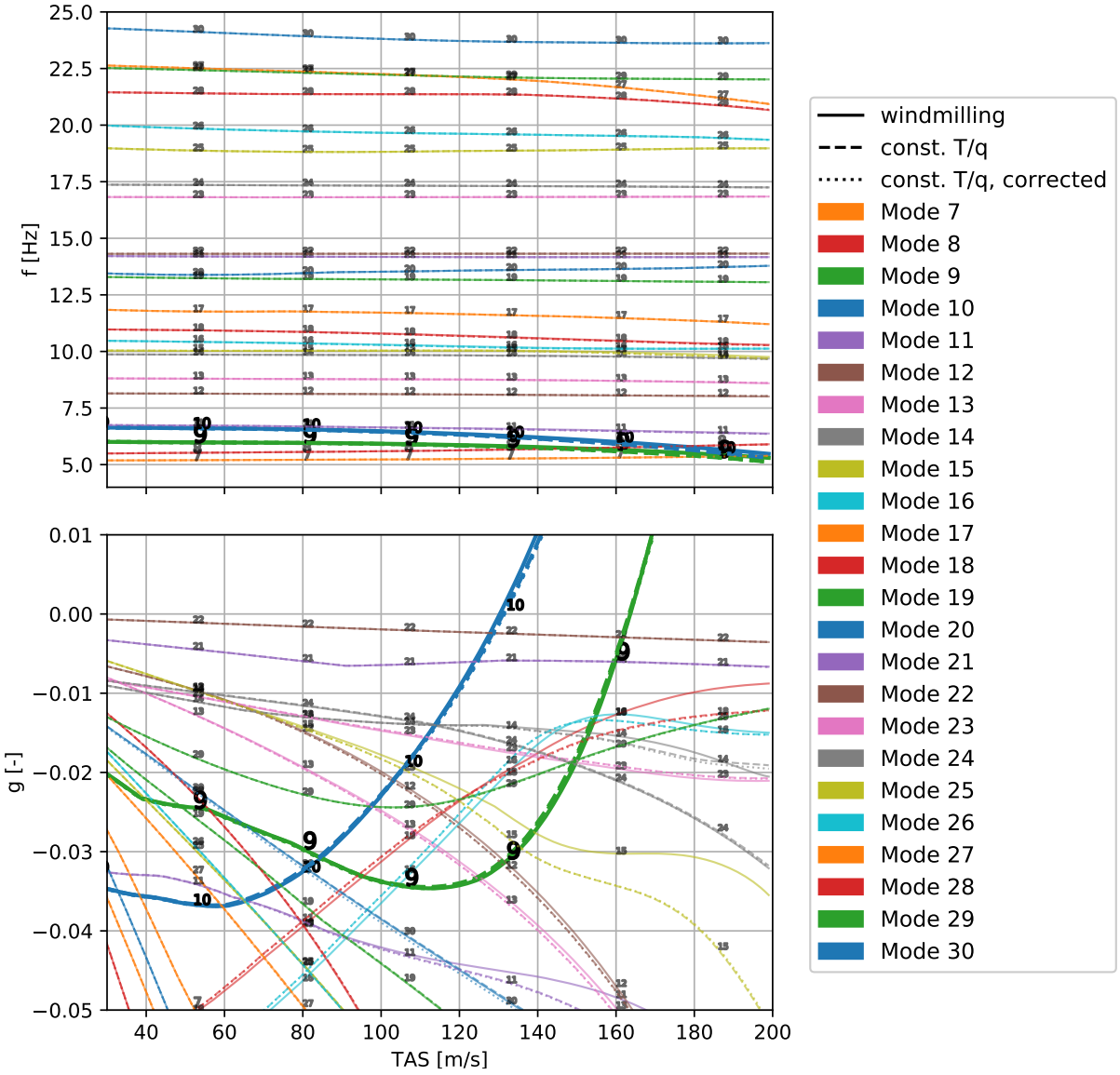

Figure 5.11.: Frequency and damping trends for the Tuned WF model with TM-method for rigid blades and different trim conditions (corrected = with slipstream correction), see figure 5.12 for close-up of damping at flutter point

First of all, it can be noticed in figure 5.11, comparing the dashed and dotted lines, that the influence of the slipstream correction on the frequency and damping values is for all modes, as expected, very low. That is the case, not only for the unstable modes 9 and 10, but also for the other modes that can be seen transparently in the background of the figure. In the close-up in figure 5.12, it can be observed that including the slipstream correction factor leads to slightly higher flutter speeds for both unstable modes. But, the difference is still very small.

Comparing the windmilling condition with the other two conditions with thrust, in this case again it can be seen that the thrust has a quite low effect on most modes. Especially, the unstable modes 9 and 10 show nearly no difference in frequency and damping and also the flutter velocities for both modes differ less than 1 % for the different trim conditions. Also, it can be seen in figure 5.12 that the impact of thrust is either destabilising (subplot (a), Mode 9) or stabilising (subplot (b), Mode 10) and the influence on Mode 10 is a bit higher than on Mode 9, just as for the maximum power condition.

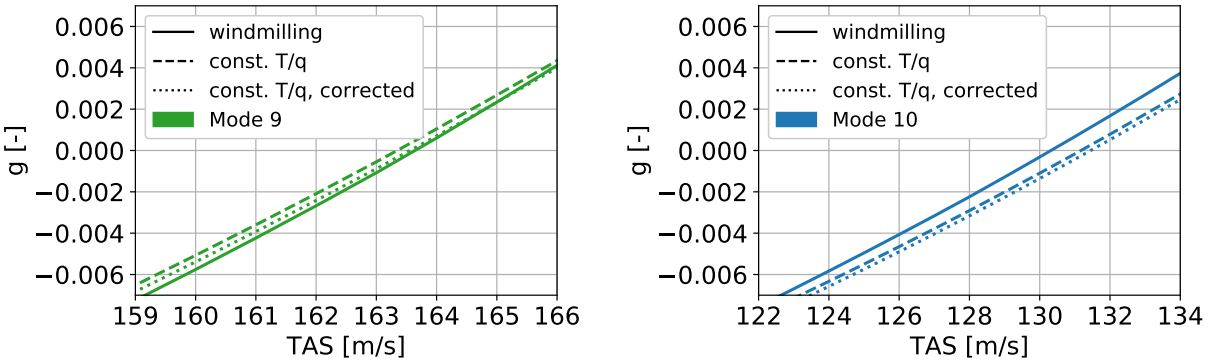

(a) Mode 9 (antisym. whirl)

(b) Mode 10 (sym. whirl)

Figure 5.12.: Close-up of damping at flutter point for both flutter modes from figure 5.11

Next, the stability analysis for the elastic propeller model with constant T/q trim is presented. Figure 5.13 shows again the frequency and damping trends. The modes that become unstable for the rigid propeller case are again highlighted. It can be seen that the correction according to the slipstream effect has still a small impact on the frequency and damping values. As for the maximum power trim with elastic propeller blades (see figure 5.9), here a higher thrust increases the damping for both modes 9 and 10. In this case, however, the effect is smaller in the lower velocity range and amplifies for higher velocities. This can be explained by the definition of the trim condition which leads to less thrust when the velocities are small to keep the thrust to dynamic pressure constant. Contrary to that, in the max. power trim, the thrust even increases for lower velocities to retain the desired constant power (compare figure 3.3).
The thrust to dynamic pressure ratio is relatively small. The assumed value for trim has been determined by taking the thrust and pressure value from the reference point at V_D. The effect of the slipstream correction might be larger for T/q values using the maximum thrust at lower velocities. As it can be seen in the lower right plot from figure 3.3, T/q becomes for the maximum power trim much higher at lower velocities. If the reference condition is not determined at V_D, but, for example, at the Design Manoeuvring Speed of $V_A = 72\ m/s$ of the aircraft, the ratio increases to a value of approximately $T/q = 2$. In this case the factor w_{kk} becomes 1.38. This is much higher than the calculated value before, but the influence of such a factor has not been tested because for whirl flutter usually a higher velocity range is relevant. But, for load analysis this factor might have a larger impact as those are performed also at lower velocities.

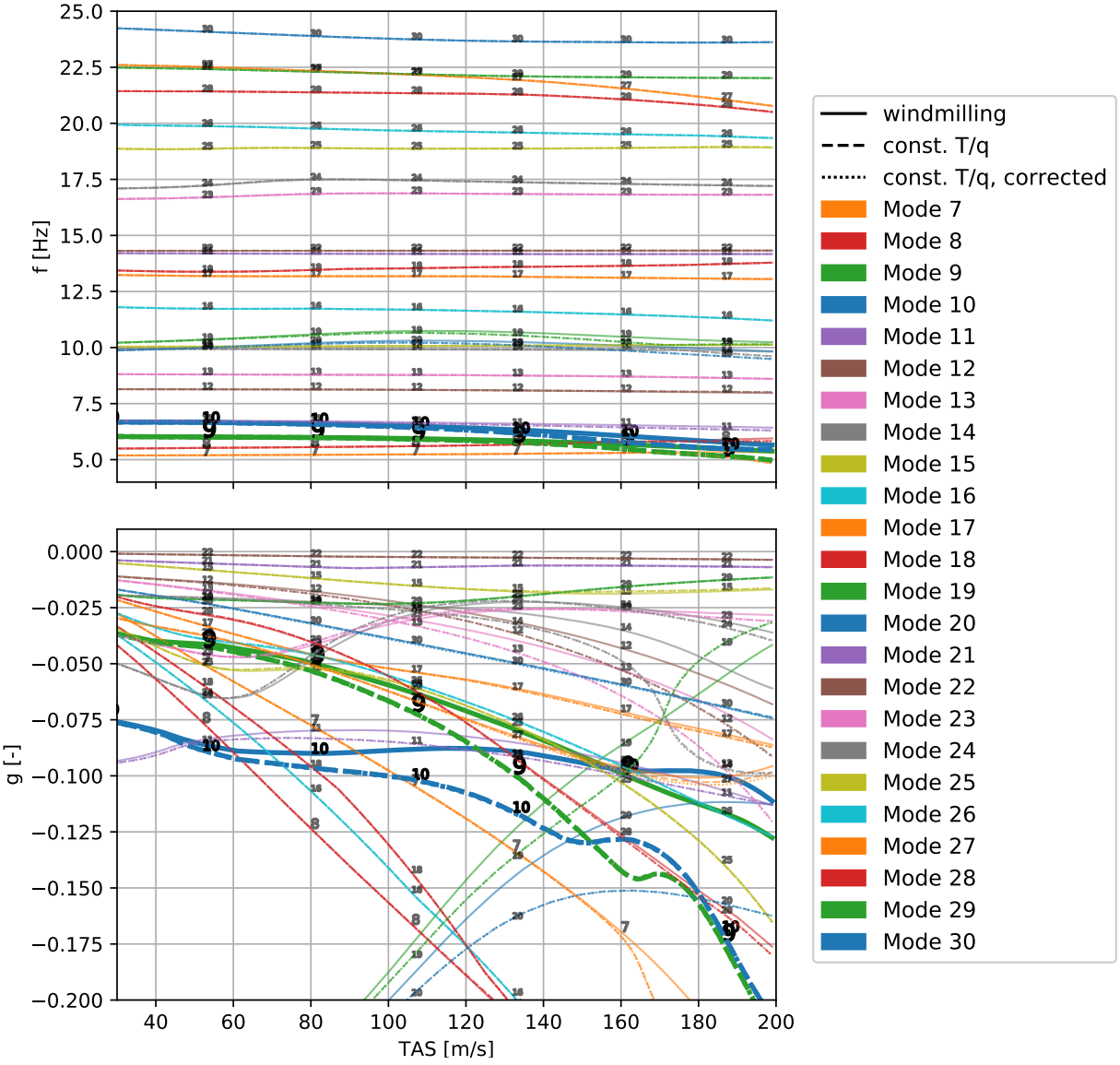

Figure 5.13.: Frequency and damping trends for the Tuned WF model with TM-method for elastic blades and different trim conditions (corrected = with slipstream correction)

5.4. Stability analyses with the Tuned BTF model

To evaluate the influence of the accuracy of propeller modelling on the flutter stability regarding other flutter phenomena, the Tuned BTF structural model has been created. The aeroelastic analysis of this model with the classical HR propeller approach shows a symmetrical bending-torsion flutter instability. The influence of the TM-method modelling with and without blade elasticity on this instability is shown in the following. After that, the influence of thrust is also studied.

As for the Tuned WF model, the influence of the mask definitions of the TM-method on the flutter results is small. No comparison plot is shown here, but as before, mask 1 is the most conservative approach and closest to the classical HR model results. Therefore, the

mask 1 definition is applied for all presented TM-method results in this section. The flutter speeds of all in the following analysed configurations are listed in table 5.2.

	V_F $[m/s]$		
Trim	HR	TM rigid	TM elastic, $k_{scale} = 1$
windmilling	159.84	160.39	162.34
max. power	-	160.18	164.13
const. T/q, without correction	-	160.08	164.99
const. T/q, with correction	-	160.14	164.98

Table 5.2.: Flutter velocities for the Tuned BTF model, different trim conditions and propeller modelling approaches

5.4.1. Influence of TM-method and blade elasticity

Figure 5.14 shows the results of flutter analysis for the Tuned BTF model with the HR propeller and the TM-method propeller for rigid and elastic propeller blades. All cases show the instability due to symmetrical bending-torsion flutter in Mode 11, which is therefore highlighted. For all three methods, there is no big difference in the frequency over the whole velocity range. Comparing the solid line (HR-method) and the dashed line (TM-method with rigid propeller) in the lower subplot shows that a difference in damping is present, but also small. The damping level is slightly higher for the TM-method results. The flutter speed is accordingly increased, but by less than 1 %, as can also be seen in the close-up on the zero-crossing of the curves. Having a look on the damping results for the elastic propeller modelling (dotted line) shows that the damping increases even more, especially in the lower velocity range. The flutter velocity is also increased, but the impact on that is still small (+1.22 %).
All in all, it can be noted that the influence of propeller blade elasticity on the bending-torsion flutter stability is much lower than on the whirl flutter stability. That is not so unexpected as this flutter mechanism is based on the motion of the whole wing and the propeller forces take only a small part in it. However, it still has a slight impact on the damping levels.

5.4.2. Influence of thrust

The rigid and elastic propeller modelling with the TM-method has also been examined regarding the impact of thrust on the wing bending-torsion flutter stability. In the following, both trim conditions with thrust (max. power and const. T/q) are compared together. Also the slipstream correction factor is applied in the analyses.
It could be noticed, that the overall impact on the flutter analyses with the rigid propeller model is marginal. Therefore, the detailed flutter results are not shown here. Only the resulting flutter speeds are listed in table 5.2. The comparison of the flutter speeds for the rigid propeller shows a slightly destabilising effect due to thrust. However, the change in flutter speed is very small (less than 0.2 % difference for all trim conditions), so the influence can be assumed as neglectable.

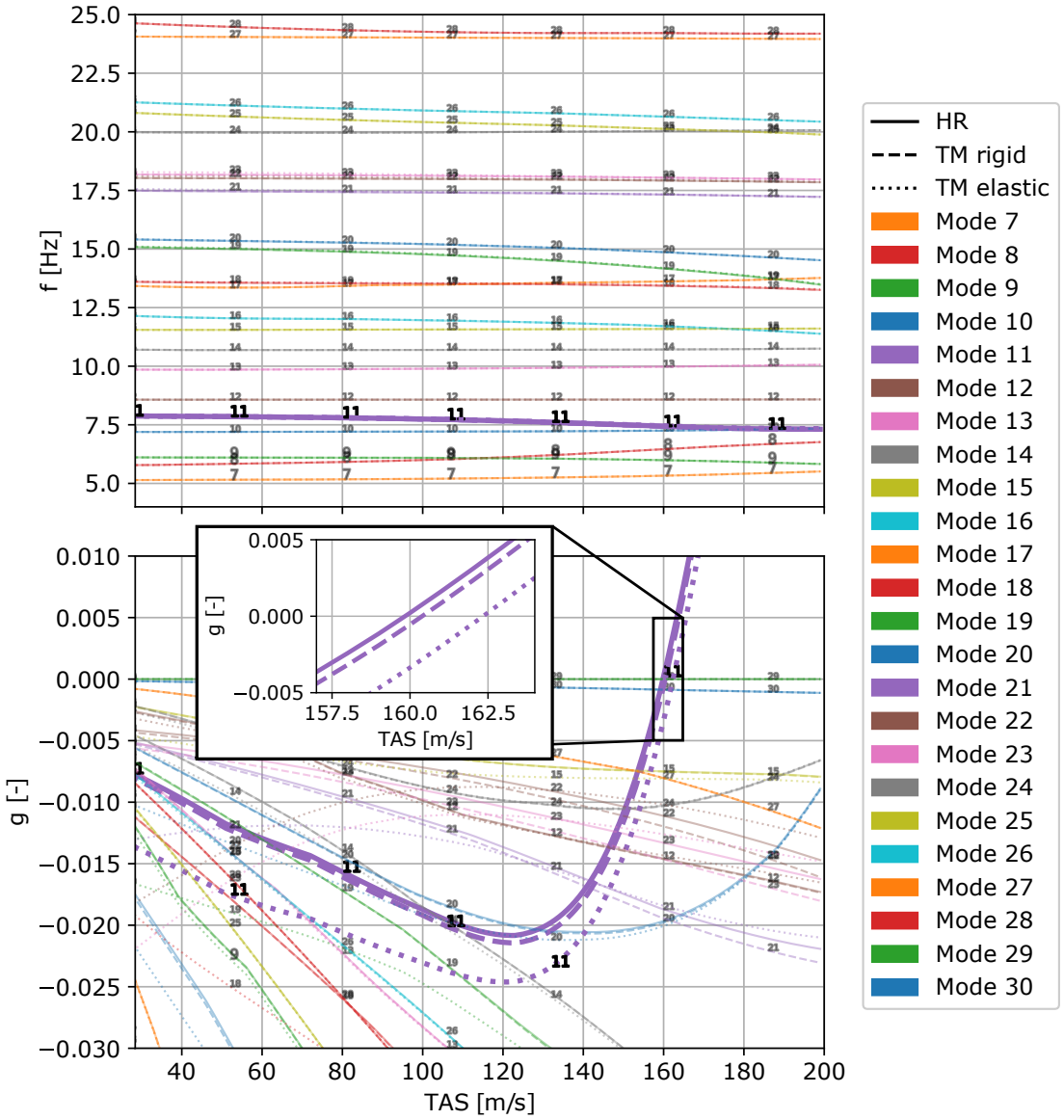

Figure 5.14.: Frequency and damping trends for the Tuned BTF model with HR- and TM-method for rigid and elastic blades, windmilling condition

Figure 5.15 shows the frequency and damping results for the elastic propeller analysis, with a close-up view on the flutter mode at the zero-crossing. No change in frequency, but a few differences in damping appear between the trim conditions.
First of all, no influence of the slipstream correction for the constant T/q trim can be noticed. In the flutter point, the two curves (dotted and dot-dashed) even overlap nearly exactly, leading to a difference in flutter speed of only 0.01 m/s which can be neglected. However, compared to the zero torque trim, the damping curves for the constant T/q trim show deviations. The biggest effect on damping can be found at around 130 m/s where the damping levels are the highest. At low velocities, the impact fades out, probably due to the low generated thrust at low velocities which comes from the definition of the trim condition. But, also close to the flutter point, the influence is small, even though the thrust is higher

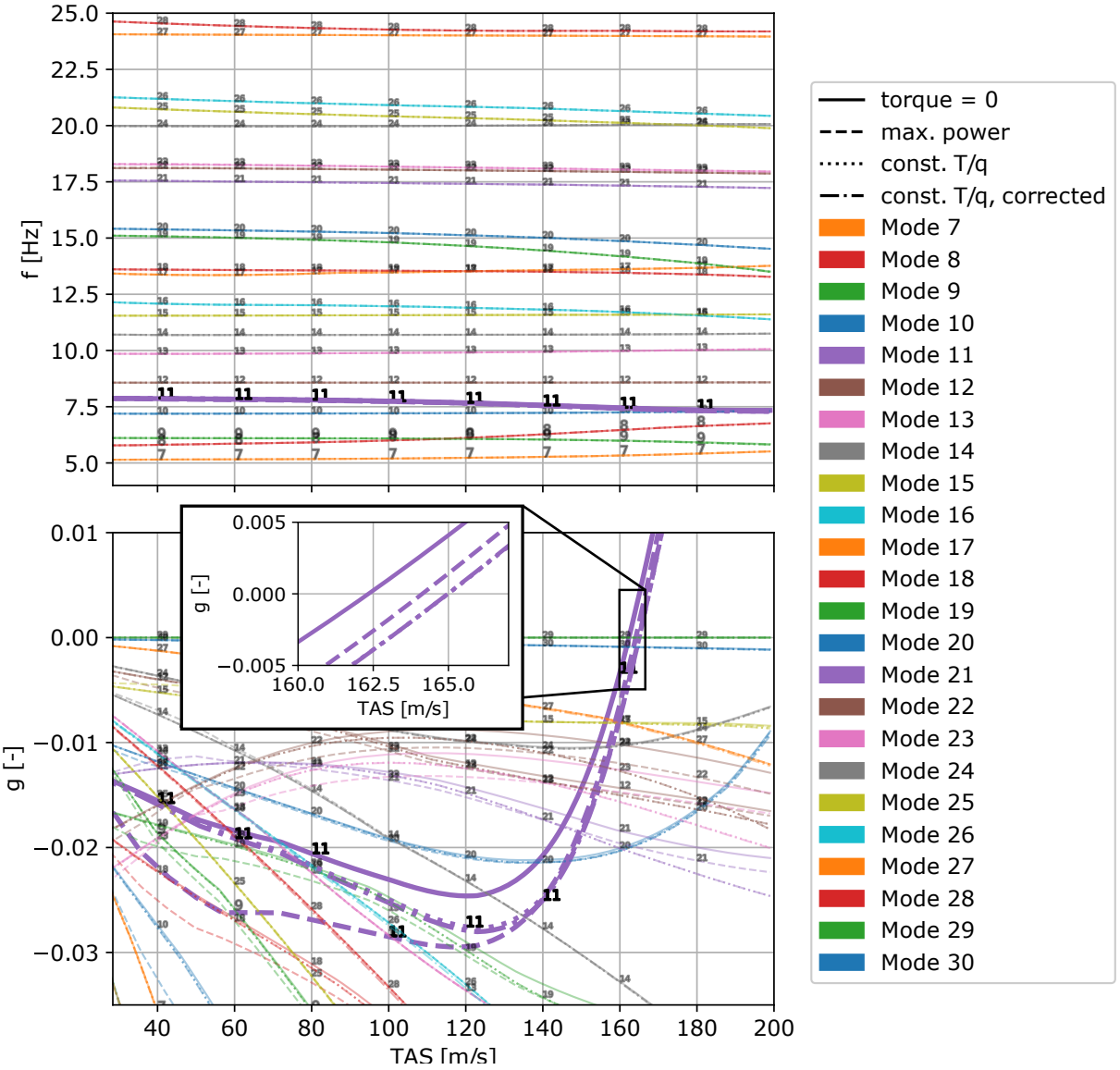

Figure 5.15.: Frequency and damping trends for the Tuned BTF model with TM-method for elastic blades and different trim conditions

at that point. The flutter speed increases only by 1.63 % compared to the windmilling condition. A possible explanation for that effect is that the impact of propeller thrust on the wing motion is smaller at higher velocities because there the aerodynamic forces on the whole wing are much higher.

The maximum power trim is represented in the plot by the dashed lines. It can be seen that, besides the velocity range where the power is still ramping up to full power, the impact of thrust becomes higher the smaller the velocity is. In this trim condition, the thrust is the highest at low velocities (see figure 3.3). Furthermore, in that range also the remaining aerodynamic forces on the wing are smaller. At the flutter point, the flutter speed is again only slightly increased by approximately 1.1 %.

To summarise, while the thrust does not affect the results with the rigid propeller model nearly at all, considering the thrust with elastic propeller blades increases the damping of the wing bending-torsion flutter mode and might lead to a slight stabilisation. But, the influence for higher velocities is low and the flutter point itself effectively does not change much. That is the case even for the maximum power trim, representing a upper limit for possible thrust conditions.

6. Conclusion and outlook

The aim of this thesis was to demonstrate the applicability of the TM-method for flutter stability analysis on full aircraft level and study the influence of this modelling approach on the stability results. The TM-method is capable of considering parameters, such as blade elasticity and thrust. Before this work, the TM-method has only been used for stability analyses of simple two degrees of freedom models of a single, isolated propeller. Even though some interesting insights, especially regarding the influence of blade elasticity on the whirl flutter stability, have already been gained by these investigations and could even be reproduced in preliminary studies on 2DOF level in this work, whirl flutter analysis on full aircraft level should show in this work that the detected stabilising effects also occur for complex aircraft configurations.

Before the stability analyses on the full aircraft could be performed, the TM-method as known from literature has been extended in this work to make it possible to apply the method on complex aircraft models. For that, three main modifications on the TM-method were introduced. First, the influence of propeller mass that derives from the mass of the elements in the time-domain model used for transfer-matrix generation has been successfully eliminated from the transfer-matrices. This development improves the applicability of the method for parameter studies with different structural configurations because the model of the structure usually already contains the propeller mass. So, the structural models do not need to be changed and the mass of the propellers is not accounted twice in the calculations neither. Furthermore, an interpolation routine for the transfer-matrices could be implemented in the process to make the number of velocity steps necessary for the transfer-matrix generation independent from those necessary for the flutter analysis. This brings a big advantage regarding the computational effort of the whole process because the transfer-matrix generation based on time-domain simulation is a time-consuming procedure and can now be performed for less velocity steps than necessary for the flutter analysis. Lastly, it was found that an alignment of the coordinate system of the transfer-matrices (determined by the time-domain simulation model) with the coordinate system of the structural model was necessary to gain correct flutter results. This problem has been solved by deriving transformation matrices that can be multiplied with the transfer-matrices before integrating them in the flutter calculation.
Similar adaptions were necessary for the classical HR-method, because the implemented definition of the propeller derivatives differed from the coordinate system definition of the examined full aircraft model. Additionally, also the propeller rotation direction was different. For both deviations, also transformation matrices for the propeller stiffness and damping matrices could be derived and implemented in the calculation procedure to solve the issue.

The performed whirl flutter stability analyses revealed that the stabilising effect due to blade elasticity occurs not only for the 2DOF model, but also on full aircraft level. The flutter results have been stabilised by incorporating the blade elasticity with the TM-method in

the calculations. Investigations on the 2DOF model showed further that this stabilising effect is based on the blade deformation changing occurring forces and moments, as already stated in literature. It could be demonstrated for a 2DOF system with constant polar inertia that scaling the blade eigenfrequency by the blade stiffness has a much greater effect on the whirl flutter stability than scaling the blade mass. However, for both the 2DOF model and the full aircraft model, it could be observed that the stabilising effect due to higher blade elasticity has a certain limit. For very low stiffness values, the system becomes unstable again. Because the whirl flutter stability map of the 2DOF model changes strongly in shape compared to the nominal blade stiffness case, the assumption arises that the instability mechanism changes for these configurations. Further examinations would be necessary to gain detailed knowledge about the effect, but have not been performed in this work. For that, also other methods should to be used to verify that the TM-method results are fully reliable for these new effects. Still, it can be concluded that the stabilisation due to blade elasticity seems to be only exploitable up to a certain extent and aircraft with propellers with very low blade stiffness need to be handled with care.

For the influence on thrust, it could be determined that thrust has a low impact on flutter stability of the full aircraft configuration for rigid propeller blades. The examination showed even different tendencies for the two present whirl modes, one has been slightly stabilised and the other destabilised. In contrast to that, for the elastic propeller modelling, the higher thrust increases the damping of all whirl modes.
Two trim conditions have been used for the investigations, from which similar results for the impact of thrust on stability could be derived. One of the trim conditions has also been used to examine a slipstream correction factor defined in literature to consider the effect of the propeller wake on the wing aerodynamics in the calculations. This correction factor was shown to be relatively low for the determined trim condition. Analogously, it appeared to have nearly no impact on the aeroelastic stability of the system. The correction factor might be relevant for other design aspects, such as loads analysis, though. Furthermore, it needs to be remarked that only the effect of the propeller wake on the axial velocities on the wing has been taken into account. Neither the tangential velocity impact, nor the opposed influence of the wing aerodynamics on the propeller have been considered. These effects might increase the influence of the propeller-wing interaction on stability and could be an issue of future work.

Investigations on bending-torsion flutter showed that the propeller modelling has a much lower influence on this flutter instability for the given aircraft configuration. Especially for higher velocities, at which also the flutter point of this model appears, the damping only differs little between the results from HR-method and TM-method with rigid or elastic blades. For lower velocities, the impact of blade elasticity on the damping level is a bit higher (towards higher damping for elastic blades).
The influence of higher thrust conditions is similar. While for rigid blades, thrust has a neglectable impact on the frequency and damping trends, for elastic blades, there is a noticeable effect on damping level, but again mostly for the lower velocities. The flutter point is not really shifted due to thrust. Also, the slipstream correction factor applied has proven to have no impact on bending-torsion flutter.

However, the different aspects might have a greater influence on bending-torsion flutter for different overall aircraft configurations.

All in all, the analyses with the generic aircraft configuration showed that the TM-method has been successfully modified to enable its application on complex aircraft models in an efficient way, as it has been the aim of the thesis. It can be concluded that the effects detected on the 2DOF model still occur on full aircraft level. While thrust has a lower impact, considering blade elasticity increases the whirl flutter stability range decisively. Therefore, the TM-method results indeed reveal an additional margin of flutter stability compared to the more conservative HR-method results on full aircraft level. It seems favourable to exploit that in the aircraft design to optimise the overall aircraft configuration. However, the found results need to be validated either experimentally or by validation studies with aerodynamic modelling on higher fidelity levels. In practical applications, the aircraft aerodynamic also needs to be modelled via more sophisticated modelling approaches, which could also capture aerodynamic interaction with the propeller directly. Additional work could also target more detailed investigations on the origin of the stabilising effect, for example by analysing the impact of more specific blade properties than the general scaled stiffness to increase understanding and enable directed use of the effects by changing specific blade properties. For future work, there is also a big potential for integrating more accurate aerodynamic propeller modelling in the process to investigate the effects of non-axial flow, inflow, propeller wake and more on the flutter stability.

Bibliography

[1] Long term global aspirational goal (LTAG) for international aviation, . URL https://www.icao.int/environmental-protection/Pages/ClimateChange_Trends.aspx. Accessed: 2023-11-14.

[2] Reducing emissions from aviation. URL https://climate.ec.europa.eu/eu-action/transport/reducing-emissions-aviation_en#aviation-emissions. Accessed: 2023-11-14.

[3] Trends in Emissions that affect Climate Change, . URL https://www.icao.int/environmental-protection/Pages/LTAG.aspx. Accessed: 2023-11-14.

[4] Ideen für elektrische Flugzuegantriebe von morgen. URL https://www.dlr.de/de/forschung-und-transfer/themen/emissionsfreies-fliegen/wie-gelingt-die-energiewende-in-der-luftfahrt-ideen-fuer-elektrische-flugzuegantriebe-von-morgen. Accessed: 2023-11-14.

[5] W.H. Reed. Propeller-rotor whirl flutter: A state-of-the-art review. *Journal of Sound and Vibration*, 4(3):526–544, November 1966. ISSN 0022460X. doi: 10.1016/0022-460X(66)90142-8. URL https://linkinghub.elsevier.com/retrieve/pii/0022460X66901428.

[6] C. Koch and B. Koert. Including Blade Elasticity into Frequency-Domain Propeller Whirl Flutter Analysis. *Journal of Aircraft*, pages 1–11, October 2023. doi: 10.2514/1.C037501. URL https://doi.org/10.2514/1.C037501.

[7] C. Koch. WHIRL FLUTTER STABILITY ASSESSMENT USING ROTOR TRANSFER MATRICES. In *International Forum on Aeroelasticity and Structural Dynamics (IFASD) 2022*, Madrid, Spain, June 2022.

[8] J.C. Houbolt and W.H. Reed III. Propeller-nacelle whirl flutter. *Journal of the Aerospace Sciences*, 29(3):333–346, 1962.

[9] S.R. Bland and R.M. Bennett. Wind-tunnel measurements of propeller whirl-flutter speeds and static-stability derivatives and comparison with theory. NASA Technical Note NASA TN D-1807, Langley Station, Hampton, Va., August 1963.

[10] W.P. Rodden and T.L. Rose. Propeller/nacelle whirl flutter addition to MSC/NASTRAN. In *Proceedings of the 1989 MSC World User's Conference*, 1989.

[11] J. Cecrdle. Whirl flutter-related certification according to FAR/CS 23 and 25 regulation standards. In *International Forum on Aeroelasticity and Structural Dynamics 2019, IFASD 2019*, Savannah, GA (USA), June 2019. URL https://www.scopus.com/inward/record.uri?eid=2-s2.0-85082242391&partnerID=40&md5=2a06c166ea4ab937227d55b3b6246ba1.

[12] M.I. Young and R.T. Lytwyn. The Influence of Blade Flapping Restraint on the Dynamic Stability of Low Disk Loading Propeller-Rotors. *Journal of the American Helicopter Society*, 12(4):38–54, 1967.

[13] R.A. Johnston. Parametric Studies of instabilities associated with large, flexible rotor propellers. In *28th Annual National Forum of the American Helicopter Society*, Washington, D.C., May 1972. American Helicopter Society.

[14] W. Johnson. Dynamics of tilting proprotor aircraft in cruise flight. NASA Technical Note NASA TN D-7677, NASA, May 1974.

[15] J. Shen, P. Masarati, B. Roget, D.J. Piatak, J.D. Singleton, and M.W. Nixon. Modeling a stiff-inplane tiltrotor using two multibody analyses: A validation study. In *Annual Forum Proceedings - AHS International*, volume 3, pages 2307–2315, 2008. URL https://www.scopus.com/inward/record.uri?eid=2-s2.0-50049105267&partnerID=40&md5=5c1854f68e7093e5e3b71c3cac2ed718.

[16] C.B. Hoover, J. Shen, and A.R. Kreshock. Propeller Whirl Flutter Stability and Its Influence on X-57 Aircraft Design. *Journal of Aircraft*, 55(5):2169–2175, September 2018. ISSN 0021-8669, 1533-3868. doi: 10.2514/1.C034950. URL https://arc.aiaa.org/doi/10.2514/1.C034950.

[17] C.B. Hoover and J. Shen. Parametric Study of Propeller Whirl Flutter Stability with Full-Span Model of X-57 Maxwell Aircraft. *Journal of Aircraft*, 55(6):2530–2537, November 2018. ISSN 0021-8669, 1533-3868. doi: 10.2514/1.C035081. URL https://arc.aiaa.org/doi/10.2514/1.C035081.

[18] H. Yeo and A.R. Kreshock. Whirl Flutter Investigation of Hingeless Proprotors. *Journal of Aircraft*, pages 1–11, March 2020. ISSN 1533-3868. doi: 10.2514/1.C035609. URL https://arc.aiaa.org/doi/10.2514/1.C035609.

[19] R.E. Donham and D.J. Osterholt. Utilizing test results to show adding flexibility of propeller blades is more representative than the classical rigid blade propeller whirl flutter analysis. In *Proceedings of International Forum on Aeroelasticity and Structural Dynamics (IFASD)*, pages 18–20, Stockholm, Sweden, 2007.

[20] Z. Wang and P.C. Chen. Whirl flutter analysis with propeller aerodynamic derivatives computed by unsteady vortex lattice method. In *56th AIAA/ASCE/AHS/ASC Structures, Structural Dynamics, and Materials Conference*, Kissimmee, Florida, 2015. American Institute of Aeronautics and Astronautics. doi: 10.2514/6.2015-1419. URL https://www.scopus.com/inward/record.uri?eid=2-s2.0-84937945388&partnerID=40&md5=25d9da500ced2527e096deef1e00db18.

[21] M. Gennaretti and L. Greco. Time-Dependent Coefficient Reduced-Order Model for Unsteady Aerodynamics of Proprotors. *Journal of Aircraft*, 42(1):138–147, January 2005. ISSN 0021-8669, 1533-3868. doi: 10.2514/1.4817. URL https://arc.aiaa.org/doi/10.2514/1.4817.

[22] M. Gennaretti and L. Greco. Whirl flutter analysis of prop-rotors using unsteady aerodynamics reduced-order models. *The Aeronautical Journal*, 112(1131):261–270, May 2008. ISSN 0001-9240, 2059-6464. doi: 10.1017/S0001924000002207. URL https://www.cambridge.org/core/product/identifier/S0001924000002207/type/journal_article.

[23] J. Serafini, M. Molica Colella, and M. Gennaretti. A finite-state aeroelastic model for rotorcraft–pilot coupling analysis. *CEAS Aeronautical Journal*, 5(1):1–11, March 2014. ISSN 1869-5582, 1869-5590. doi: 10.1007/s13272-013-0086-8. URL http://link.springer.com/10.1007/s13272-013-0086-8.

[24] R. Gori, J. Serafini, M. Molica Colella, and M. Gennaretti. Assessment of a state-space aeroelastic rotor model for rotorcraft flight dynamics. *CEAS Aeronautical Journal*, 7(3):405–418, September 2016. ISSN 1869-5582, 1869-5590. doi: 10.1007/s13272-016-0196-1. URL http://link.springer.com/10.1007/s13272-016-0196-1.

[25] Prof. Dr.-Ing. L. Tichy. Lecture notes "Einführung in die Aeroelastik 1", TU Braunschweig, Version WiSe 2017/18.

[26] J. Schwochow. Die aeroelastische Stabilitätsanalyse - ein praxisnaher Ansatz zur intervalltheoretischen Betrachtung von Modellierungsunsicherheiten am Flugzeug. Technical Report DLR-FB-2012-21, 2013.

[27] H.W. Försching. *Grundlagen der Aeroelastik*. Springer Verlag, 1974. ISBN 978-3-642-48285-4. doi: 10.1007/978-3-642-48285-4.

[28] H.J. Hassig. An approximate true damping solution of the flutter equation by determinant iteration. *Journal of Aircraft*, 8(11):885–889, November 1971. ISSN 0021-8669, 1533-3868. doi: 10.2514/3.44311. URL https://arc.aiaa.org/doi/10.2514/3.44311.

[29] P. C. Chen. Damping Perturbation Method for Flutter Solution: The g-Method. *AIAA Journal*, 38(9):1519–1524, September 2000. ISSN 0001-1452, 1533-385X. doi: 10.2514/2.1171. URL https://arc.aiaa.org/doi/10.2514/2.1171.

[30] J. Cecrdle. *Whirl Flutter of Turboprop Aircraft Structures*. Elsevier, 2015. ISBN 978-1-78242-185-6. doi: 10.1016/B978-1-78242-185-6.50017-9.

[31] C. Koch. Parametric whirl flutter study using different modelling approaches. *CEAS Aeronautical Journal*, 13:57–67, October 2021. ISSN 1869-5582, 1869-5590. doi: 10.1007/s13272-021-00548-0. URL https://link.springer.com/10.1007/s13272-021-00548-0.

[32] B. Koert. Einfluss von Blattelastizität auf die Whirl-Flatter-Stabilität von Propellerkonfigurationen, 2022. Master thesis.

[33] Hexagon AB. *MSC Nastran 2022.3 Quick Reference Guide*, 2022.

[34] Dassault Systemes. *SIMULIA Simpack 2023 Refresh 2*, 2023. URL https://www.3ds.com/de/produkte-und-services/simulia/produkte/simpack.

[35] F. Hitchens. *Propeller Aerodynamics : The History, Aerodynamics & Operation of Aircraft Propellers*. Andrews UK Ltd., 2015. URL http://ebookcentral.proquest.com/lib/dlr-ebooks/detail.action?docID=4460965.

[36] ZONA Technology Inc. *ZAERO User's Manual, Version 9.3*, 2020. URL https://www.zonatech.com/Documentation/ZAERO_9.3_Users_Full_Electronic.pdf.

[37] ZONA Technology Inc. *ZAERO Theoretical Manual, Version 9.3*, 2020. URL https://www.zonatech.com/Documentation/ZAERO%209.3_THEO_Full_Electronic.pdf.

[38] P Vacher, B Jacquier, and A Bucharles. Extensions of the MAC criterion to complex modes. In *Proceedings of the international conference on noise and vibration engineering*, pages 2713–2726. ISMA Leuven, Belgium, 2010.

List of Tables

List of Figures

A. Appendix

A.1. Transformation of propeller matrices for HR-method

Following the derivations from Cecrdle's book about whirl flutter [30], the different elements of the propeller matrices $\underline{K}_{prop}$ and $\underline{D}_{prop}$ can be derived analytically. To align the determined propeller matrices on different propeller orientations than the classical HR-method assumption, transformation matrices are derived and presented in section 4.2. To determine the transformation matrices for the propeller matrices, the derivation for other orientations are stated and compared with the classical definitions. In the following, the derivation for the transformation matrix to turn the rotational direction is presented shortly.
To derive the propeller matrices, the aerodynamic forces and moments in the coordinate directions y and z are determined dependant on the velocities and displacements in and around these axis. In the following, only the quasi-steady derivation is shown. For the full transformation matrices as shown in section 4.2 also the lift lag effect needs to be incorporated which can be performed similar. For the derivation, a four-bladed propeller is considered as displayed in figure A.1. In the figure two cases, the classical HR-method definition (a) and the case with opposite propeller rotation direction (b), can be seen. In the upper part of the subplots, the propeller area is displayed as viewed from the front. For both cases, the x-axis points vertically out of the page, as well as the velocity V_∞ (directed in flight direction). In the lower part of the subplots, a section of one blade (labelled as "Blade 1" in the upper plot) is displayed with all occurring velocities and forces.

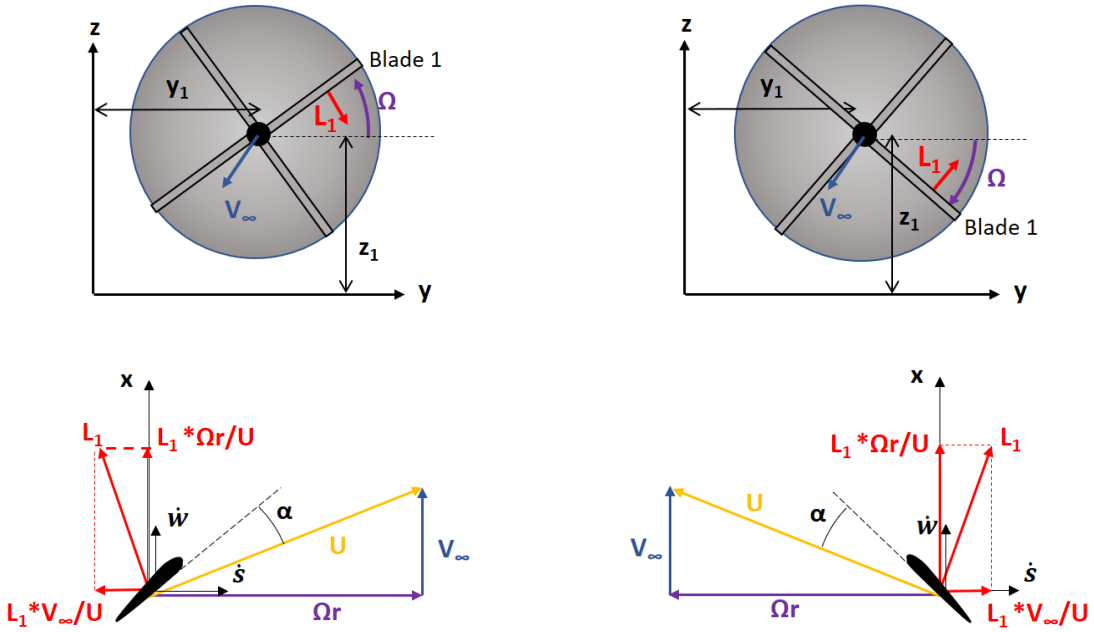

(a) Classical HR definition

(b) Opposite rotation direction

Figure A.1.: Orientation of propeller and blade section for the derivation of the propeller matrices

The perturbations due to a local blade angle of attack α_1, a velocity in the propeller plane $\dot{s}$ and a velocity out of the propeller plane $\dot{w}$ are considered. The propeller plane is pitching and yawing around the hub leading to these perturbations at a blade section. With the definitions from figure A.1 following definitions can be determined:

Classical HR definition:

$$\begin{aligned}
\alpha_1 &= \psi \cdot sin(\Omega t) + \theta \cdot cos(\Omega t) \\
y &= y_1 + r \cdot cos(\Omega t) \\
z &= z_1 + r \cdot sin(\Omega t) \\
w_1 &= -\psi \cdot r \cdot cos(\Omega t) + \theta \cdot r \cdot sin(\Omega t) \\
\\
\dot{s} &= -\dot{y} \cdot sin(\Omega t) + \dot{z} \cdot cos(\Omega t) \\
\dot{w} &= \Omega\theta r \cdot cos(\Omega t) + \dot{\theta} r \cdot sin(\Omega t) \\
&\quad + \psi r\Omega \cdot sin(\Omega t) - \dot{\psi} r \cdot cos(\Omega t)
\end{aligned}$$

Opposite rotation direction:

$$\begin{aligned}
\alpha_1 &= \psi \cdot sin(\Omega t) - \theta \cdot cos(\Omega t) \\
y &= y_1 + r \cdot cos(\Omega t) \\
z &= z_1 - r \cdot sin(\Omega t) \\
w_1 &= -\psi \cdot r \cdot cos(\Omega t) - \theta \cdot r \cdot sin(\Omega t) \\
\\
\dot{s} &= +\dot{y} \cdot sin(\Omega t) + \dot{z} \cdot cos(\Omega t) \\
\dot{w} &= -\Omega\theta r \cdot cos(\Omega t) - \dot{\theta} r \cdot sin(\Omega t) \\
&\quad + \psi r\Omega \cdot sin(\Omega t) - \dot{\psi} r \cdot cos(\Omega t)
\end{aligned}$$

All these perturbations together with the inflow from propeller rotation and airstream velocity and the stationary blade angle of attack α_0 determine the effective angle of attack α_{eff} and inflow of the blade section U_{eff}:

Classical HR definition:

$$\begin{aligned}
\alpha_{eff} &= \alpha_0 + \alpha_1 - \dot{w} \cdot \frac{\Omega r}{U^2} + \dot{s} \cdot \frac{V_\infty}{U^2} \\
U_{eff} &= U + \dot{w} \cdot \frac{V_\infty}{U} + \dot{s} \cdot \frac{\Omega r}{U}
\end{aligned}$$

Opposite rotation direction:

$$\begin{aligned}
\alpha_{eff} &= \alpha_0 + \alpha_1 - \dot{w} \cdot \frac{\Omega r}{U^2} - \dot{s} \cdot \frac{V_\infty}{U^2} \\
U_{eff} &= U + \dot{w} \cdot \frac{V_\infty}{U} - \dot{s} \cdot \frac{\Omega r}{U}
\end{aligned}$$

With this velocity and angle of attack, the lift of the blade section $L1$ can be determined, for a blade section with a lift curve slope of a_0 and an airfoil chord of c_0:

Classical HR definition:

$$\begin{aligned}
L1 &= \frac{1}{2} a_0 \rho c_0 U_{eff}^2 \alpha_{eff} \\
&= \frac{1}{2} a_0 \rho c_0 [(V_\infty^2 \psi - \Omega\dot{\theta} r^2 - V_\infty \dot{y}) \cdot sin(\Omega t) \\
&\quad + (V_\infty^2 \theta + \Omega r^2 \dot{\psi} + \dot{z} V_\infty) \cdot cos(\Omega t)]
\end{aligned}$$

Opposite rotation direction:

$$\begin{aligned}
L1 &= \frac{1}{2} a_0 \rho c_0 U_{eff}^2 \alpha_{eff} \\
&= \frac{1}{2} a_0 \rho c_0 [(V_\infty^2 \psi + \Omega\dot{\theta} r^2 - V_\infty \dot{y}) \cdot sin(\Omega t) \\
&\quad + (-V_\infty^2 \theta + \Omega r^2 \dot{\psi} - \dot{z} V_\infty) \cdot cos(\Omega t)]
\end{aligned}$$

This lift force $L1$ that can be separated in an in-plane and an out-of-plane component, as already seen in the lower parts of figure A.1. The lift forces generated by the other propeller blades can be determined similarly. All lift force components of the four propeller blades can be summed up to propeller hub forces and moments in and around the y- and z-axis and a few further conversions lead to these definitions for the sectional forces and moments:

Classical HR definition:

$$\Delta L_y = \frac{V_\infty}{U}\rho a_0 c_0 (V_\infty^2 \psi - \Omega \dot{\theta} r^2 - V_\infty \dot{y})$$
$$\Delta L_z = \frac{V_\infty}{U}\rho a_0 c_0 (-V_\infty^2 \theta - \Omega \dot{\psi} r^2 - V_\infty \dot{z})$$
$$\Delta M_y = \frac{\Omega r^2}{U}\rho a_0 c_0 (V_\infty^2 \psi - \Omega \dot{\theta} r^2 - V_\infty \dot{y})$$
$$\Delta M_z = \frac{\Omega r^2}{U}\rho a_0 c_0 (-V_\infty^2 \theta - \Omega \dot{\psi} r^2 - V_\infty \dot{z})$$

Opposite rotation direction:

$$\Delta L_y = \frac{V_\infty}{U}\rho a_0 c_0 (V_\infty^2 \psi + \Omega \dot{\theta} r^2 - V_\infty \dot{y})$$
$$\Delta L_z = \frac{V_\infty}{U}\rho a_0 c_0 (-V_\infty^2 \theta + \Omega \dot{\psi} r^2 - V_\infty \dot{z})$$
$$\Delta M_y = \frac{\Omega r^2}{U}\rho a_0 c_0 (-V_\infty^2 \psi - \Omega \dot{\theta} r^2 + V_\infty \dot{y})$$
$$\Delta M_z = \frac{\Omega r^2}{U}\rho a_0 c_0 (V_\infty^2 \theta - \Omega \dot{\psi} r^2 + V_\infty \dot{z})$$

These section forces and moments need to be integrated over the blade radius to gain the final force and moment values at the propeller hub. The obtained equations for the classical HR definition case are then used to derive the propeller derivatives as they are implemented in the used procedure. However, at this point, differences in sign in front of different geometrical perturbations ($\dot{\psi}$, $\dot{\theta}$, ψ, θ, $\dot{y}$, $\dot{z}$) can be noticed between the two cases already for the sectional forces. These changes are passed forward in the further derivation and can be translated already at this point into an change in sign of the propeller derivatives. These changes, together with the changes that can be obtained when including unsteady aerodynamics, lead to the definition of the transformation matrix stated in equation 4.12. This matrix can be multiplied element-wise with the propeller matrices $\underline{K}_{prop}$ and $\underline{D}_{prop}$ determined based on the classical HR definition to generate the suitable matrices for a propeller with opposite propeller rotation direction.

$$\underline{D}_{prop,neu} = \underline{D}_{prop} \circ \underbrace{\begin{bmatrix} 1 & -1 & -1 & 1 \\ -1 & 1 & 1 & -1 \\ -1 & 1 & 1 & -1 \\ 1 & -1 & -1 & 1 \end{bmatrix}}_{\underline{T}_\Omega} \quad ; \quad \underline{K}_{prop,neu} = \underline{K}_{prop} \circ \underbrace{\begin{bmatrix} 1 & -1 & -1 & 1 \\ -1 & 1 & 1 & -1 \\ -1 & 1 & 1 & -1 \\ 1 & -1 & -1 & 1 \end{bmatrix}}_{\underline{T}_\Omega}$$

Similar to this derivation, the case of an opposite flight direction can be studied, leading to the transformation matrix as already stated in equation 4.14:

$$\underline{T}_{FD} = \begin{bmatrix} 1 & 1 & -1 & -1 \\ 1 & 1 & -1 & -1 \\ -1 & -1 & 1 & 1 \\ -1 & -1 & 1 & 1 \end{bmatrix} \tag{A.1}$$

A.2. Transfer-matrix transformation for opposite propeller rotation

From transfer-matrices that have been generated using a different propeller model in Simpack, that has been existed already for different propeller rotation definitions, a transformation matrix for an opposite propeller rotation direction could be derived as follows:

$$\underline{H}_{prop,neu} = \underline{H}_{prop} \circ \begin{bmatrix} 1 & 1 & 1 & 1 & 1 & 1 \\ 1 & 1 & -1 & 1 & -1 & 1 \\ 1 & -1 & 1 & 1 & 1 & -1 \\ 1 & -1 & -1 & 1 & -1 & -1 \\ 1 & -1 & 1 & 1 & 1 & -1 \\ 1 & 1 & -1 & 1 & -1 & 1 \end{bmatrix} \tag{A.2}$$

This transformation matrix has not been used in the present thesis and not verified more precisely. It is given here only as an additional information because it might be interesting for future applications of the method.

A.3. Structural modes of the generic aircraft model

Mode	Description	Frequency [Hz]
1-6	Rigid body modes	$0 - 0.1$
7	Fuselage yaw and roll + 1st asym. wing bending (in- and out-of-plane)	5.3
8	1st sym. wing bending (out-of-plane)	5.6
9	Fuselage yaw and roll + 1st asym. wing bending (in-plane) + asym. pylon pitch	6.2
10	1st asym. wing torsion and out-of-plane bending	7.7
11	1st sym. wing torsion	8.1
12	1st sym. wing bending (in-plane) + fuselage pitch	8.9
13	HTP yaw and roll	9.9
14	HTP yaw and roll + sym. pylon torsion/lateral	10.7
15	Asym. pylon torsion/lateral	11.7
16	Asym. HTP bending + pylon torsion	12.4
17	Fuselage bending (out-of-plane) + sym. HTP bending + pylon torsion	13.7
18	Fuselage bending (in-plane) + asym. HTP bending + 2nd asym. wing bending (out-of-plane) + asym. pylon torsion and pitch	14.1
19	Asym. pylon torsion/lateral	17.5
20	Sym. pylon torsion/lateral	17.9
21	Fuselage bending (in-plane) + HTP yaw + VTP bending + 2nd asym. wing bending (out-of-plane) + asym. pylon pitch/torsion/lateral	19.1
22	1st sym. wing bending (in-plane) + asym. pylon torsion/lateral + sym. HTP bending	19.2
23	Fuselage bending (out-of-plane) + 1st sym. HTP bending + 2nd sym. wing bending (out-of-plane) + sym. pylon pitch	20.2
24	Fuselage bending (in-plane) + HTP yaw + VTP bending + 2nd asym. wing bending (out-of-plane) and torsion + pylon pitch and x-motion	22.6
25	Fuselage bending (out-of-plane) + sym. HTP bending + 2nd sym. wing torsion	22.9
26	Fuselage bending (in-plane) + VTP bending + 2nd asym. wing bending (in-plane and out-of-plane) + asym. pylon pitch and x-motion	24.3
27	Aileron control rod mode	25.2
28	VTP bending + asym. wing torsion + asym. pylon pitch	25.5
29	Fuselage bending (out-of-plane) + HTP bending + 2nd sym. wing torsion + sym. pylon pitch	26.4
30	Aileron control rod mode	30.5

Table A.1.: First 30 structural modes of the unmodified generic aircraft configuration

A.4. Flutter results for different stiffness scales for all modes

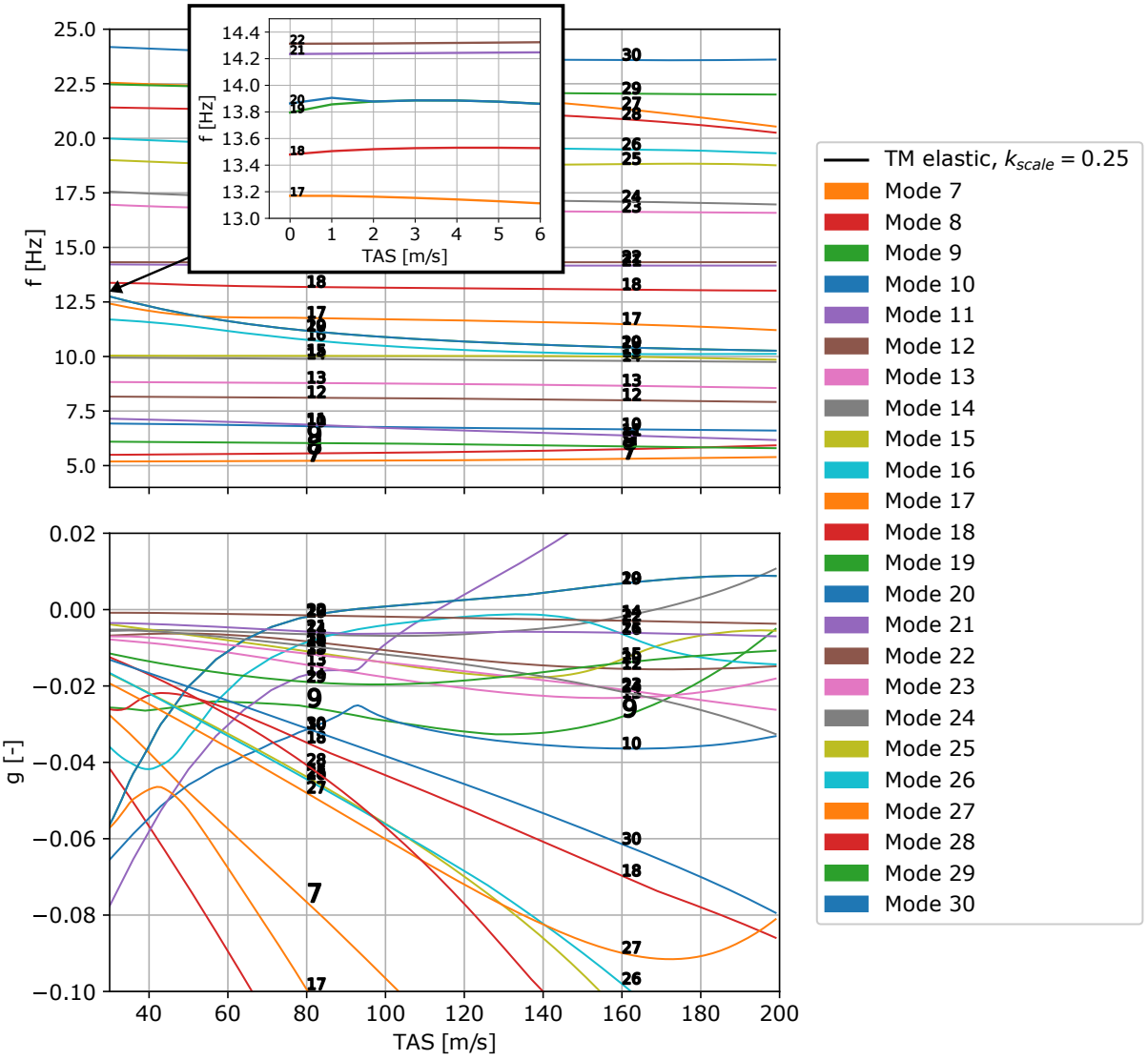

Figure A.2.: Frequency and damping trends from TM-method results for elastic propeller blades with $k_{scale} = 0.25$

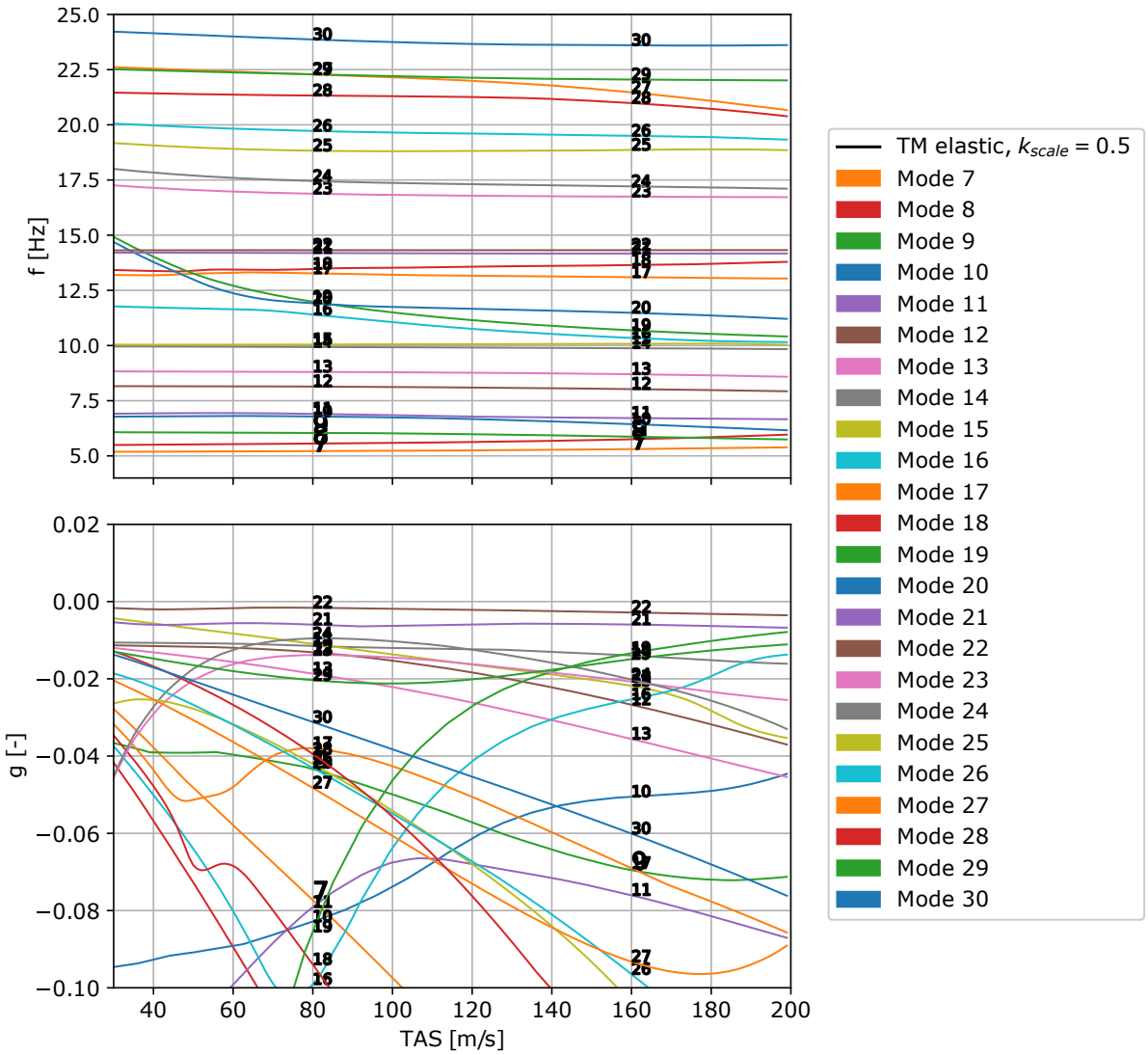

Figure A.3.: Frequency and damping trends from TM-method results for elastic propeller blades with $k_{scale} = 0.5$

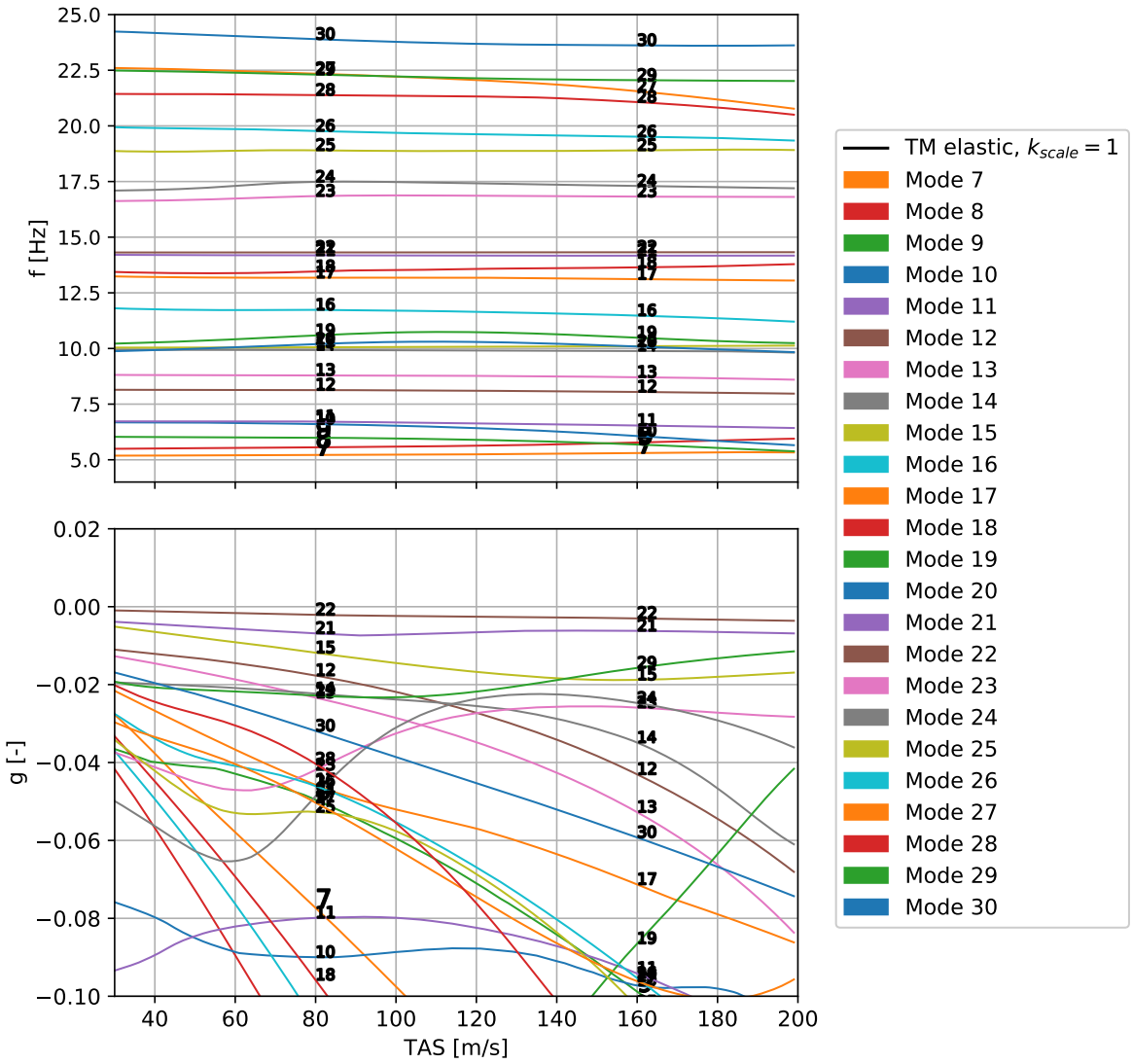

Figure A.4.: Frequency and damping trends from TM-method results for elastic propeller blades with $k_{scale} = 1$

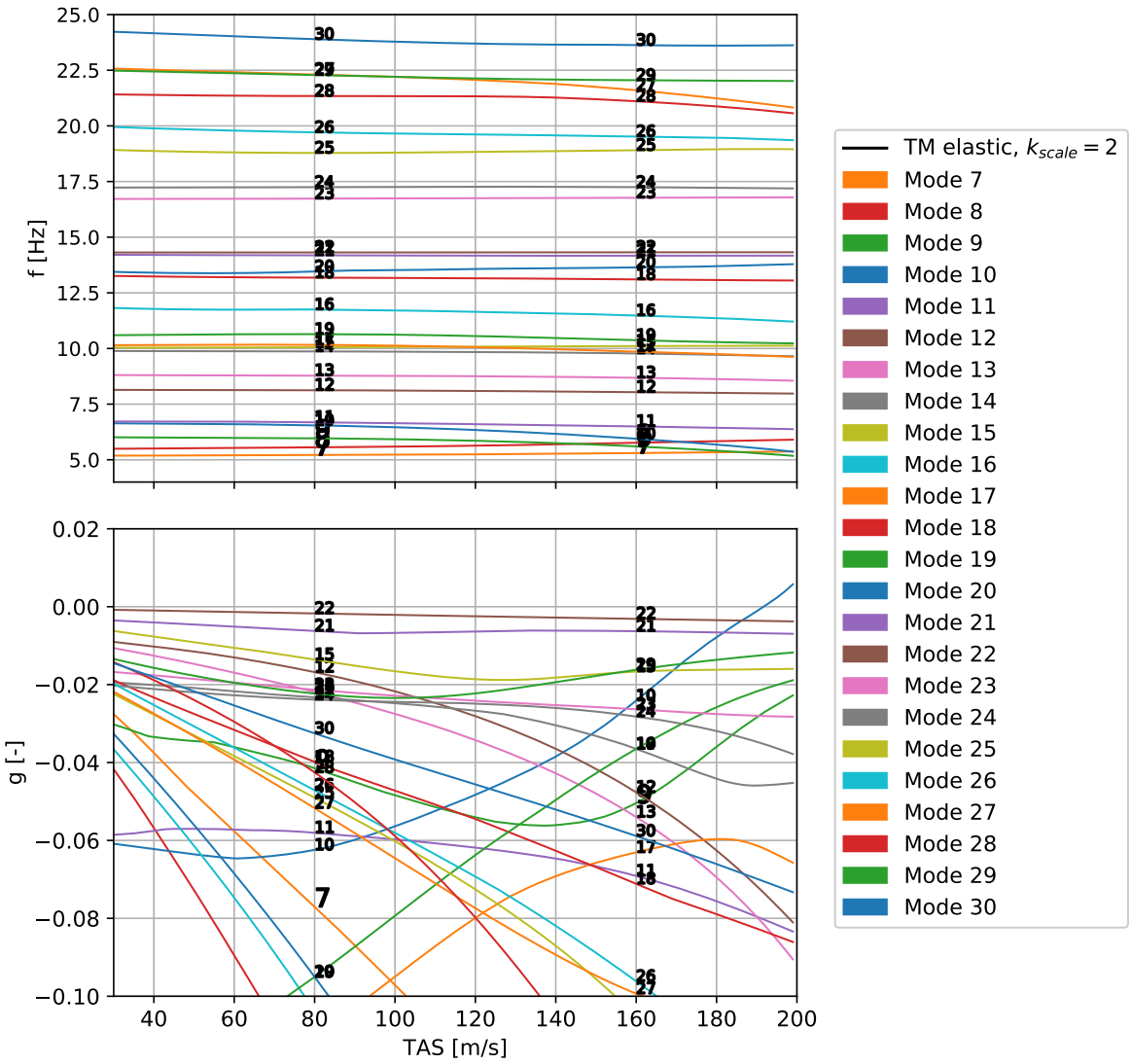

Figure A.5.: Frequency and damping trends from TM-method results for elastic propeller blades with $k_{scale} = 2$

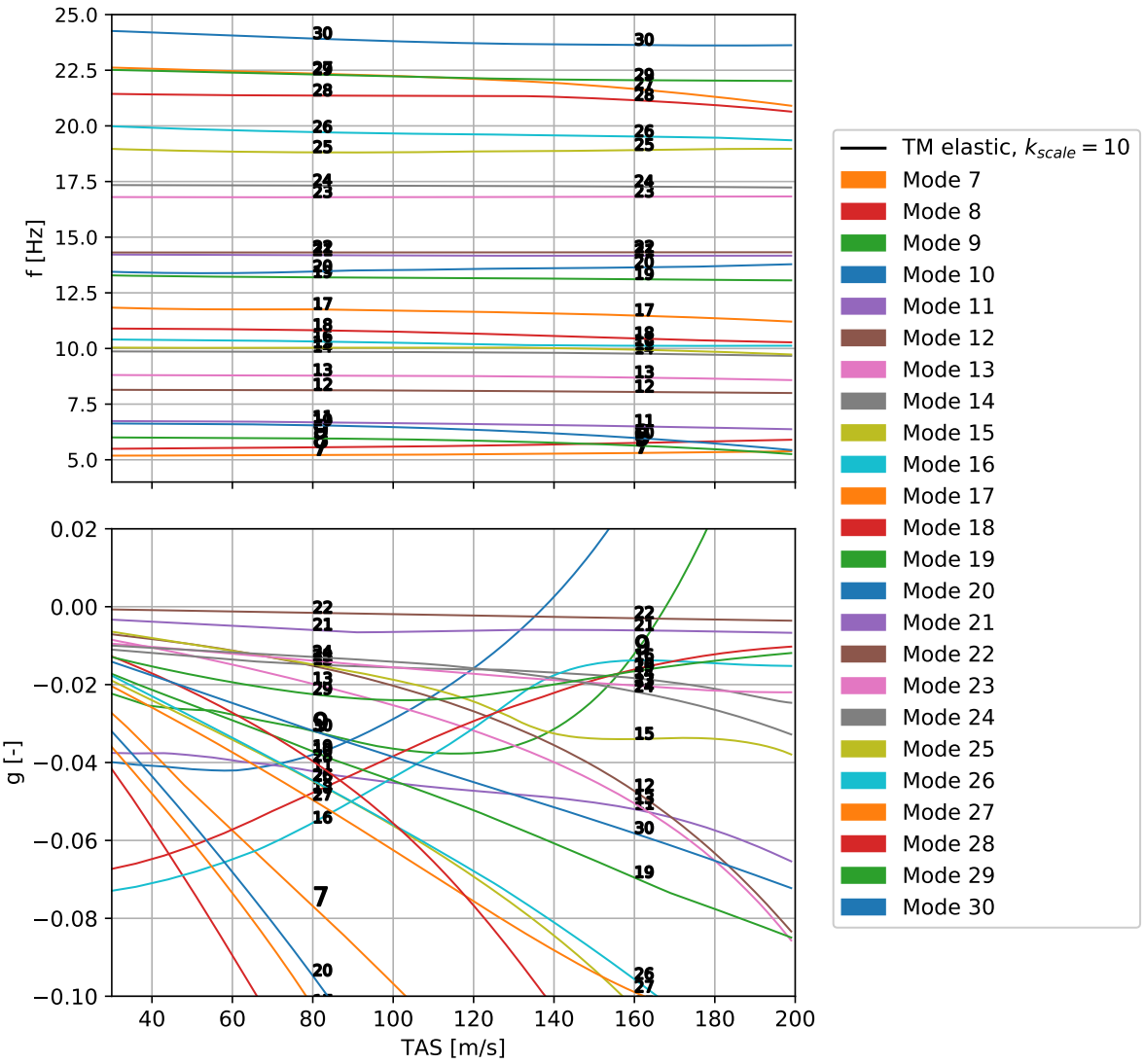

Figure A.6.: Frequency and damping trends from TM-method results for elastic propeller blades with $k_{scale} = 10$